University of Alberta

Detection of Clandestine Tunnels using Seismic Refraction and Electrical Resistivity Tomography

By

Grey Riddle

A thesis submitted to the Faculty of Graduate Studies and Research
in partial fulfillment of the requirements for the degree of

Master of Science
in
Geophysics

Department of Physics

Spring 2012
Edmonton, Alberta

ABSTRACT

The detection of clandestine tunnels is a major issue along the U.S.-Mexico border. These tunnels provide access to illegal transportation of drugs, weapons, and people. This study tests the use of high resolution seismic refraction techniques and electrical resistivity tomography to detect tunnels. The target sites are (i) surrogate tunnel sites along an abandoned railway track in Oxford, MS, and (ii) a plugged clandestine tunnel that runs from Agua Prieta, MX, to a warehouse in Douglas, AZ. The results show that the use of seismic and electrical techniques can detect the presence of a tunnel anomaly and can increase reliability and confidence in the location of tunnels.

TABLE OF CONTENTS

LIST OF FIGURES

LIST OF TABLES

LIST OF SYMBOLS AND ABBREVIATIONS

NCPA	National center of Physical Acoustics
UofA	University of Alberta
MS	Mississippi
AZ	Arizona
US	United States
DHS	Department of Homeland Security
CBP	Customs and Border Patrol
MX	Mexico
ERT	Electrical resistivity tomography
SRI	Stanford research institute
GPR	Ground penetrating radar
EM	Electromagnetic
FDEM	Frequency domain electromagnetic method
TDEM	Time domain electromagnetic method
MASW	Multichannel analysis of surface waves
KGS	Kansas geological survey
RMS	Root mean square
GPS	Global positioning system
VSP	Vertical seismic processing
CA	California
SEG	Society of exploration geophysicist
SARIS	Scintrex automated resistivity imaging system
DC	Direct Current
FDVEP	Finite difference viscoelastic program
FD	Finite difference
GSLS	Generalized standard linear solid

SRT	Seismic refraction tomography
P-wave	Compressional wave
S-wave	Shear wave
SV wave	Vertical surface wave
QC	Quality control
CSG	Common shot gather
GLI	Generalized linear inversion
NMO	Normal moveout correction
LMO	Linear moveout correction
WET	Wavepath eikonal traveltime
AGC	Automated gain control
FWI	Full waveform inversion
S/N	Signal to noise
V_s	Shear wave
V	Compressional wave
fc	Central frequency
DH	Grid spacing
DT	Time sampling
Q	Quality factor
T	stress relation time/tortuosity
J	Electric current density
ρ	Density
E	Electric field
L	Length
A	Cross sectional area
C	Curvature
I	Current
Δ_v	Potential difference
k	geometric factor
Δq	Resistivity model parameter change vector
F	Resistivity smoothness constrain matrix

f	Resistivity model response vector
g	Resistivity discrepancy vector
J	Jacobian matrix
y	Resistivity data vector
2D	Two dimensional
3D	Three dimensional
k	Bulk modulus
μ	Shear modulus
v	Velocity
λ	Wavelength
E	Least squares error
P	Probability
T	Temperature of annealing

CHAPTER 1
1.0 OUTLINE

The work presented here is the result of joint cooperation between the University of Alberta, Alberta, Canada, and the National Center for Physical Acoustics (NCPA), Olemiss, MS, USA. The author contracted with the Department of Homeland Security (DHS) to investigate the feasibility of using high resolution seismic methods to detect clandestine tunnels and electrical methods to help delineate features identified at the two test sites. The first site was in Oxford, MS, along an abandoned railway track that had numerous cavities cutting underneath it. The second site was in Douglas, AZ, where a real clandestine tunnel crosses the U.S.-Mexico border. The work is divided into eight chapters; a brief description of each chapter is given below.

Chapter 1 describes the project premise and summarizes the contents of each chapter.

Chapter 2 is an overview of geophysical methods used in the past to detect tunnels and describes how these methods detect a void in the subsurface. The motivation to initiate this project and a description of the prevailing issues associated with tunnels across the U.S.-Mexico border are provided. A description of geophysical techniques used to detect subsurface voids and a review of the literature on methods of tunnel detection are included. Methods of tunnel construction are reviewed and limitations and advantages of these methods are considered.

Chapter 3 gives an overview of the data acquisition and equipment that were used at the tunnel sites. Methods used to explore the target sites and the surrounding terrain are explained along with a description of the equipment used and how it was implemented in the field.

In chapter 4 the detection of subsurface tunnels with seismic and electrical methods is described. It is shown how synthetic modeling can optimize parameters of the data acquired and a signature of what should be seen in the real data is

presented. The simple geological models used were guides for acquiring data using seismic and electrical methods. Electrical modeling was used to figure out which electrical array was needed to image the subsurface model and also to detect the effects of an air filled void on both Wenner and dipole-dipole arrays. Using a finite difference forward modeling program, synthetic seismograms were used to display the effect of a tunnel on a seismic wave. Descriptions of the program and the parameterization of the modeling program are given.

Electrical method theory and its application are described in chapter 5; examples are given. The chapter starts by going over some basic resistivity theory followed by a description of the electrical resistivity tomography (ERT) method. How electrical data are displayed and how the subsurface is imaged for both dipole-dipole and Wenner arrays are explained. The data collected at Oxford, MS, is analyzed and the results are fed into the interpretation of the real clandestine site in Douglas, AZ. The main objective of this chapter is to show how electrical methods can detect tunnels.

Chapter 6 discusses the seismic method and how it can be used for tunnel detection. It starts with a description of elastic wave theory and describes different types of seismic waves. Seismic resolution is described and it is explained how refraction tomography and seismic ray tracing can image the subsurface. The inversion algorithm and seismic refraction data are discussed. Refraction profiles from Oxford, MS, and Douglas, AZ, are analyzed and both surface and borehole models are interpreted.

Both seismic and electrical methods can help delineate false anomalies, as shown in chapter 7. The data are reviewed to discover what could be improved in a future project.

Joint surface and borehole interpretation shows why some surveys fail and why others are interpreted in certain ways. The interpretation also shows what could be done with other parts of the seismic wave to detect tunnels using diffractions off the tunnel itself. The final part of the chapter discusses feasibility, repeatability, and criteria needed for the next level of tunnel detection.

Chapter 8 includes a short summary of how refraction and electrical methods can be used for tunnel detection. It describes what was done in the project, what was learned, and the conclusions reached.

The Appendix at the end of the dissertation contains details that expand on the chapter information and a brief description of some of the key acquisition parameters of each tunnel site. Site information, field record notes, a basic description of the tunnel sites, and pictures associated with each test site can be found in the Appendix.

CHAPTER 2

2.0 BACKGROUND INFORMATION

The following chapter discusses how geophysical techniques can be used to detect subsurface voids such as tunnels, cavities, and karst features. Different geophysical methods are analyzed to determine how they measure basic physical properties of the terrain and the limitations and advantages of each method are considered. Previous case studies on tunnel detection are reviewed with respect to how they have helped develop new advances in processing and data acquisition in detection of near surface voids. Tunnel construction is discussed later in the chapter. Equipment and software provided for this study by the University of Alberta and the University of Mississippi are described.

2.1 INTRODUCTION

Near surface tunnel detection is a difficult field of research because most tunnels and subsurface cavities have a large amount of surface and subsurface heterogeneity and are often in are in densely populated regions. Thus a geophysical search for a tunnel is undertaken on a site to site basis. The geophysical methodology is the same as that for finding other subsurface voids such as bunkers, caves, karst features, tombs, and culverts. Geophysically speaking, a subsurface void is just a zone of high contrast in physical properties with a solid wall and a fluid interior. In the near surface the void is completely fluid filled, in most cases with air and water. The way the subsurface void is created affects the surrounding rocks by changing the stress on the surrounding material. The type of tunnel casing also greatly affects what type of geophysical technique can be used to study the tunnel; with this in mind the interpretation of tunnel data must be made with caution. Multiple methods should be used to limit false artefacts and increase reliability in detecting tunnels.

Clandestine tunnels crossing the U.S.-Mexico border have been used for years to transport drugs and illegal immigrants. The U.S. government began to take notice and held its first symposium on tunnel detection in 1977 at

the Colorado School of Mines; since then more attention has been given to near surface clandestine tunnels. Conventional intelligence methods do not detect all tunnels, so more attention has been given to direct methods of locating tunnels allowing more border security and greater control of illegal drug and immigrant transportation. The progression of tunnel detection and the involvement in this project of the University of Alberta and the University of Mississippi are discussed later in the chapter.

Due to the cost and the lack of reliability of most geophysical methods, the best way to find a clandestine tunnel is still indirect, using intelligence methods (i.e., rumours, tips) rather than science. But as data acquisition technology progresses, cheaper and more effective ways are being found to detect tunnels. Multiple geophysical methods have been used in the past to detect tunnels, but all have limitations from both scientific and data acquisition perspectives. New advances in date acquisition have made it possible to obtain cheap and reliable data, but the small sizes of underground voids make them nearly impossible to detect. The goal of the research is to test the practicality of using seismic and electrical resistivity tomography to detect clandestine tunnels. Other geophysical methods that are used to detect subsurface voids are compared and discussed.

Later in this chapter information is given about tunnel construction and how the construction changes the physical properties of the surrounding rock. The construction technique used depends on the lithology in the region and the region's accessibility to heavy machinery. The main type of tunnel construction in urban environments is known as the cut and cover method. Another method popular in clandestine tunnel construction is boring, in which a tunnel is cut through the subsurface without removing the material above it. Tunnel construction is considered to help with data interpretation later in the dissertation but will not be discussed in detail.

2.2 MOTIVATION

Most clandestine tunnels are constructed with the aim of escaping detection. Besides the tunnels passing through the U.S.-Mexico border, tunnels have been

detected at the Canada-U.S. border and a series of tunnels to enable military or terrorist access have been discovered across borders between North and South Korea and between Israel and the Palestinian territories. As human intelligence is useful but unreliable, this research evaluates the reliability of near surface geophysical methods of tunnel detection.

To do this, multiple types of geophysical methods were considered, but only a few available geophysical methods were field tested as appropriate for the test sites selected in this project. The work was supported by the U.S. Department of Homeland Security under Grant Award Number 2007-ST- 108-000003.

The first few conferences on tunnel detection were convened to see if geophysical techniques could be used effectively to detect a subsurface tunnel. The first technical symposium on tunnel detection tunnels (Anon 1981) found that geophysical methods could be used to detect tunnels, and the second technical symposium on tunnel detection (Anon 1988) was held to see if new research made detection more accurate. A major report was issued by SRI International to evaluate the technology used in tunnel detection in 1979 (Vesecky, Nierenberg and Despain 1980). This report revealed that there was a resolution issue in nearly all geophysical techniques. Multiple other conferences were held to try to remedy this issue but resolution is still a problem in all geophysical techniques used for tunnel detection.

Ongoing conferences attempt to determine if newer data acquisition technology has increased the resolution for detecting subsurface voids. A conference held in Oxford, MS, was the first to suggest that tunnels might be detected during construction (Sabatier and Muir 2006). In particular, attendees discussed the use of passive techniques that record the unavoidable noise created during tunnel construction in the subsurface. Other active techniques were also discussed but it was decided that more data were needed to find tunnels. Although other assemblies around the same time were dedicated to the detection of tunnels or voids (Halihan and Nyquist 2006, Mckenna and Ketchum 2006), the resolution issue of tunnel detection is still the main source of unpredictability. A combination of multiple methods is now used to detect tunnels. For instance, joint

inversion of data from two different approaches can decrease false anomalies (Cardarelli et al. 2010). In this thesis electrical resistivity is used to estimate a model of the subsurface and that model is used as the initial model for refraction tomography. The goal of this research is to use multiple methods and process them individually to limit false artefacts in interpretation of data (Riddle, Hickey and Schmitt 2010).

The University of Mississippi became involved with the U.S. Department of Homeland Security during a convention in 2006 (Sabatier and Muir 2006). The goal of the grant for the present project from the U.S. Department of Homeland Security was to determine if refraction tomography has advanced far enough to enhance the detection of tunnels using high resolution seismic technology. The idea first came from looking at infiltration of water through a test earthen damsite; researchers were trying to determine if the movement of water could be detected in a time lapse sense (Hickey and Howard 2006). What was seen was that as the water went through a buried pipe, a void of air was created and it was possible to detect the void by looking at the seismic ray coverage. The goal of this study was to detect tunnels using a 2-D ray coverage plot and velocity tomography with the methodology that proved successful at the earthen dam. It was also considered to use electrical methods to look at basic geological structures because of their previous success in finding high contrast voids. The University of Alberta got involved in this project through a collaboration between Dr. Doug Schmitt and Dr. Craig Hickey that provided field experience and equipment available at the university. The goal of the University of Alberta was to use electrical resistivity tomography to test other high resolution seismic methods such as reflection for the ability to detect tunnels.

2.3 TUNNEL DETECTION REVIEW

There are multiple methods for finding geological information in the vadose zone—the partially saturated zone from the earth's surface to the ground water table; but all the methods have drawbacks. The vadose zone is the region where a clandestine tunnel is most likely to be constructed, as below the water table opening and maintaining a dry tunnel is problematic. In the vadose zone rocks are

unsaturated to partially saturated with water. To detection a subsurface void, one looks for large changes in the physical properties of the void compared to the surrounding rock. The main issue is that the resolution of the tunnel site is on par or smaller than that of surrounding terrain. The literature review presented below illustrates methods and problems involved in the detection of subsurface voids; the limitations, advantages, and disadvantages of the geophysical techniques used in these studies are discussed.

Tunnel discovery is most common during construction or use. For this reason a quantity of permanent seismometers and sensors are in place along the U.S.-Mexico border to find tunnels that are being constructed. Noise in the seismic data from tunnel construction is picked up by the sensors and signals can be correlated to find the general location of the activity (Sabatier, Matalkah and Ieee 2008). Many seismometers are needed to get an accurate location of a tunnel, but information on the general location can be easily confirmed. The installed sensors can detect tunnel location by comparing similar signals from different sensors and by back-propagating the location of the noise. The way sound waves propagate through a tunnel (Ketcham et al. 2006) can be used to help find a tunnel signature. The activity in a tunnel pulsates in a harmonic motion that is reflected in the seismic data and can be cross correlated to create maps of possible tunnel locations (Ketcham et al. 2006). Other types of permanent geophysical sensors can be implemented and used to gather data to help limit false artefacts in clandestine tunnel detection by using statistical measures and comparing them to synthetic measurements (Senglaub et al. 2010). The advantage of passive methods is that once the sensors are in place they can survey a large area for possible tunnel sites. Unfortunately, in urban environments the energy caused by tunnel construction may be weak relative to the urban noise at seismometer locations. In these locations geophysical methods need to be applied to detect clandestine tunnel construction. However, geophysical techniques have limitations in urban environments due to situational noise and large man-made obstacles that block optimal data acquisition.

Techniques used in an urban environment depend on the situation and the type of terrain. In situations of very resistive soil with very little surface metal in

the ground, penetrating radar (GPR) is usually the best imaging technique. GPR uses high frequency electromagnetic (EM) waves and pulsates a signal into the ground using an antenna. Two antennas are used, one to transmit signal into the ground (the source) and the other to receive the signal (the receiver). The transmitted signal is a polarized short pulse of a given frequency; the wave propagates through the ground and when it hits a buried object of different dielectric constant it is reflected back. The depth of penetration depends on the electrical conductivity of the subsurface and the transmitted frequency. In situations where the soil conductivity is high this method works only in the very near ground surface and will miss a deeper anomaly (Telford, Geldart, and Sheriff 1990). In these regions using GPR is a poor choice and other techniques need to be used. Due to its high accuracy, GPR was one of the first techniques used effectively to detect tunnels and has been used extensively to map karst features (Benson 1995, Chamberlain et al. 2000). The method is popular because it employs onsite data analysis, enables fast data acquisition, and can distinguish very small subsurface features; in practice GPR has been used to map subsurface cavities (Kruse et al. 2006). Due to the fast data acquisition inherent in the GPR technique it is feasible to combine interpretations of GPR and geoelectrical data (El Khammari et al. 2007) in regions with many large cavities. Interpretation of GPR can be difficult in regions of large laterally variant near surfaces; combination with microgravity, data can be used in regions of sinkholes and karstic features to help delineate lateral density changes (Leucci and De Giorgi 2010). A new way to use the GPR technique to look for tunnels is with multiple antennas that create a radio frequency tomography (3D structure) of the subsurface (Lo Monte et al. 2010). This technique uses diffraction scattering from the void and multiple antennas to look for shallow tunnels. The main disadvantage of using GPR techniques is that the data inversion depends on the conductivity of the subsurface.

In a technique known as microgravity, gravity is used to search for tunnels or near surface voids. A gravimeter records the relative value of gravity at the earth's surface, so the change in ground density due to a near surface void causes a gravity anomaly that can be seen in the gravity measurements (Telford et al. 1990). Since microgravity looks at relative gravity measurements, the

technique is used extensively in geotechnical studies to look for buried voids (Debeglia and Dupont 2002) or other subsurface cavities (Butler 1984). Microgravity can also be used to detect karstic features in mining operations; safety is increased by locating these voids (Bishop et al. 1997). Whether the void is filled with water or air, the change in density will cause a gravity anomaly. Since only relative gravity changes are measured the microgravity technique can be used efficiently without giving false artefacts. The problem associated with the microgravity technique is that in urban environments with large basements the change in density due to buildings can mask tunnel locations. To avoid this problem a detailed structural model of the region being surveyed needs to be created and information necessary to the model may not be available.

Electromagnetic (EM) methods are popular in near surface studies due to their high frequency content and ability to map large areas. One type of EM technique is the frequency domain electromagnetic (FDEM) method; the FDEM method measures induced electromagnetic current which can used to calculate a volume in the subsurface, and can be continuously measured for quick mapping of the subsurface. Although data for the subsurface volume are gathered, FDEM surveys generally have poor vertical resolution; but FDEM surveys can be used to obtain lateral changes such as those produced by cavities (Sogade et al. 2004).

Time-domain electromagnetic (TDEM) methods are near surface techniques commonly used in hydrogeological and geotechnical studies but which can also be used to look for tunnels. Time domain methods use induced electric current to create a magnetic field to induce a secondary electric current in the ground. The electric current then pulsates and between injections of electric current the time decay response is measured, which can then be related to the electrical conductivity of the subsurface. Nabighian and Macnae provide information about different types of TDEM methods (Nabighian and Macnae 1991). TDEM methods are useful in detecting conductive anomalies, but can also be used to see changes in lithology and ground water (Legchenko et al. 2009). For tunnel detection TDEM methods can be employed in detecting saline water filled voids or metal lined cavities. Most tunnels are filled with air, but if they are not lined the water table may fill the cavity. In regions of salty sands a TDEM method

may be able to detect the saline water in the tunnel. The main disadvantage of TDEM methods is that air filled tunnels may not be detected due to the surroundings being more conductive. These techniques are used to advantage when a tunnel is water filled and/or has a metal lining. TDEM methods are used as secondary techniques to supplement other methods.

Magnetic surveys can also be used to detect subsurface tunnels or voids lined with a metal exterior or otherwise containing a large amount of iron or steel. The magnetic technique is used mainly to find larger tunnels that have cart tracks or are concrete lined with rebar reinforcements. Due to the rapid data acquisition of this technique it can be useful if there is prior information about steel or iron in the tunnel, but is usually not used in the field.

In near surface geophysics, geoelectrical methods are one of the more common geophysical techniques. The reason for this is that resistivity changes in the subsurface can be related to changes in fluid, mineral content, porosity, water saturation, and rock salinity. Since the near surface physical properties of rocks can change drastically it is necessary to image both vertical and lateral changes. Electrical resistivity tomography (ERT) was developed because imaging the subsurface complex geology is faster with ERT than with the conventional sounding approach (Griffiths and Barker 1993, Zhou, Beck and Stephenson 2000) using Wenner array geometry. Different arrays can also image complex geology; for instance, the dipole-dipole array (Zhou et al. 2000) specializes in lateral changes in the subsurface. ERT is useful in imaging the near surface and has been used widely to image sinkholes and karst geology (van Schoor 2002, Kruse et al. 2006, Leucci, Margiotta and Negri 2004, Dobecki and Upchurch 2006). Sinkholes resemble collapsed tunnels in geophysical images; that is, the ground shows up as either a highly resistive or conductive anomaly depending on whether it is air or water filled, respectively. Using the same methodology as tunnel detection, ERT can be used to detect archeological targets such as tombs and graves (Negri, Leucci and Mazzone 2008, Papadopoulos et al. 2010, Cardarelli et al. 2010). When using ERT at archeological tombs the anomaly that is seen is a highly resistive block due to weak soils and air filled chambers. Since air is highly resistive, ERT methods can be used in joint interpretation methods to limit uncertainty (Cardarelli et al. 2010,

Piro, Tsourlos and Tsokas 2001). The main advantage of ERT compared to other methods is that electrical methods work quite well in complex geology. Electrical methods can map the subsurface quickly and fairly inexpensively due to fast data acquisition and easily interpretable results. The main disadvantage of ERT is that in very conductive soils the current may not penetrate to where a highly resistive anomaly may be, and thus the subsurface feature of interest may be imaged incorrectly. As ERT gives only apparent resistivity values of the subsurface, the actual values cannot be directly interpreted for a given geological feature.

In the detection of clandestine tunnels, both seismic refraction and reflection techniques are popular. The reason for this is that seismic methods can detect contrasts in rigidity, compressibility, and density of the subsurface. The physical properties of fluid filled voids are much different from those of surrounding materials. In all seismic methods the velocity of the subsurface is related back to the physical properties for interpretation. The main issue in most void sites is that the highest resolution of the seismic data is on par or smaller than that of the void.

Grandjean and Leparoux conducted seismic modeling experiments to see if using seismic methods could be used to detect subsurface voids (Grandjean and Leparoux 2004). The researchers observed that both P-wave and Rayleigh waves are important in the detection of tunnels. Grandjean and Leparoux described how both direct and diffracted waves are attenuated and changed by the presence of a cavity in the subsurface. In general, due to the size of the void, seismic reflection is too small to treat a tunnel like a layer. Therefore, instead of reflecting off the void site, the void scatters secondary waves and is treated as a second point source, or as a source of diffraction (Xia et al. 2007). Diffraction imaging is useful in detecting subsurface voids and has been used to back-propagate tunnel locations (Lee et al. 1989). Using a similar technique, the diffractions can be stacked to look for small sized voids (Belfer et al. 1998). A newer approach attempts to image the subsurface using diffraction imaging, where the diffraction is separated using a moveout function (Xia et al. 2007), or a display similar to semblance (Keydar, Pelman and Ezersky 2010), to find the anomaly. The reason that so many different types of diffraction imaging must be used is that the first diffractions arrive at the surface receiver at times similar to the times of the surface waves. Further, the time-

receiver offset trend of the diffractions looks similar to that of the reflections, and thus is processed similarly. Since diffractions can have small amplitude, enhancement may be needed to remove the energy of other seismic waves (Khaidukov, Landa and Moser 2004). This is exceptionally useful when there are numerous strong reflectors, since most diffractions have significantly lower amplitude then the reflections. The main disadvantage of using diffraction imaging is that it is hard to discriminate between a diffraction caused by a void and a diffraction produced by a local heterogeneity. To circumvent this problem, seismic tomography can be carried out in addition to diffraction and the results of the two methods can be correlated. The main advantage of this diffraction method compared to other seismic techniques is that the diffractor comes directly from the tunnel so it is easy to locate the void.

The first arrival of a refracted wave—that is, the first wave that comes from the source to the sensors located on the ground—can be used to detect a tunnel. The larger the spread length of the sensors from the source point, the deeper and faster is the refracted wave, generally. Since the P-wave velocities of air and water are quite a bit lower than the P-wave velocity of sedimentary rocks, the location of a void causes a delay in the arrival of the seismic wave (Engelsfeld, Sumanovac and Pavin 2008). Markiewicz and Rodriguez used travel time data alone to estimate void locations underneath a concrete road (Markiewicz and Rodriguez 1986).

Refraction tomography uses the first arrival travel time and uses the changes in arrival times of waves to calculate the velocity structure of the subsurface. Due to the small size of voids, the velocity information estimated by refraction tomography is only slightly lower than that of the surrounding material (Sheehan, Doll and Mandel 2006a). The reason for this is that when inverting for the velocities using the travel times from direct arrivals, the regularization of the inversion causes a smooth velocity change. The method uses ray tracing to calculate the velocity of the structure; at lower velocity, fewer rays travel through the tunnel (Hickey and Howard 2006). Since the physical properties of the tunnel contrast with those of the surrounding terrain, the rays bend around the tunnel because the seismic waves can travel through the surrounding rock while

transmission of seismic energy through the air filled void is minimal. The velocity tomogram is still able to see a small decrease in velocity around the tunnel site. Another way to detect subsurface tunnels using refraction tomography is to use joint interpretation. Using the information from ERT surveys one can estimate a subsurface initial model for refraction tomography to increase the accuracy of the tomogram and decrease false artefacts (Cardarelli et al. 2010). Multiple refraction tomography programs have been tested to determine their effectiveness in characterizing near surface features (Sheehan, Doll and Mandell 2006b). Doll et al. discusses some of the limitations and disadvantages of using tomography (Doll et al. 2006). Due to the low cost of near surface seismic studies, much research is dedicated to seeing how well seismic methods can characterize near surface features.

Some waves in a seismic study are surface bound. These waves travel near to the surface and are thus called surface waves. The strongest surface wave is known as the Rayleigh wave, or the ground roll in geophysical jargon. The Rayleigh wave is dispersive and loses amplitude very quickly in the subsurface. The reason it is used in near surface studies is due to the high amplitude of the signal which can be used extensively in urban environments. The technique most associated with surface waves for near surface studies uses multichannel analysis of surface waves (MASW), a method developed by the Kansas Geological Survey (KGS) (Zhang, Chan and Xia 2004). The technique uses dispersion curves to estimate the velocity of the subsurface and due to the nature of surface waves (S-waves) the presence of any fluid can indicate the presence of a near surface void (Nasseri-Moghaddam et al. 2007). The technique can be applied quite well in busy urban environments where most techniques fail because of high noise levels (Karray and Lefebvre 2009). Karray and Lefebvre study found cavities underneath pavement in an urban environment using surface waves. The key to characterizing voids using MASW techniques requires good spatial and frequency sampling. That is, both low and high frequencies need to be covered well since the velocity image relies on the dispersive nature of the waves. Good spatial resolution is needed to detect narrow subsurface cavities, such as dipping cavities in abandoned mine shafts (Xu and Butt 2006). The history of MASW in the

search for tunnels is described in Miller et al.; the authors suggest that MASW techniques are the best ways to find clandestine tunnels (Miller et al. 2006). The main disadvantage of using surface techniques is that without low frequency geophones, which can be costly, the depth of the investigation is limited. The main limitation of this technique is that for now the inversion from a dispersive curve to a velocity image is all 1-dimensional, so large spatial sampling is needed to accurately image the subsurface.

Surface techniques for detecting subsurface tunnels are the most cost effective and but in general are limited in an urban environment. Since surface techniques are also limited in estimating the initial subsurface model, artefacts and interpretation errors can be prominent. One way to ameliorate this problem is to ground truth the geophysical data by carrying out additional measurements in shallow boreholes at the investigation site. This is quite common in oil and gas exploration to "tie" seismic reflections to the real geology. One can place a sensor in a borehole and a source in another and look at 1-way travel times for seismic waves, this technique is known as cross-borehole tomography. The technique has been used effectively to detect tunnels due to the simplicity of the inversion and the large effect a tunnel can have on higher frequency seismic waves that can be used in such environments (Vesecky et al. 1980). The tunnel can affect the seismic response in two ways. First, the seismic wave must refract or diffract around the tunnel due to the air filled cavity retarding the travel time considerably. Second, the size of the tunnel changes the incoming amplitude of the seismic waveform (Rechtien, Greenfield and Ballard 1995). Drilling boreholes to gather information in the near surface is quite expensive and in general is not physically possible. The main advantage of using cross-borehole tomography is the simplicity of inversion and the acquisition of ground truth results. The disadvantage is that it is impractical to have boreholes at a survey site. Thus cross-borehole tomography is only used in certain situations.

The method used to find subsurface voids depends on the site characteristics and the equipment available. This research project looks at how seismic methods can be used and describes some key features in tunnel detection. The University of Alberta has two major program licenses for seismic refraction tomography,

Raygui (Song and ten Brink 2004), and SeisOpt Pro™, (provided by Optim Software and Data Solutions, USA). Raygui is an open source ray tracing program used for imaging refraction tomography where the user manually creates the initial velocity model. SeisOpt uses a 2-D eikonal solver for ray tracing and starts with a homogeneous layer and continues to forward the results until the lowest RMS is calculated using a Monte Carlo method. University of Mississippi researchers use Rayfract™ (Intelligent Resources Inc.) which updates the velocity model using the residual from synthetically figured out first breaks. Along with seismic techniques the ERT uses a program called RES2DINV (Loke 2002) to invert the calculated apparent resistivity pseudosection in the subsurface, and also has its own forward modeling software, RES2DMOD (Loke 2002). In the end, GPR was not used for the reason that the soil at the tunnel sites of interest had a large amount of conductive clay rendering the GPR signal ineffective. Table 2-1 lists advantages and limitations of the common geophysical techniques used to detect tunnels and near surface voids.

Technique	Advantages	Limitations
GPR	-Fast acquisition. -Good lateral andvertical resolution. -Can resolve very small anomalies. continuous profiling	-Depth of penetration depends on local geology -Need goodcontact with antennas totransmit and receive signal.
Passive Seismic	-Continuous measurements.	-Expensive to set up. -Need large amount of sensors to image tunnel.
Microgravity	-Very accurate. -Interpretation can give depth, size, and type of anomaly. -Can be used on any terrain.	-Slow acquisition. -Sensitive to vibrations. -Basements in urban environments need to be modeled and post processed.
EM	-Good lateral resolution. -Fast acquisition, no ground contact.	-Limited vertical resolution. -Tough to use in urban environments.
Magnetics	-Fast measurement. -Very sensitive to conductors. -Non intrusive.	-If no conductors is useless.-Sensitive to any surface conductor.
ERT	-Vertical and lateral resolution. -Simple interpretation.	-Interference from any conductor. -Not as effective in very conductive regions.
Seismic reflection/ diffraction	-Gives information of depth and composition. -Good lateral resolution	-Sensitive to acoustic noise. -Extensive processing.
Seismic Refraction	-Good lateral resolution - Can resolve multiple layers	- Sensitive to acoustic noise. -Need large spread lengths.
MASW	-Not as sensitive to acoustic noise. -Fast acquisition.	-Very Frequency dependent. -Low resolution.
Borehole Seismic	-Gives ground truth. -Very accurate. -Limited processing.	-Site needs boreholes. -Impracticable to drill at test sites.

Table 2-1 Advantages and limitations of the common geophysical techniques used to detect tunnels and near surface voids.

2.4 TUNNEL CONSTRUCTION

In general, the construction of a clandestine tunnel occurs long before a survey is performed. The type of construction is hugely important in the detection of the tunnel. The tunnels in this study were constructed by two methods “cut

and cover" (Mouratidis, Lambropoulos and Sakoumpenta 2005) and mechanical excavation. The main difference between the two methods is that in mechanical excavation the ground is excavated by boring through the rock, while in cut and cover the top layer of earth is removed and the tunnel is placed inside the cavity. Most clandestine tunnels along the U.S.-Mexico border were built with some sort of mechanical excavation to evade detection by the U.S. border patrol. Tunnels were/are usually built from a basement on the Mexico side of the border in a straight line to a basement on the U.S. side. The method of excavation required removal of bored rock causing the stress field around the excavation site to become fractured. Because of this a support or casing (a shield) was created during construction. In some cases the clandestine tunnel was completely cased in to keep water out and this complete casing was usually built after the construction of the tunnel. For a cut and cover construction, the surrounding material is excavated from the ground and the cased tunnel was placed in the excavation. This method is usually used in urban environments where secrecy is not an issue as it is a safer and more accurate method of building a tunnel. The reason these types of tunnels may need to be found is that in some situations the clandestine tunnel may bore into a service tunnel. Geologically speaking, a cut and cover tunnel will have its native material removed and reset, while a mechanically excavated tunnel will have the original native material around it.

2. 5 SUMMARY

In near surface geophysics, characterization of near surface features generally depends on the local geology. A tunnel is a subsurface void that is fluid filled and is generally lined with a competent material. The detection of clandestine tunnels is important to the security of the U.S.-Mexico border with respect to illegal immigration, drug transportation, and terrorist activities. Detection of tunnels is a major issue and many conferences and workshops have been devoted to this topic. The University of Alberta and the University of Mississippi have collaborated to detect tunnels using near surface seismic techniques. ERT was also performed to help classify geological information. The different geophysical techniques used for void detection and the advantages and limitations of these techniques are listed in Table 2-1.

CHAPTER 3
3.0 DATA ACQUISITION AND EQUIPMENT

3.1 FIELD SITES

A tunnel is a subsurface void, which in most cases is cased with a competent material to keep dirt and water from intruding into the air filled void. Many study sites can be used as surrogate tunnels to study tunnel physics and possible data acquisition parameters. In most geotechnical operations the tunnels are underneath concrete roads and are used as service tunnels in urban environments. These tunnels are not suitable for use as surrogate sites as electrical wiring runs through them. Other options are drainage tunnels that act as culverts and resemble real subsurface clandestine tunnels. Culverts or pseudotunnels are used as surrogate tunnel sites to perfect data acquisition and processing methods in order to obtain a better idea of the geophysical responses that can be expected at a real clandestine tunnel site. Two different study sites were used in this project. The first site is in Oxford, Mississippi, where multiple surveys were gathered along an abandoned railway surface where culverts have been inserted to lessen erosion on the bank of the valley. This provided a wide range of depths and dimensions for testing. The second and main site is in Douglas, Arizona, where an actual clandestine tunnel was discovered in 1990; it is now the property of U.S. Customs and Border Protection and is used for research purposes. Details about the field notes and basic information about individual tunnel sites are presented in the Appendix.

The first study site was performed February 1–20, 2009, in Oxford, MS, where seismic and ERT surveys were performed of multiple tunnel sites of varying depths and compositions. The study site is several kilometers from the main town and is now used extensively as a walkway. The reason this study site was chosen was its varying depths and compositions but also its proximity to the National Center for Physical Acoustics (NCPA) (a research center at the University of Mississippi) where the equipment was stored. The goal of studying the Oxford, MS, site was to experiment with varying acquisition parameters to see if there are pitfalls or limitations in detecting tunnels. Multiple sources were tested to see the

effects on clipping and energy at the tunnel sites. The data were collected and processed at a later date at the University of Alberta and at the NCPA where Dr. Craig Hickey performed refraction tomography.

At the second study site in Douglas, AZ, seismic and ERT data were collected from September 31–August 4, 2009. This site is a known clandestine tunnel discovered in 1990 when it was being used to smuggle cocaine from Agua Prieta, MX, to Douglas, AZ. The tunnel is approximately 70m long and on average about 10m deep. The tunnel is now used for research purposes and multiple small boreholes have been dug around the tunnel for cross bolehole tomography. The purpose of studying this site was to detect whether a void exists, and, if so, to measure its thickness and depth. To accomplish this multiple surveys were performed at this site during the week of date acquisition.

3.1.1 THE UNIVERSITY OF MISSISSIPPI TEST SITE

As described earlier, the reason for collecting data at the Oxford, MS, site was to validate that geophysical methods could be used for tunnel detection. The site is an abandoned railway track just south of the University of Mississippi campus and is currently used as a walking path. The site is approximately 2 km from a major highway and the only major source of error is pedestrian traffic. The abandoned railway track has multiple drainage culverts inserted into the sides of the structure; they were probably installed during its construction 150 years ago. Some metal culverts were surveyed that were probably installed after construction to deal with other local drainage issues. Table 3-1 lists the various tunnels sites, their physical characteristics, and their GPS parameters. Figure 3-1 shows a Google earth image of the plan view with the approximate locations of tunnel sites projected onto the surface.

Tunnel	Tunnel Casing	Depth (m)	Size (m)	Latitude (N)	Longitude (W)
Tunnel 1	Sandstone Block	9.0-10.0	1.5x1	34°20'11.04"N	89°33'34.14"W
Tunnel 2	Metal Pipe	5.5-6.0	1.25	34°20'42.06"N	89°32'58.80"W
Tunnel 3	Cast Iron Pipe	4.0	0.5	34°20'45.54"N	89°32'56.52"W
Tunnel 4	Sandstone Block	5.5	0.5x1	34°19'47.52"N	89°33'58.32"W
Tunnel 5	Small Concrete Pipe	2.0-2.5	0.75	34°20'3.00"N	89°33'48.12"W
Tunnel 6	Concrete Blocks	6.0	0.6x1	34°19'30.54"N	89°34'12.48"W
Tunnel7	Concrete Pipe	1.5-2.0	0.5	34°20'18.96"N	89°33'19.68"W
Tunnel 8	Sandstone Block	5.5	0.9x0.9	34°19'29.19"N	89°34'14.64"W
Dam	Concrete pipe	4.0-6.0	0.6	34°21'5.45"N	89°33'21.96"W

Table 3-1 Tunnel sites and physical properties; data are from surveys at the Oxford, Mississippi, test site

The tunnels all varied in depth and size but in general the layout for most of the sites was similar. The data acquisition showed a similar layout at each test site; because the railway track was only 5–6 m wide, causing all sites to be surveyed perpendicular to the tunnel location. Except for the dam site, most test sites had similar subsurface structure and native material due to the proximity of the surveyed sites. Figure 3-1, a Google map image of the tunnel sites, shows that tunnel sites are quite far from major roads, and that most of the land near the sites is farm land. A hand held GPS was used to locate the tunnel sites as dense tree coverage limited access. The general terrain showed very little change in

elevation, so static corrections would not be needed in processing, therefore, handheld GPS data were considered to be sufficient.

Figure 3-1 Google earth image © 2011. Google map of the plan view of the tunnel sites located in Oxford, MS. The University of Mississippi is north of Highway 6.

The subsurface view of the each tunnel site varied slightly, but in general all tunnels followed a similar construction. The layout of a deeper tunnel can be seen in Figure 3-2 which depicts a subsurface view of the tunnel and casing material; an example of a surrogate tunnel is also shown. This is one of the tunnels built during the construction of the railway. Most of the tunnel sites are similar to the tunnel shown in Figure 3-2. The exception is the dam site which is made of mostly clay and silt and was still quite moist when the survey was performed. Like the tunnel shown in Figure 3-2, most tunnels were completely air filled and very few were saturated with water.

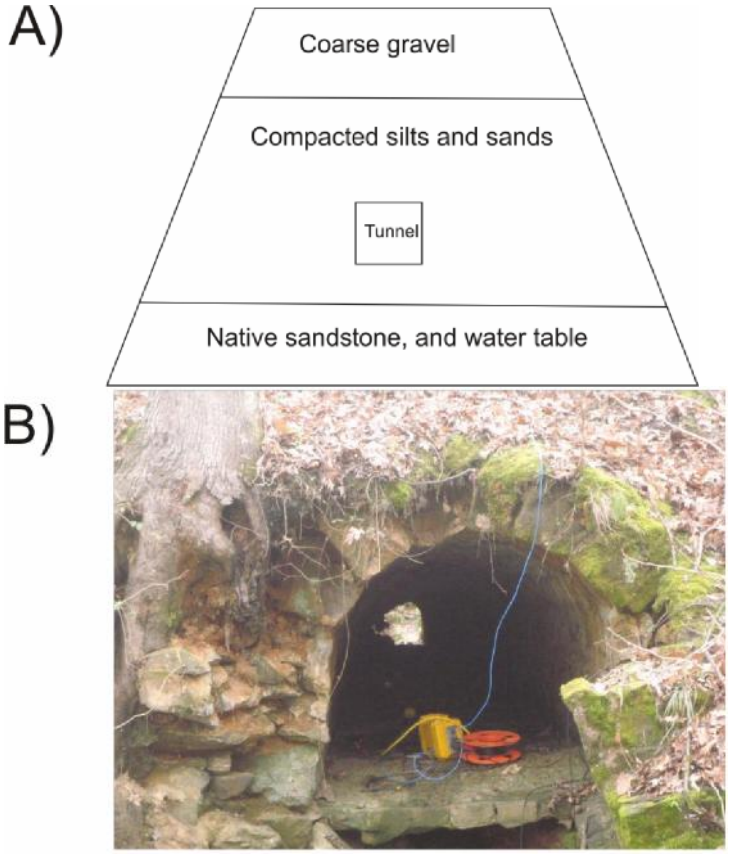

Figure 3-2 (A) A schematic view of the railway study site in Oxford, MS. (B) Tunnel 1 in Oxford, MS. The sandstone blocks casing is visibly spread through the tunnel.

3.1.2 DOUGLAS ARIZONA TEST SITE.

The clandestine tunnel used in this project as a test site crosses the U.S.-Mexico border and is controlled by U.S. Customs and Border Protection (CBP). The purpose of this facility was to research methods of tunnel detection. The tunnel is concrete lined and about 70 m long. It begins in a basement in Mexico and ends in a warehouse in Douglas, AZ. The tunnel is on average around 5–10 m deep and is generally filled with water unless it is pumped out. The site was drained prior to data acquisition. The geophysical surveys were performed August 31–September 5, 2009, and were focused at this tunnel site. To do this, two different locations—a ditch and a road—were surveyed with ERT and seismic refraction and are thus referred to as "ditch" data and "roadside" data. The ditch, as implied, was about 4 m shallower than the tunnel, while the road ran by the warehouse on the Douglas, AZ, end of the tunnel.

These were the only two viable options for surveying a 50 m spread at the tunnel site. Figure 3-3 displays the tunnel site layout for both seismic and ERT surveys in Douglas, AZ. There were a lot more surface heterogeneity and local cultural interferences with the layouts in Douglas, AZ, compared to the Oxford, MS, test site. Both Wenner and dipole-dipole arrays surveyed by ERT and multiple surveys were performed with seismic refraction using different sets of geophones. The roadside data contained noise from the presence of a metal fence and a road that ran nearby. The ditch data suffered from unconsolidated loose sands that made it hard to make good contact with the surface. The ditch had been dug to slow down illegal immigration, and was in the process of being lined with concrete during the time of data acquisition. Along the roadside there were multiple boreholes specially constructed for crosshole tomography. One of the surveys had three component geophones on the surface complemented with a gimbaled 3-C geophone package placed at the bottom of the borehole. Data were then simultaneously collected from all geophones, including the geophone down the borehole and on the surface.

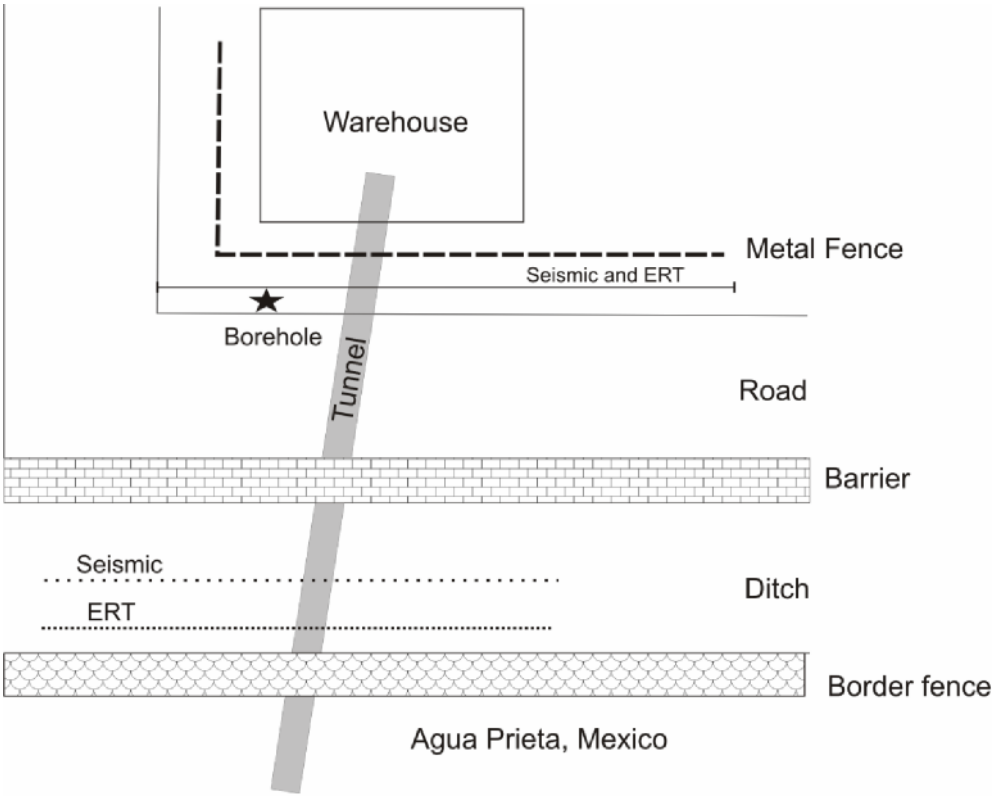

Figure 3-3 A plan view of the Douglas, AZ, test site. The tunnel is 8–10 m deep along the road and 4–6 m deep in the ditch. The border fence is approximately 10 m high and made of closely spaced steel square tubing.

The tunnel stretches from a warehouse in Douglas, AZ, to a villa in Mexico. The tunnel is reinforced by a few centimeters of concrete and has electrical wiring and a ventilation system in place. In its heyday, the tunnel was operated from the Mexico side where the tunnel entrance was disguised with a hydraulic lift floor. There was evidence in the tunnel of dolly tracks indicating some sort of tram being used for transportation of contraband though the tunnel. Because the tunnel depth is below the water table, the water was pumped out before data acquisition. The tunnel is rectangular and approximately 1 m tall and about 75 cm wide. Due to safety hazards no one was allowed to enter the tunnel and hence no sensors could be placed inside nor could any photographs be obtained. Looking at the ditch side wall there were loosely consolidated soils for the first 2 meters of the roadside, and then laminations are evident on the bedrock showing more competent material near the location of the ditch surface.

3.2 FIELD EQUIPMENT

The geophysics department at the University of Alberta (UofA) has an array of geophysical equipment used for near surface and monitoring studies. The grant proposal for this project was submitted by Dr. Craig Hickey and the University of Alberta was subcontracted out for equipment and near surface expertise. The contract included the use of near surface seismic tomography and reflection profiling to detect tunnels. Since the UofA has other types of geophysical equipment, additional techniques were tested to see which might benefit the study. In particular, electrical resistivity tomography (ERT) was carried out due to its previous success in detecting subsurface voids (van Schoor 2002), (Griffiths and Barker 1993), (Kruse et al. 2006). Other techniques such as ground penetrating radar (GPR) have been used to detect tunnels (Benson 1995) but this was not attempted for various logistical and geophysical reasons. In the end only seismic and electrical methods were used in the surveys. To determine accurate locations, a differential GPS was employed at the Douglas, AZ, test site.

3.2.1 SEISMIC EQUIPMENT

The seismic system used in this project employed "planted" geophone sensors on the surface to measure the ground displacement. During a measurement, the geophones transduced the ground surface particle velocity into an analog voltage signal to a digital converter which was then transferred to a computer using an ethernet cable. The geophones are activated by any acoustic or elastic wave energy that will displace the earth's surface; a source of elastic wave energy is required to provide a coherent signal for reception. This seismic energy travels through the earth and the time it takes to travel from the source to the sensor can be used to calculate the velocity of the subsurface. The University of Alberta achieves this by using a GeodeTM (Geometrics Ltd., Santa Clara, CA) system which digitizes the geophone signal for direct storage on a laptop. These data are discussed in detail later. The seismic source generally consisted of using a hammer blow or an accelerated weight drop in these studies.

3.2.1.1 Sensors and Digitizer

A variety of geophone sensors were used at the study sites but in general the most common type were the GS-20DM 40Hz OYO and the GS-20M 14Hz OYO geophones (OYO Corp., USA). These are similar geophones with the difference being the bandwidth of the frequencies the geophones can record. The 14 Hz geophones will not record a good signal below 14 Hz and the 40 Hz geophones will not record a good signal below 40 Hz. In general in a region of high traffic noise, a higher frequency geophone will limit the low frequency surface wave energy contaminating the site. In the Oxford, MS, site, 10 Hz geophones were used at the end of the line during one of the surveys and this generally showed more surface wave energy.

The only different type of sensor used was the 3-C geophone which is a three component sensor that has different orientations to record energy coming from different directions. This geophone is encased in a plastic tube with a hydrometer attached to it and is used extensively for borehole studies. This was used in Douglas, AZ, and was placed at the bottom of the boreholel; orientation was not important since only travel times were used from these data.The geophones are connected to a takeout cable which can transfer the analog signal to be recorded to a digitizer. Each Geode records up to 24 geophones per box. A yellow Geode box with the ethernet and trigger cable attached to it is shown in Figure 3-2. The Geode then is connected to an ethernet cable which transfers the data to a computer where the information can be displayed. Multiple Geodes can be used simultaneously for larger surveys. The Geode options are controlled by a program called Seismic Module Controller where the data are stored. The Geode can handle one shot gather (a shot is a hammer blow on a plate that sends waves of energy into the ground; gather refers to the data collected at the site of the shot) location at a time where stacking of the data can be done in the field or after. The information is stored in SEG-2 format and can be directly transferred to most seismic processing programs. The program also uses a real time noise monitoring, so bad geophones or remnant acoustic energy can be seen. This is very useful on surveys in urban environments and high traffic areas.

3.2.1.2 Source

The source in seismic surveys can vary but in general there are three types.

1) Force in the vertical direction
2) Force in the horizontal direction
3) Explosive force (i.e., in all directions)

These three types of force indicate the type of energy that will be forced into the ground. In general, force in the vertical direction for studies that measure P-wave velocities and force in the horizontal direction for S-wave studies is preferred. Explosive forces direct energy in all directions and are the most common type of geophysical source in seismic studies. For the Oxford, MS, data site, two types of surveys were performed, a manually hefted 5 kg sledge hammer and an accelerated weight drop.

The hammer system involves using a metal plate or strike pad and a hammer connected to some sort of trigger. The trigger is attached to the Geode and in this case a motion sensor trigger was used. When the hammer is swung toward the plate the Geode starts recording at a specified delay time before the impact occurs. This is done to minimize data transfer and reduce postfield processing.

The accelerated weight drop runs on a similar system but instead of being swung, the hammer is forced down by its weight and the additional energy of a 2 m long industrial elastic band. This system is attached to the hitch of a truck where the engine sits in the truck bed. The engine sits on an inner tube to reduce vibration noise. A hydraulic lift energized by a 5 hp Honda engine lifts the steel "hammer" (90.7 kg in this case) and tightens the elastic band. For additional force the band can be tightened around more turns to create higher elastic potential energy and provide more force. Instead of a motion sensor trigger, a contact trigger was used. The strike pad had an electrical wire attached to it and the weight drop had a wire attached to it. When the two wires meet an electrical circuit is closed; the Geode senses the current and commences digitization. The source used depends on spread length and accessibility, in Douglas, AZ, manual

swinging action was used as shown in Figure 3-4(A) to produce seismic waves; an accelerated weight drop is shown in Figure 3-4(B).

3.2.2 ELECTRICAL RESISTIVITY EQUIPMENT

DC electrical resistivity data were collected along similar or the same lines as seismic data. The electrical system used was a Scintrex Ltd. (Toronto, CA) automated resistivity imaging system (SARISTM). The electrical system uses stainless steel electrodes, a smart cable, and the SARIS recoding/activation module. The electrodes are attached to the smart cable using alligator clips which are connected to the SARIS unit. Each smart cable can handle up to 25 electrodes and the UofA has 2 cables. Both imaging and sounding surveys can be surveyed, but imaging surveys were performed in this survey. The two smart cables are attached to the SARIS unit which acts as a switchboard for the electrodes and also for the computer to record the data. By changing the current potential electrode spacing, differing depths of penetration in the subsurface can be obtained. However, the deeper the survey the greater the offsets required and hence the larger the electrical current must be. The system runs on a 24 V battery; power can be obtained from two car batteries in series to supplement the system's smaller internal battery. The system can handle up to 100 watts and 1A of current. Different electrical arrays can be uploaded to the system but most common array types are already included. Wenner and dipole-dipole arrays were surveyed on most tunnel sites; not all locations were surveyed due to time constraints.

3.2.3 GPS

To establish survey locations at the Oxford, MS, test site, a handheld GPS was sufficient since there were only very slight variations in terrain in the location of the surveys. For the Douglas, AZ, test site a Trimble differential GPS was used to accurately determine where the surveys were performed. The Trimble GPS system involves a base rover attached to a tripod which has a set elevation over a control point. When the system is initialized over this control point, real time data can be uploaded with the receiver unit. The mobile rover is attached to a 2 m metal pole and used to get differential GPS from the base point. The control point

in Douglas, AZ, was a borehole cover since accurate GPS data were known at this point. The data are collected and then can be postprocessed for exact locations if the control points are given. The differential GPS has an accuracy of about 1–3 cm while the handheld GPS accuracy is around 1–2 m.

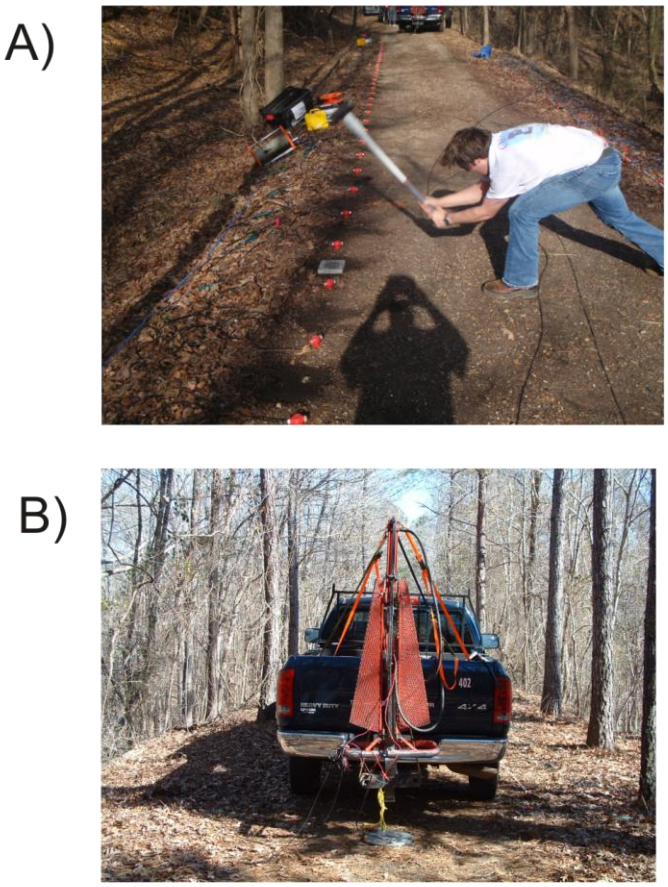

Figure 3-4 A) Swinging the hammer along tunnel 6 in Oxford, MS. The shotpoint locations are taken in-between each geophone. B) An accelerated weight drop; straps keep the weight drop vertical while in the hitch. The strike pad can be seen dragging underneath the truck.

3.3 OVERVIEW

The test sites in this study were in Douglas, AZ, and in Oxford, MS. The Oxford, MS, test site was used to test acquisition parameters and to understand some limitations seen in the field after processing the data. The Douglas, AZ, test site was the location of a known clandestine tunnel and

information gathered from Oxford, MS, made it possible to get very good and accurate data from the Douglas, AZ, site. The large amount of data collected was used to evaluate limitations and advantages of seismic and electrical methods in a search for subsurface voids. The equipment was from the University of Alberta and the surveys were performed through collaboration between the University of Alberta and the University of Mississippi.

CHAPTER 4
4.0 SYNTHETIC MODELING

4.1 INTRODUCTION

It is prudent to carry out some sensitivity testing for the responses that may be encountered prior to carrying out field tests. Here, modeling of both seismic and electrical responses of hypothetical voids was carried out to see how these responses were changed and to assist in finding clues to the interpretation of real (complex) data. Seismic modeling was accomplished using the program FDVEPS_MPI while electrical modeling used RES2SMODTM. A parallel 2-D viscoelastic finite difference seismic modeling program (FDVEPS) was used. Seismic modeling uses numerical computation to predict seismic wavefields based on an initial model, and imaging of how the waves are affected by subsurface features. RES2DMOD, a finite difference or finite element forward modeling program, was used to model subsurface resistivity. An apparent resistivity map, called the pseudosection, is estimated from a given model grid constructed by the resistivity structure of the subsurface. The expected section can give details about which type of resistivity array should be used in the field and how the anomaly may look in real data. The synthetic modeling results are estimates made before the real surveys are performed.

The goal of using synthetic modeling programs in geoelectrical studies is to best define the most efficient array to interpret the geology of the subsurface. RES2DMODTM is a forward modeling program used to test this using a finite difference/finite element technique which will estimate the apparent resistivity of the subsurface given a user defined model. The estimated model is based on known resistivity values; that is, it is a model of what is expected to be seen in the subsurface based on previous studies or rock physics models. In the near surface the 2D model will consist of sedimentary rock containing an air filled cavity. Differing observational electrode arrays applied such as Wenner and dipole-dipole will be applied to show what effect the air filled cavity will have on their responses. The array types are based on the work of Edwards (Edwards 1977) who describes some of the practical uses of multiple types of arrays. The results

are used as a guideline for data acquisition at the field sites; the estimated results help to resolve what type of survey spread is needed and which surveys may best work. The criteria used in this study are: depth of investigation, resolution, and practicality. More details about the theory of electrical methods can be found in chapter 5

4.2 ELECTRICAL METHODS

The goal of modeling was to look at the theoretical electrical response of a clandestine tunnel at the approximate depth that would be seen at the Douglas, AZ, test site. The model incorporates values (see Table 4-1) of resistivity and seismic compressional velocities that were found experimentally in laboratory and field measurements and reported in the literature. Velocity values used for seismic modeling later in the chapter are also listed in Table 4-1. The goal of the synthetic measurements was to see how the resistivity values in the subsurface change. An initial model is built to represent the underground tunnel and the surrounding material. Then a detailed description of the forward modeling program operations are given. The theory can be seen in detail in Loke (Loke 2002). When the initial model and theory have been described, the inversion results of the models will be interpreted and some of the conclusions will be used for data acquisition. This modeling was done before the field measurements at the Oxford, MS, test site.

Material	**Resistivity (Ω.m)**	**Seismic Velocity (m/s)**
Sandstone	50-1000	1450-1650
Shale's	5-100	2200-4000
Conglomerates	1000-10000	2000-6000
Fresh Water	5-100	1480
Brine	0.25-1	1530
Sands (unconsolidated)	600-10000	500-1000
Soil	5-25	180-450
Near surface rocks (average)	10-100	500-2000

Table 4-1: Rock resistivities (Palacky 1987) and seismic velocities (Marion et al. 1992).

.2.1 *INITIAL MODEL*

Using hypothetical geological models allows for a basic understanding of the technology that is being applied and how this may best be used to limit poor

data acquisition. The goal in the electrical modeling here was to assess what was the preferred geometry of the electrode array and to see what the limitations of the method would be. To do this, multiple models were created using RES2DMOD, a program used to first construct the 2D initial model, and from this forward model the apparent resistivity pseudosection from a given initial model. The different array geometries used can be tailored to detect different types of features in the subsurface. Loke discusses applications and pitfalls of the different arrays (Loke 2002).

Here, apparent resistivity pseudosections were calculated for both Wenner (Figure 4-2) and dipole-dipole (Figure 4-2) arrays; the reader is referred to chapter 5 for more details.

In geophysical studies, every tunnel site is different; and unique difficulties with near surface heterogeneity are encountered. However, in these models a homogeneous near surface was used in order to maximize the geophysical response of the tunnel and to avoid confusion with additional effects introduced by the heterogeneity of the earth. From experience, a value for the near surface of 25 Ω.m is representative of simple sandstone rock. Further, it was assumed that the subsurface was fully water saturated in order to eliminate any vertical resistivity gradients. One complication was the air filled void that for practical purposes would have an infinite resistivity. However, the modeling program does not allow for such numbers and a high unique value for air of 100000 Ω.m was used. A metal casing was also used in some of the modeling tests but the effects of high conductivity casings were otherwise ignored. The tests of high conductivity casing showed a low resistivity anomaly zone that was exaggerated in location and depth but was conclusive in detecting the anomaly. When a 0.5 m cement casing of 100 m was used there was no significant difference compared to a 2 m × 2 m air filled void.

Effects of casing on resistivity data are seen in chapter 5. The air filled cavity is a 2 m × 2 m square block 5.5 m from the ground surface. An electrode spacing of 1 m was used with 50 m spread length, this value was used due to the inversion giving results of up to about 10 m depth. The void

was centered in the middle of the spread in these models, this was to ignore any edge effects seen in the modeling.

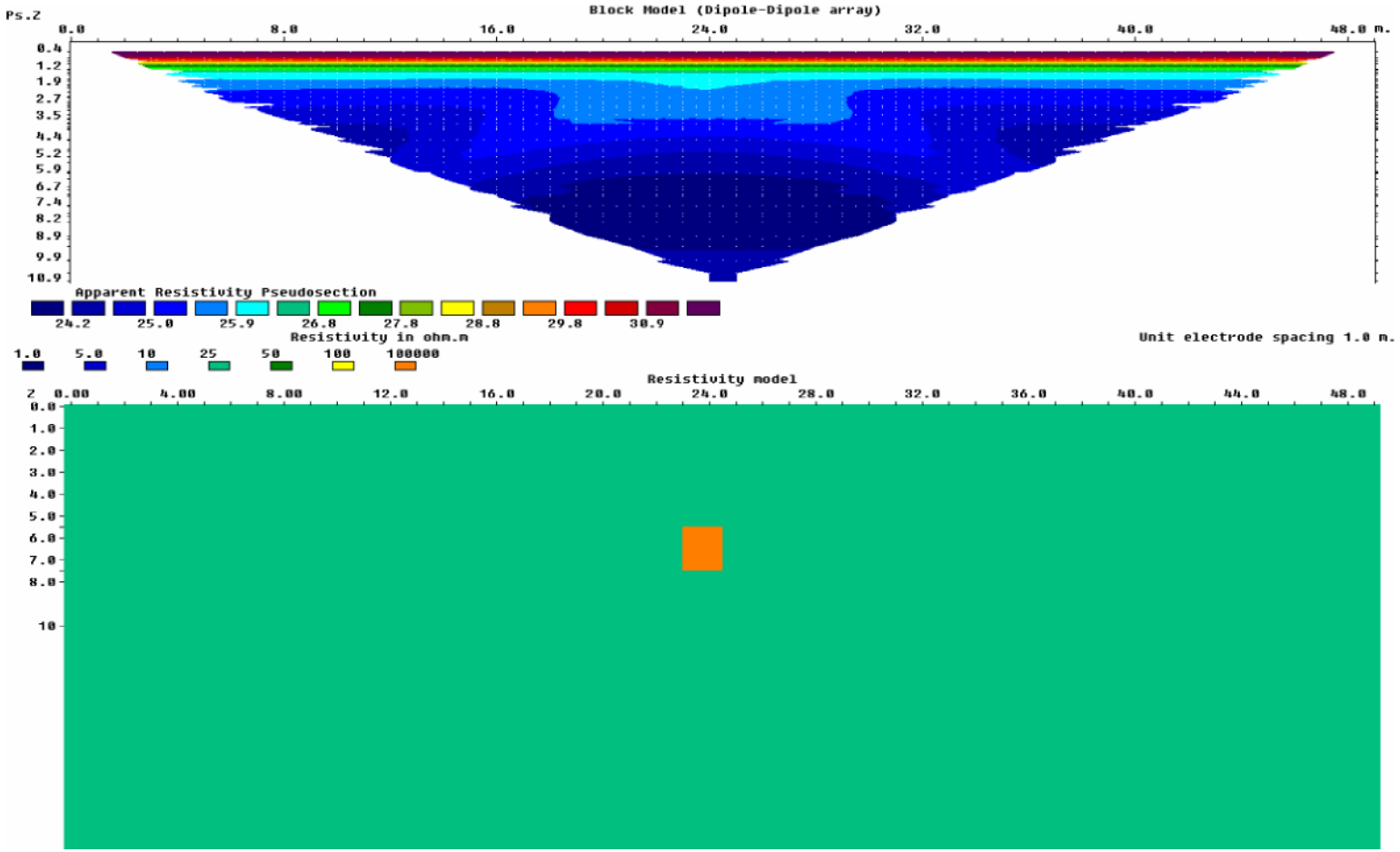

Figure 4-1 The initial model of an air filled void with a homogeneous subsurface using a dipole-dipole array. Top: the apparent resistivity pseudosection created from the model. Bottom: the initial model with a homogeneous subsurface at 25 Ω.m and an air filled cavity of 100000 Ω.m.

Once the initial model is built in RES2DMOD it is used as the inverse true apparent resistivity pseudosection; basically, it is the expected result. The program then forward models the electrical response using a finite element technique (Silvester and Ferrari 1990) that segments the resistivity structure into trapezoid blocks. The number of blocks controls the resolution and this depends on the mesh size. For the finer mesh a 0.25 m block size was used in the horizontal direction. The vertical direction starts with 0.25 m spacing and increases gradually each layer to 2 m at the bottom of the initial model. There is a maximum of 16 layers in the model and the highest sensitivity is near the surface. The model resolution can be seen in Figure 4-5 which displays where the highest resolution is for a given array. This follows what is seen in a resistivity array of real data, where there are more data in the near surface and less and less data as the depth increases. Overall, there were 16 layers in the vertical direction where the last layer had a mesh size equal to 2 m. Using finite element methods increases computing time but the inversions are still completed in less than 1 minute. The initial model then fits the resistivity value into each trapezoid block and is placed in a measured apparent resistivity model section. This model resembles the given field data once it is put into a pseudosection. The first geometry used was the dipole-dipole array; this can be seen in Figure 4-1. The model consists of just a homogeneous layer (light green) and an air filled void (orange) in the middle. A small resistivity change can be seen in Figure 4-1 around the location of the tunnel but it is only on the order of a few meters above the void near the surface. The array is seeing a slight perturbation due to the anomaly but it is doubtful this could be detected in a real situation when noise is included.

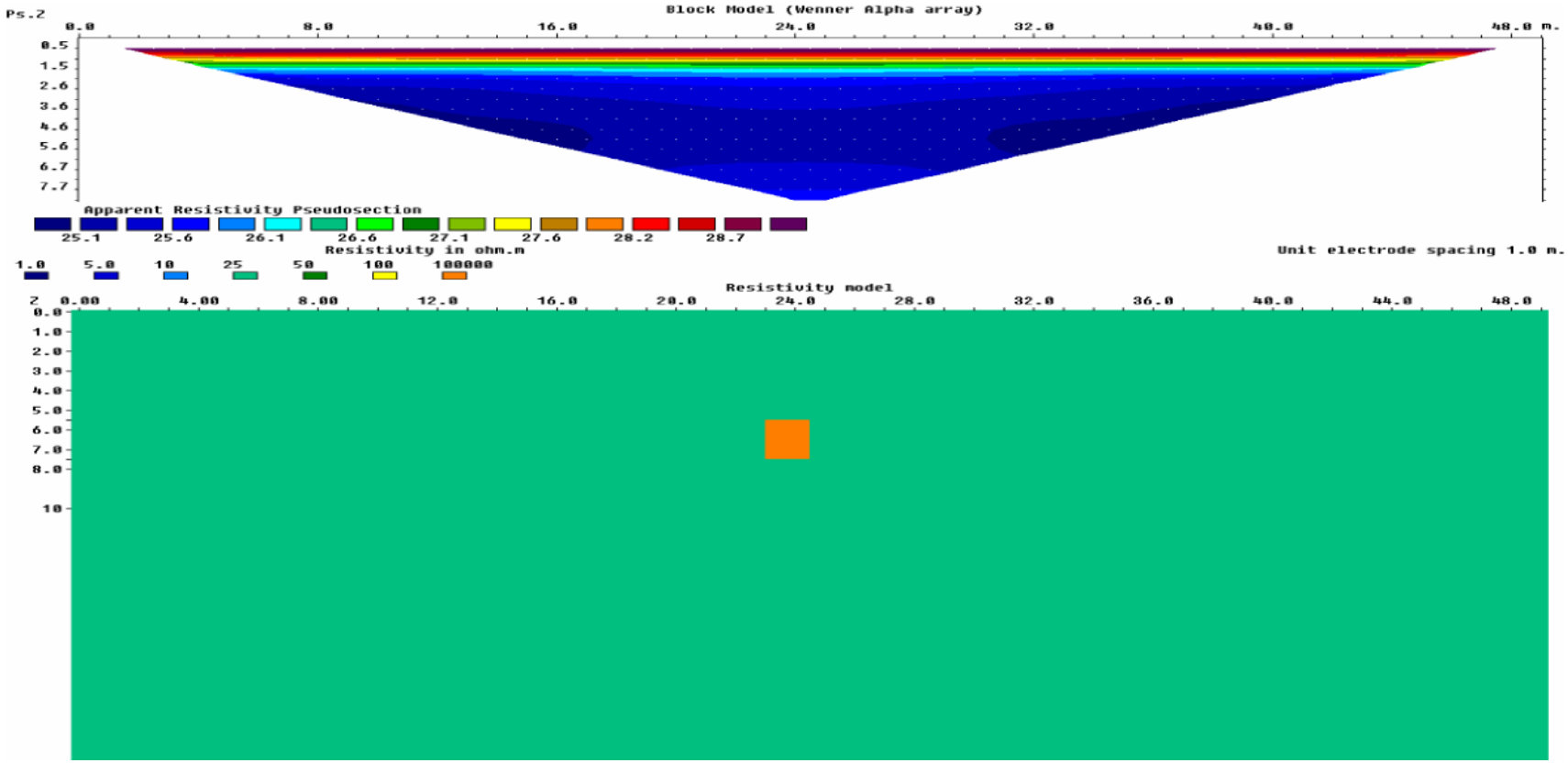

Figure 4-2 The initial model for an air filled void with a homogeneous subsurface using a Wenner array. Top: the apparent resistivity pseudosection created from the model. Bottom: the initial model where there is a homogeneous subsurface of 25 Ω~m and an air filled cavity of 100000 Ω.m.

The next model was the Wenner array seen in Figure 4-2; the model parameters are the same as in the dipole-dipole array but the geometry of the array is different. The Wenner array is sensitive to vertical changes of resistivity in the ground. More information about electrical methods is discussed in chapter 5, but for now the relative effects of the tunnel are considered. The main difference is that the apparent resistivity anomaly is even smoother. The anomaly is resolved even less than in the dipole-dipole array and there is a resistivity greater than 25 Ω.m around the surface; also, a slightly higher resistivity is diffused through most of the apparent resistivity pseudosection. The interpretation is that due to the large resistivity contrast and the small size, the forward modeling causes a large area to have a relatively higher resistivity but does not image the tunnel. Once the initial models are in a calculated resistivity form they can be used as the initial dataset for the inversion to invert the model.

4.2.2 MODELS

The initial models are forward modeled to obtain the apparent resistivity section and then these are used for the inversion program known as RES2DINV. The program and how it works is discussed in chapter 5. The inversion works by modeling a calculated resistivity section and comparing it to the input data that inverts the residual between the models to update the inverse resistivity modeled section. If the inversion process is perfect, the final section will reproduce the initial model. A finite element inversion using a fine mesh for the largest horizontal resolution was used. When imported into RES2DINV the data had 1 % Gaussian noise added to produce a somewhat practical dataset.

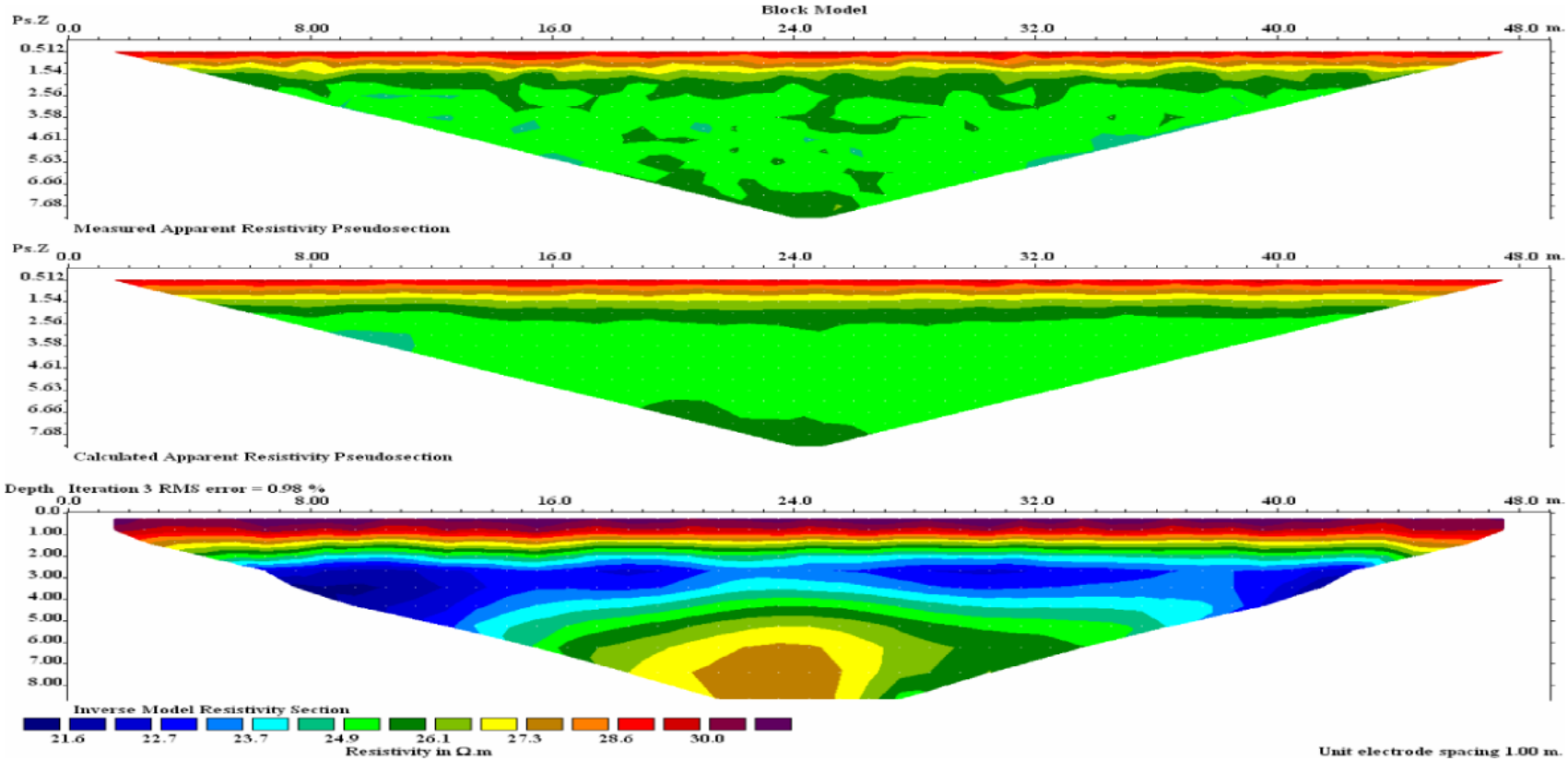

Figure 4-3 The Wenner array using the air filled void initial model with 392 data points. Top: the measured apparent resistivity pseudosection with 1% noise added. Middle: the calculated apparent resistivity pseudosection; this is the forward modeled result of the top picture for use in inversion. Bottom: the inverse model resistivity section; this is the inverted result showing different layers of resistivity but no clear indication of the tunnel.

The 1% noise added was found to be as much as the inversion could tolerate because the anomaly was so small that corresponding larger amounts of noise would overwhelm the response of the tunnel. Figure 4-3 shows the Wenner array inverted section; since the Wenner array is very good at resolving vertical changes in the subsurface it treats the tunnel anomaly as a smeared layer. As such, the inversion of the Wenner array results in a layer-like appearance with a conductive upper layer (blue) and a more resistive layer (yellow-brown) at the approximate location of the tunnel. The contrasts of the layers here are less than 5 Ωm. The inverted results produce a three layer model but do not show any horizontal features resembling a tunnel. The model converged after three iterations with only a 0.98% root mean squared (RMS) error.

The dipole-dipole array forward modeled apparent resistivity plot is shown in Figure 4-4 for the same case with the same 1% Gaussian noise added to it. The inverted section shows a localized zone with a $\sim$ 7 Ωm higher resistivity at the tunnel location. As seen with the Wenner array the inversion of the dipole-dipole geometry underestimates the resistivity of homogenous rock and the air filled void. The response of the tunnel is also smoothed out over a larger region, and thus expands the general location of the tunnel anomaly. The reason the dipole-dipole dataset looks so much noisier is that due to its survey design it obtains about 4–5 times the number of data points relative to the Wenner array.

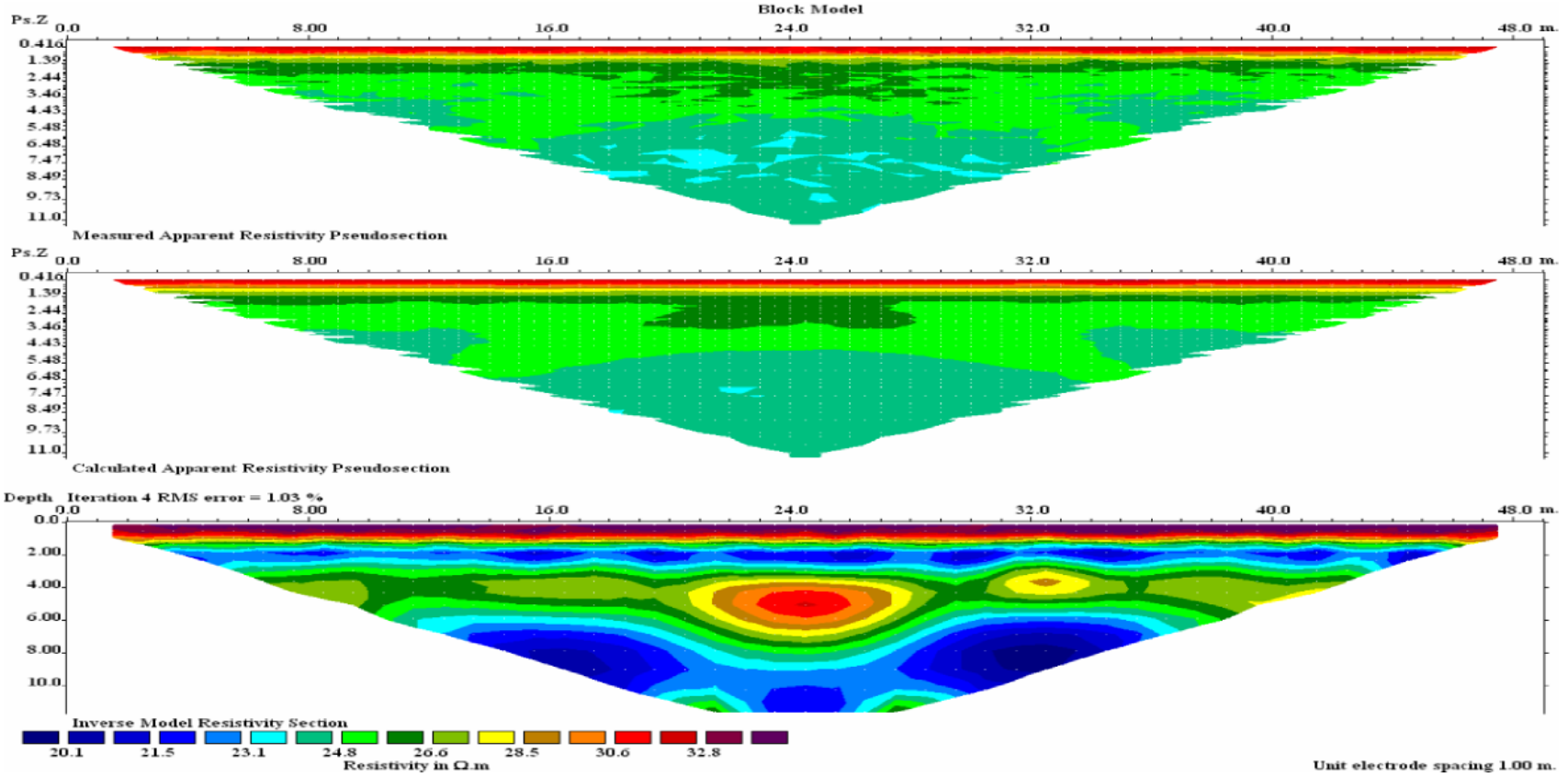

Figure 4-4 The dipole-dipole array using the air filled void initial model; there are1594 data points. Top: the measured apparent resistivity pseudosection with 1% noise added. Middle: the calculated apparent resistivity pseudosection. Bottom: the inverse model resistivity section; this is the inverted result; the result shows that the anomaly is a hot spot of around 32Ωm.

4.2.3 RESOLUTION

The electrical resistivity array gives a continuous spectrum of apparent resistivities through the subsurface. The actual depth of penetration and the resolution of the array depends on the electrode spread length and electrode spacing, respectively. In general the depth of penetration is approximately 1/4 of the array spread length. A qualitative estimate for the depth of penetration can be imaged using a sensitivity function that is the Frechet derivative of the array (Edwards 1977, Loke 2002). The sensitivity function is calculated by measuring the change in potential at the surface as it goes though small horizontal layers. The sensitivity is calculated for the entire subsurface and then can be plotted as a pseudosection to give a sensitivity map imaging the model resolution. The sensitivity of the Wenner and the dipole-dipole arrays can be seen in Figure 4-5. Both models have their highest resolution near the surface but behave differently around the tunnel. The sensitivity function is normalized so the larger the value the larger the effect to influence the resistivity value of that model block. This is the reason why there is a smooth result and not a perfect inverted section (Loke 2002). Both Wenner and dipole-dipole arrays show the tunnel having little influence on the model. The dipole-dipole array has stronger influence around the tunnel, that may be why the dipole-dipole array images the tunnel anomaly slightly better than the Wenner array.

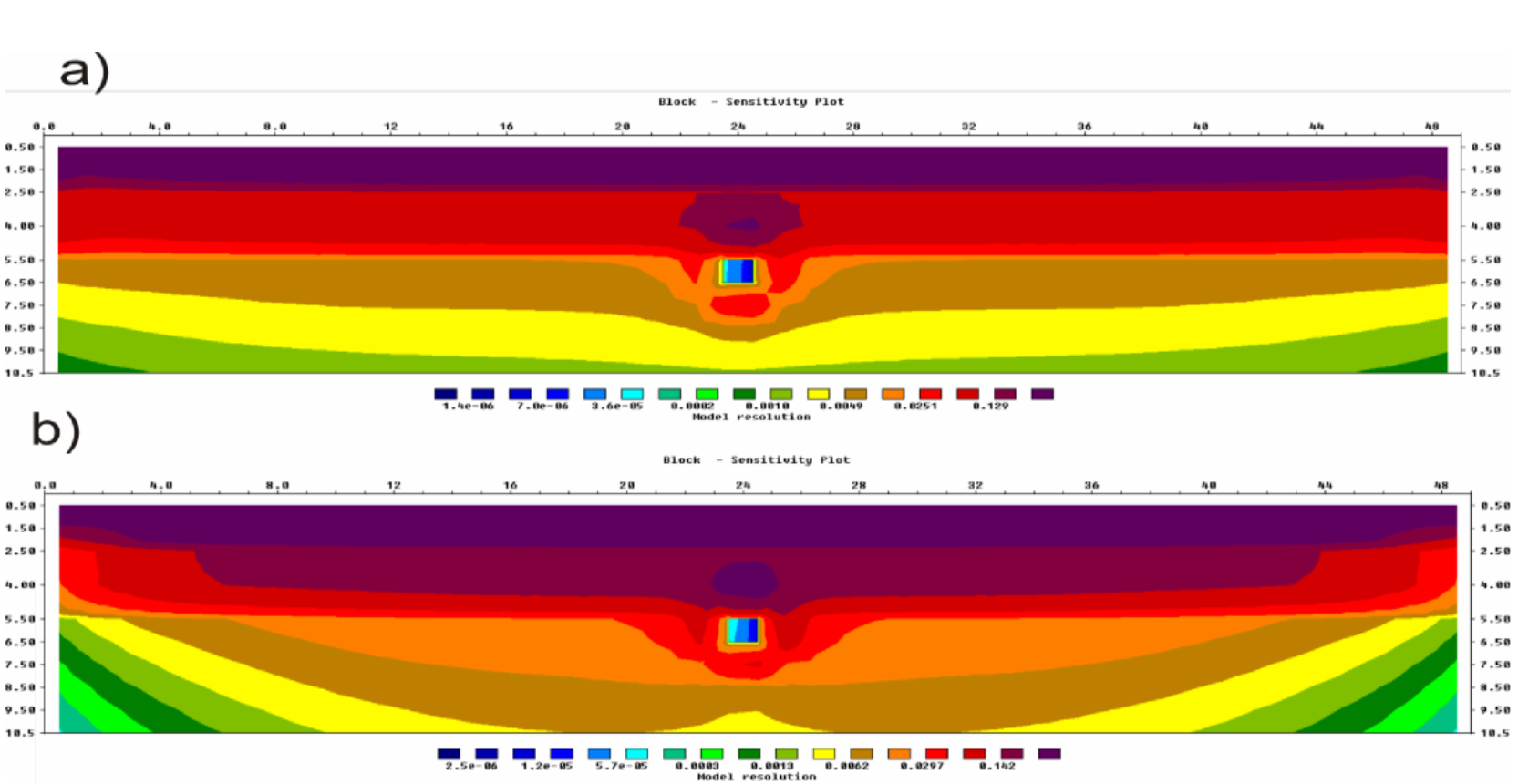

Figure 4-5. Sensitivity plots of the initial model displaying where the pseudosection has the highest model resolution—the darker the color the greater the model resolution. (a) the Wenner array; the highest resolution is above the tunnel location (b) the dipole-dipole array sensitivity plot; the highest resolution is around the tunnel and near the surface.

4.2.4 DISCUSSION

The use of synthetic modeling helps decide what type of electrical array should be used in the field, by looking at the practicality, cost, and depth of investigation. The models that were chosen to be used for modeling were the dipole-dipole array which is sensitive to horizontal changes in the subsurface, and the Wenner array which is sensitive to vertical changes in the subsurface. The goal was to see how these models could be used and to evaluate the limitations of each model in regard to the detection of tunnels.

The Wenner array smoothed the tunnel resistivity laterally across the entire spread and could not properly detect the tunnel. The Wenner inversion is quickly computed. Although the Wenner array was not successful in detecting a tunnel that crosses the array profile perpendicularly, it could be useful in cases where the tunnel runs at a small angle or parallel to the array profile.

The dipole-dipole array was also tested. What was found was that inversion of the dipole-dipole array allowed for detection of an anomaly coincident with the tunnel but it did not "resolve" the tunnel dimensions. Instead, the tunnel's high resistivity was smeared over a large area. A small disadvantage of the dipole-dipole geometry is that more data points are obtained and this requires an increase in computational time over the Wenner array by about a factor of 10. At most this represents a few minutes of time on a ca. 2005 computer.

The results of the modeling indicated that the dipole-dipole geometry should be used in preference to the Wenner array. A decision was also made that if the tunnel was sufficiently small the electrode spacing would be reduced to enhance the lateral resolution (but at the cost of the overall coverage). The rule of thumb obtained from the experience is that for reasonably conductive (50 Ω.m) material the depth of penetration is about 1/5 of the surface spread length. This means, for example, that the 50 electrode spread at 1 m electrode spacing would reasonably sense to 10 m of depth.

Overall, this modeling study suggests that tunnels can be detected using ERT techniques, but their small size does not allow for true resolution of the void. Practitioners would instead look for anomalously high (for air filled voids) "bulls-eye" type resistivity anomalies.

4.3 SEISMIC MODELING

The goal in modeling the seismic response differs slightly from the goal in modelling the ERT. The goal in electrical modeling is to assess whether the tunnel can be detected at all and, if so, what technique is most appropriate. In the seismic studies, the tunnel dimensions will be smaller than or on the same order as the interrogating seismic wavelengths; and hence before we start we realize the tunnel cannot be directly imaged. Instead, the goal is to determine the degree to which the wavefield will be disturbed and how this disruption might be used in tunnel detection.

How different seismic waves are affected by a subsurface tunnel is investigated in detail in this chapter. A discussion of the theory of different seismic waves is discussed in more detail in chapter 6. The finite difference algorithm used is FDVEPS which is a parallel 2-D elastic/viscoelastic finite difference seismic modeling algorithm freely available to the academic community (Bohlen 2002). Below, in advance of presenting the modeling itself, a brief and basic introduction to the theory of finite difference calculations is given. This is followed by a description of the model and what was involved in this project. Some examples of the modeling are shown to see the effects of the tunnel on the seismic wave field.

4.3.1 THEORY

Finite difference modeling is in principle a method to give an analytical solution of the wave equation for an elastic wave. The reason forward modeling is used is to understand the effects of complex media in the subsurface. The goal is to see if modeling the wavefield through a tunnel location

causes a distortion in the seismic wave field. To do this the theory behind the method is discussed so the reader will understand the parameters and why they were chosen for the modeling.

Finite difference (FD) calculations have been widely used to model wave propagation in the subsurface in both 2-D and 3-D elastic mediums. Finite difference methods are popular because researchers are able to construct complex heterogeneous subsurface geological structures in terms of their seismic velocity and density. FD methods have been used to model complex tunnels to assist their construction (Jetschny, Bohlen and De Nil 2010) to determine what their effects on the seismic wavefield as measured at the surface might be (Kneib and Leykam 2004). The FD method used here is referred to as a "formulated fourth-ordered staggered grid finite difference system" (Levander 1988, Virieux 1986); it is based on first-order coupled elastic equations using seismic velocities and stresses as variables. Using finite difference to solve for stresses and velocities was developed to calculate synthetic seismograms for 2D elastic geometries; as a result they cannot incorporate seismic anelasticity. This was later developed by (Robertsson, Blanch and Symes 1994) who replaced the elastic model with a viscoelastic rheology described by a generalized standard linear solid (GSLS) following the work of Korn (Korn 1987). The new method which is used here is a viscoelastic staggered grid modeling program that can include both attenuation and seismic wave dispersion (Bohlen 2002).

The viscoelastic wave equation is a good way to model the subsurface but the main drawback is that the computational resources used for such FD methods can be quite intensive. Each of the calculated test shots shown require approximately 24 hours to run using a cluster of 6 processors (ca. 2002). To do this the model is split up into multiple parts and the parts are run in a parallel environment.

We avoid a discussion of the mechanics of the FD solution and the reader is directed to Bohlen and Robertsson et al. (Bohlen 2002, Robertsson et al. 1994) for the details. What is more important here is to present some practical

limitations and important considerations in using the modeling to assist in tunnel detection. The FD method solves for the seismic wavefield at every time location in the total seismogram and is a sum of all of the individual time steps. The propagation of each time step is saved as the seismic wave goes through the ground. The tunnel affects the wavefield if the time steps are small enough that the wavefield should be able to resolve the small lateral changes in the subsurface. To do this some considerations need to be taken into account; the first is discretization or how the subsurface is gridded. Second, FD methods can cause issues with numerical dispersion, where we look at how small the units of time sampling need to be in order to sample the wave field. The final consideration is the stability and how we handle the edge of the modeled data using boundary conditions.

The order of the FD determines how the wave field is calculated, the higher the order the more the model is broken down with partial derivatives and the better the solution should be. However, this comes at the expense of increased computing (i.e., time). The 4th ordered FD method provided acceptable results, and calculations at higher orders did not noticeably change the output, while the end product from the 2nd order calculations appeared substantially smoother. Discretization is the process of gridding data from a continuous spectrum into continuous blocks. The main errors occurring in finite difference methods come from discretization, from rounding errors, and from truncation errors. Since the finite difference method is in the form of a Taylor expansion, the terms above the order are removed and thus there will be truncation error. The analytical solution of a wavefield is technically an infinite order Taylor expansion of increasing orders of partial differential equations. The higher orders of derivation show more detail of the higher frequencies sampled. Generally only a few orders are needed to sample the wavefield but the truncation of the higher orders causes truncation errors. Rounding errors come from the computer cutting off the decimal of the solved quantities of the wave equation. These errors can cause small changes in the sampled wavefield but are generally quite small.

Conversely, problems with numerical stability and dispersion arise when the time steps are too long such that the proper wavefield cannot be resolved. In the program FDVEPS with 4th ordered operations, the guidelines suggest that numerical dispersion is avoided when

$$DH \leq \frac{V_{s_{min}}}{2f_c N}, \tag{4.1}$$

where DH is the grid size and $\frac{V_{s_{min}}}{2f_c}$ is the smallest wavelength propagating though the model, and where $V_{s_{min}}$ is the smallest shear wave velocity in the model and is the central frequency. Another consideration comes from sampling theory in that a minimum number of 8 grid points per the minimum wavelength that will be detected are also needed to avoid numerical dispersion. Hence, stability requires sufficiently short time stepping and spatial node sampling. A rule of thumb stability criterion for a 4th ordered staggered grid is

$$DT \leq \frac{6DH}{7\sqrt{Dv_{p_{max}}}}, \tag{4.2}$$

where DT is the time sampling and DH is the horizontal gridding, D is the dimension of the model, for all the cases that are 2D, and $v_{p_{max}}$ is the maximum compressional velocity in the model. The program will not run unless the stability and dispersion issues are already met and so it avoids making the mistake of an erroneous calculation from the perspective of numerical dispersions, but they limit some of the parameters for the modeling, such as extremely different velocities. This can be problematic when there is an air filled void. There will be some form of numerical dispersion but the error should be quite limited if the time stepping is low enough.

The boundary conditions applied to the geological model are the final consideration that must be taken into account. There are two types: a free surface boundary (at the top) and the side boundaries. The top surface of the model is presumed to be exposed for the purpose of treating it like a vacuum so its motion will not be restricted and it will be subject to no normal stresses

(equivalently, one can allow the "material" above the free boundary to have zero wave speed) (Levander 1988) (Robertsson 1996). A similar boundary condition is often applied to the bottom surface of the model. The side boundaries are more complicated as they must present some kind of dissipative surface that can attenuate or absorb the seismic energy incident upon them. This is often done by multiplying by a weighting function to both the stress and velocity field using a value less than 1 (Cerjan et al. 1985). The goal of this is to dissipate all the seismic energy that hits the side in order to reduce side reflections from propagating back into the model. Of course these side reflections will not exist in the real earth which can be considered for all effective purposes as a laterally infinite medium.

4.3.2 GEOLOGICAL MODEL

The geometry that is used in the synthetic modeling is given in Figure 4-6, note that the dimensions of the geological model (constructed in terms of the seismic velocities) is substantially larger than the area of interest where the responses are to be found. In the model the total length L of the survey detectors is 120 m, a length larger than but comparable to that used in the field. The distance X is the distance to the tunnel from edge of the model, T is the thickness of the tunnel casing, and W is the tunnel width. These are varied during the modeling to assess the effects of size and depth on the observed wavefield. The width of the absorbing boundary changes for some surveys but generally it is 20 m. The initial model also needs the density, Q factor for shear and compressional components, the compressional wave velocity and its shear velocity.

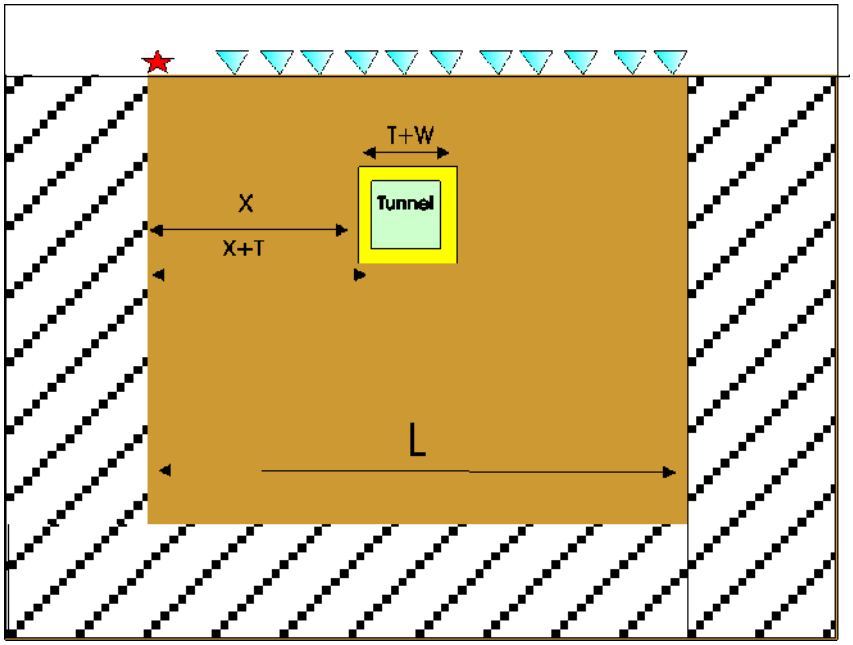

Figure 4-6 The subsurface model for seismic modeling. The subsurface (brown) has a velocity of 1000 m/s, the velocity of the concrete casing (yellow) is 2000 m/s, and the tunnel (green) has a compressional velocity of 343 m/s.

The initial model generated was to be similar to Oxford tunnel 1. The information that was known at the time was that the tunnel was approximately 10 m deep and was constructed through a geological formation consisting of partly consolidated sands with lesser amounts of shale. The presumed material properties are given in Table 4-2.

Material	**Vp (m/s)**	**Vs (m/s)**	**Density (kg/m³)**	**Qp**	**Qs**
Surrounding rock	1500	750	2000	100	100
Tunnel casing	2000	1000	2000	100	100
Void	343	1E-6	2000	100	100

Table 4-2 Parameters for the synthetic site of tunnel 1; the values for Q and density remain the same as there was no attenuation in this test.

4.3.3 SEISMIC MODELS

One processor was used for both the y and x directions in the synthetic models that were derived here. The FD mesh typically had 400 and 250 grid points in the x and y directions, respectively, and was sampled at 0.01 s (10 ms). The calculations proceeded long enough to produce a 0.250 s trace record. A symmetric 50 Hz Ricker wavelet, which is the second derivative of the Gaussian function, was used as representative of the seismic pulse used. This was the default parameter and was similar to what was seen in some sample test shots. The source duration was 0.002 s (2 ms) and thus resembled an instantaneous explosive force. The source signal had the energy needed to propagate downward, similar to that of a hammer swing. The absorbing boundary was 20 m wide; both particle velocities and stresses decayed by 95% over this boundary (Cerjan et al. 1985). The receiver array was 120m long with the receivers spaced 1 m apart and buried at 10 cm from the free surface. The depth of 10 cm must be used because with the receivers at the free surface the energy would be zero and we would see nothing. The attenuation for this array follows an approximation based on the GSLS factor, and with a simple case where we assume that there is only 1 relaxation frequency, we have

$$Q \approx \frac{2}{\tau}, \qquad (4.3)$$

where Q is the seismic quality factor which is related inversely to the attenuation for a rock; τ is the stress relation time which is dimensionless. What this means is that we can give τ a value of 0.02 to give Q an approximation of 100. More information on empirical values of the seismic quality factors for different rocks can be seen in O'Connell and Budiansky (O'Connell and Budiansky 1978). We used these parameters at the synthetic test site in Douglas, AZ. More synthetic examples were calculated and are discussed but will not be shown.

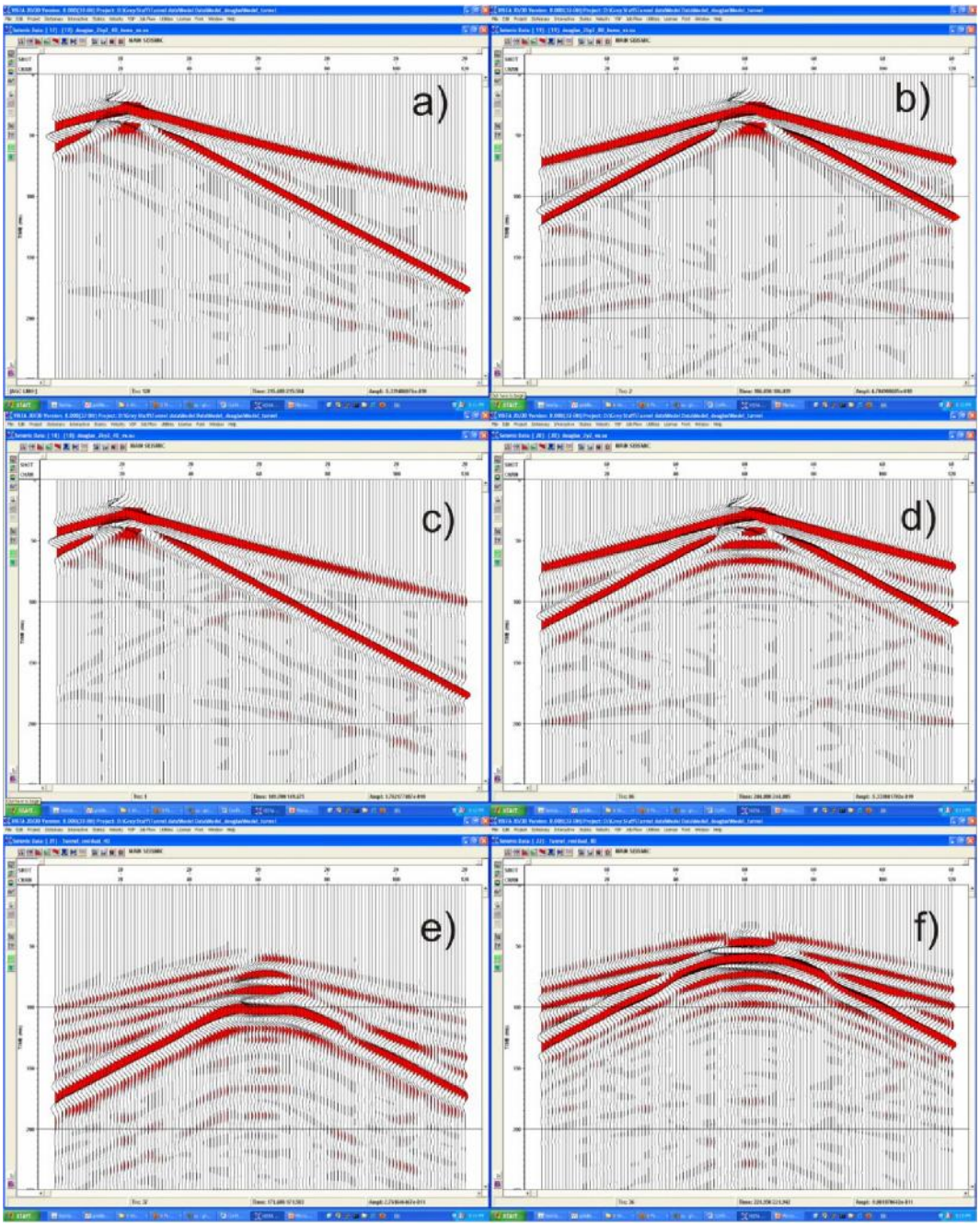

Figure 4-7 Examples of calculated shot gathers over the Oxford, AZ, tunnel 1 model. Shot gathers over a homogenous layer with no tunnel for (a) a shot point to the left of the model 40 m+ from the center of the tunnel and (b) a shot point at the centre of the model. Similar shot gathers for a model containing in its centre a 2 m × 2 m tunnel at 9 m depth for (c) a shot point 40 m left of the tunnel and (d) a shot point centered over the tunnel. Differences between the homogeneous model and tunnel model were subtracted (e) shot gathers (c)-(a) giving the residual, (f) is the residual (d)-(b). Panels (e) and (f) highlight the perturbations of the seismic wavefield introduced by the tunnel.

Figure 4-7 shows the synthetic results for the Oxford, MS, tunnel 1 test site. The calculations for the two models differ only in that those on the right are calculated in the same velocity structure as those on the left but they contain the 2 × 2 m tunnel. Both near and a far offset shot gathers were modeled to see if being closer to the tunnel and closer to being perpendicular had any effect.

Despite the application of the absorbing boundary conditions, the side boundary reflections were not completely eliminated as shown in Figure 4-7. This was one of the constraints imposed by the models; making the models wider such that the side reflections would arrive much later would increase the computational time so much that the modeling would not have been possible with the computational resources available. The side boundary reflections add noise, but taking the simple difference between the homogeneous model and the model with the tunnel (Figure 4-7e and 4-7f) yields the wave effects of the tunnel itself. As two hyperbolic waves are displayed in the residuals, there are multiples. These multiples are caused by the constant reflections going back from the surface to the tunnel creating more than 1 anomaly. The true anomaly is the first one. There is also some aliasing in the waves around where there are two sets of hyperbolic waves; this is due to wave overlap of the two different diffractions with different velocities; in this situation both diffractions are present for a certain time before the seismic wavefield detects their presence.

As will be seen later, seismic refraction tomography (SRT) uses the travel times of the refracted waves as input. These are the first arrivals in the shot gathers shown in Figure 4-7 (a)–(d) and they follow a linear "moveout" from the source. Unfortunately, for the tunnel 1 model, there is no noticeable change in this arrival and as such the tunnel cannot be detected as it is too deep to properly influence the waves using just the direct arrival. In the real world there would also be the situation of multiple layers causing the seismic wave to refract and change speeds in more than one area of the model. When the test was done with a 5 × 5 m tunnel the direct arrival did change and caused the direct wave to move significantly. The other problem that is not shown is that we

didn't forward model the ray coverage map which can also be used as an indicator for the tunnel

Of more interest to tunnel detection, perhaps, is the diffractions produced by the tunnel, these are the only anomalous arrivals between, say, Figure 4-7b and Figure 4-7d. In Figure 4-7c we have the same model except with a tunnel in (Figure 4-7d) with both the first arrival wave and the surface wave; but also a two diffractions that were seen in the residual. By fitting a hyperbolic curve to the seismogram by relating the travel time to the offset of the seismic wave, the velocity can be calculated by fitting a hyperbolic curve. This can be seen in Figure 4-8. These velocities are 1500 m/s and 1000 m/s. The first diffraction of 1500 m/s resembles the diffraction of a P-wave, and 1000m/s is the value of a P-SV wave diffraction. This happens because the wave field hits the tunnel and reflects both the P-wave and a shear component that is detected at the surface. The reason this is significant is that the wave comes in at speeds less similar to the surface wave and will most likely be detected in real data.

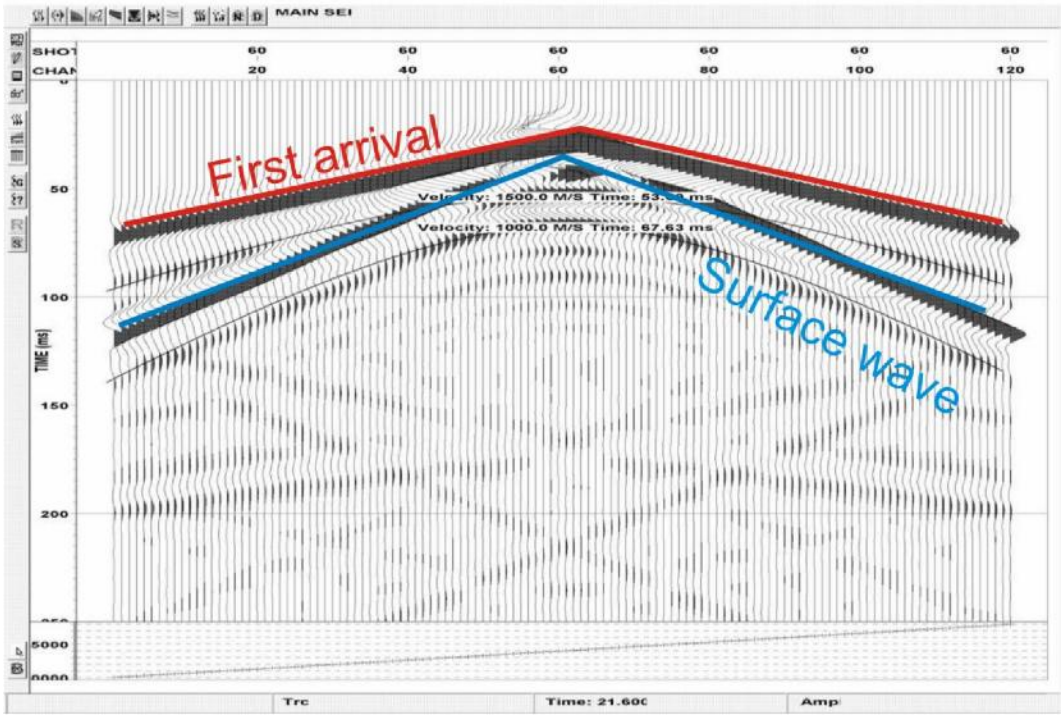

Figure 4-8 The same data set as depicted in Figure 4-7; data are collected directly over the tunnel site with two types of diffraction present. There are two that are highlighted: the first is 1500 m/s and the second is 1000 m/s. These diffractions resemble P-wave and P-SV wave diffractions, respectively. The diffractions occur when the compressional wave approaches the tunnel, hits it, then both a primary wave is reflected back and a SV wave is reflected back. These phenomena are discussed in chapter 7.

4.3.4 DISCUSSION

The calculated shot gathers illustrate that using the homogenous velocity model with a tunnel does not allow a tunnel to be detected easily by the first seismic arrivals. The tunnel did not significantly influence the first arriving waves until it reached 5 × 5 m. .Conversely, the modeling shows that diffracted wave arrivals appear centered at the approximate locations of the tunnels and that both a P and an P-SV diffractions are produced. The data are used as a prerequisite for the work at Oxford, MS, and Douglas, AZ, and are used for some of the data acquisition parameters. The synthetic data assumes a viscoelastic surface with no changes in compressional and shear wave attenuation and distortion. No anisotropy is assumed since there is not enough information before data acquisition at the field sites. The seismic modeling showed that there is little to no change in the first arrival wave field; conversely, seismic refraction methods have been used to detect small scale tunnel features (Hickey and Howard 2006). Hickey and Howard reported detecting a tunnel through the presence of a small metal pipe that carried water though the tunnel; degradation around the metal pipe made it possible to detect the tunnel.

4.4 CONCLUSION

It is useful to carry out full elastic wavefield modeling before data acquisition to get an idea of the proper parameters for a given target site. The modeling shown here was done prior to the acquisition of data in Oxford, MS, and was used as a data acquisition aid. The results show that for electrical methods using a dipole-dipole array a tunnel can be sensed. Seismic methods cause some of the energy to be diffracted back toward the surface indicating the tunnel is a diffractor point source. The main thing that was not considered in the seismic methods was noise and a more realistic and heterogeneous

subsurface. Similarly, in the electrical methods some Gaussian noise was added but no near surface heterogeneity was added.

CHAPTER 5
5.0 ELECTRICAL RESISTIVITY TOMOGRAPHY

In this chapter a brief introduction to a geophysical technique known as electrical resistivity tomography (ERT) is described followed by the theory and methods of common applications of geoelectrical methods such as Wenner and dipole-dipole arrays. Following this the data collected from Oxford, MS, and Douglas, AZ, is presented to show what can be learned through imaging subsurface voids. Methods of enhancing the techniques used in tunnel detection are considered.

5.1 INTRODUCTION

The goal of any geophysical method is to understand the structure of the subsurface and try to calculate some physical property that can be related to the actual properties of the rocks. In geoelectrical methods this is done by injecting current into the ground from one surface electrode and measuring the potential at another. The current and potential can give you an idea of the resistivity of the subsurface which can be related to subsurface materials. Electrical resistivity is a unit of measure of the degree to which a material opposes the flow of current be it electronic or, particularly in the earth, ionic conduction. By comparing the apparent resistivity values of common material to the resistivity of rock, we can elucidate the dominant rock properties of the zone we are measuring. This comparison was first started in the 1960s by comparing 1D sounding curves to analytical sounding curves from empirical data (Keller and Frischknecht 1966). Electrical methods advanced further with the invention of

high speed computers and the idea of combining tomography methods and electrical sounding curves started the technique known as electrical resistivity tomography (ERT). This method was first developed in the laboratory, measuring core using electrical tomography to compare water transport

through a rock sample (Daily, Lin and Buscheck 1987). The idea was expanded to surface data acquisition using an automated switch and multiplexer for faster deployment and was used for monitoring a steam injection site (Ramirez et al. 1993). Daily et al. and Loke provide more information on the history of electrical resistivity (Daily et al. 2005) (Loke 2002). Loke's algorithms are widely used in near surface geophysical studies.

In vadose zones there are generally three types of conduction occurring that change the resistivity of rocks quite drastically; that is why there is a wide range of resistivity in rock. The most difficult aspect of classifying an electrical (or any geophysical anomaly) in the near surface is to understand its geological history and to know if there has been any earlier disruptive urban construction in the region. If the history of the site is not well known, a common problem in urban environments, data must be carefully interpreted. Even if the history is known, how the subsurface void was created must be taken into account.

After the methodology and theory are in place, the ERT data collected from Oxford, MS, and Douglas, AZ, are presented. Not all the data collected are presented as the volume of data collected in Oxford, MS, is too high. Important surveys that definitively show that a tunnel was found and, for the sake of comparison, some of the situations where the tunnel was not detected are shown.

5.2 THEORY

In the following section there is a discussion of basic resistivity theory and the processes by which electrons or ions move through materials are considered. Understanding these basic processes leads to a discussion of the ERT method and the electrical survey designs used for tunnel detection. This is followed by a description of how electrical data is formatted to forward model problems and how the data are inverted to get a pseudosection of the subsurface

5.2.1 BASIC RESISTIVITY THEORY

Ohm's law relates an applied electric field to the displacement of charged particles creating a electric current density with field $\vec{E}$ to the displacement of charged particles creating a electric current density $\vec{J}$ with:

$$\vec{J} = \frac{1}{\rho}\vec{E}, \tag{5.1}$$

where the resistivity ρ defines how the material opposes the flow of electrons. An electric field applied to any material spreads out evenly over three dimensional space and the intensity decreases with distance from the source. Resistivity is in units of ohm-meters and the geometry of an object influences its resistance; assuming homogeneous material, the resistivity is a function of the resistance R, the cross sectional area of the material A, and the Length L.

$$R = \rho\frac{L}{A}. \tag{5.2}$$

In a porous rock which is not homogeneous, we can assume a similar relationship, but instead of length the tortuosity τ of the material is used. Tortuosity can be calculated by comparing the length L of the travel path of the charge carried through a material to the straight length C through the material.

$$\tau = \frac{L}{C}. \tag{5.3}$$

The L path depends on numerous factors such as the material porosity and the pore geometry. Although recent modeling of microscopic structures has shown promise toward the calculation of porous media resistivity, describing L can be difficult. As a result L is usually empirically reported using Archie's Law.

The key assumption made is that the electrical current will always travel through the path of least resistance. In the vadose zone (the region between the water table and the ground surface), the material is generally partially saturated unconsolidated material which implies high porosity and a

mixture of air and water in rock pores. The electrical resistivity of water has a large difference ranging from 0.5 Ω.m (brine saturated water) to 100 Ω.m (fresh water) (Palacky 1987), while air which for practical purposes is an insulator has a resistivity of nearly 10^9 Ω.m. Near surface rocks also have a fairly low resistance in the range of 10–100 Ω.m this depends on the clay content and water saturation levels. With these resistivity values one can assume that the subsurface void being pursued will be a highly resistive feature unless it is filled with brine saturated water. This has been seen in the location of subsurface voids in the past (van Schoor 2002), where highly resistive zones were interpreted as subsurface cavities.

Electrical current moves through a rock via either electronic or ionic conduction.

Electronic conduction is the means by which metals conduct electricity; the basis is due to movement of electrons from partially filled electron bands to higher conduction bands of energy. This process creates a drift velocity for the electric field through the electron band. This causes fast movement of electric current through a metal and thus makes it a very good electric conductor. In insulators there are no available bands for the electrons to go so no drift velocity is created between the bands. Electronic conduction is relatively rare in earth materials except for some base metal ores and graphite deposits.

Ionic conduction is predominant in most sedimentary and near surface rocks. The ions (e.g., Na^+, Cl^-) are displaced through the pore fluid solution or along a clay mineral surface by the applied electric field and create a diffusional flux resulting in a transport of ions through the material. In general, water is not very conductive, but as soon as there are any salts present the complete dissociation of salts in water creates an easy path for the

electric current. It is well known that even a small amount of salts causes water to be ionically conductive (Palacky 1987). More information about

how electric current can move through rocks can be found in the literature cited (Knight and Endres 2005), (Telford et al. 1990).

5.2.2 METHOD:

As described above we can relate ohm's law to how an electric field moves from a point source in a three dimensional fashion. The potential for one electrode array is given below, where V is the potential, ρ is the resistivity of the subsurface, and r is the distance from any point in the ground to the electrode. To measure the potential of the subsurface, a current is injected into the subsurface and is evenly distributed throughout the ground, dissipating in energy the farther it gets from the source. The potential created by the injected current is measured at a given electrode.

$$V = \frac{\rho I}{2\pi r}, \tag{5.4}$$

Instead of gathering a direct potential measurement, most surveys gather the potential difference between two electrodes to give information about the apparent resistivity at a given point between them. To do this a 4 electrode system is used with two potential electrodes across which the voltage is measured and two current electrodes across which an input current is applied. This can be seen in Figure 5-1 where C1 and C2 are the current electrodes and P1 and P2 are the potential electrodes. Detailed information about how the equations are set up can be found in Loke (Loke 2002), but for this geometry, the current is injected into the subsurface from the current electrodes. The current travels though the ground and the potential difference between the electrodes is measured from the injected current.

$$\Delta V = \frac{\rho I}{2\pi}\left(\frac{1}{r_{C1P1}} - \frac{1}{r_{C2P1}} - \frac{1}{r_{C1P2}} + \frac{1}{r_{C2P2}}\right), \tag{5.5}$$

Where ΔV is the potential difference between the potential electrodes and the difference between the points is related between each electrode and described by the various r. This is generally further simplified so we can calculate the apparent

resistivity ρ_a and also use a new variable known as the geometric factor. The geometric factor k combines the difference in radius from current and the difference in radius from the potential electrodes and a 2π. This changes for different survey spreads but then the calculation of apparent resistivity is the same for all surveys with

$$\rho_a = k\frac{\Delta V}{I} \qquad \text{where,} \qquad k = \frac{2\pi}{\left(\frac{1}{r_{C1P1}} - \frac{1}{r_{C2P1}} - \frac{1}{r_{C1P2}} + \frac{1}{r_{C2P2}}\right)}, \tag{5.6}$$

The main thing that has to be remembered is that since we use a potential difference between the electrodes we then only have an apparent resistivity unless the earth is completely homogeneous (a rather uninteresting hypothetical situation). To obtain the true resistivity structure, numerous observations of V must be made for a large variety of differing geometries and the apparent resistivities must be inverted (Loke 2002).

The resolution of the survey required (horizontally and vertically) and data collection configuration depend on the type of electrode array used and the kind of survey carried out. Three main types of resistivity measurement geometries are employed in near surface investigations:

1) Sounding surveys (1D)
2) Imaging surveys (2D or 3D)
3) Borehole surveys

Borehole arrays gather information about the resistivity between the surface and a borehole or between two boreholes. In general, the use of a borehole survey for tunnel detection is not feasible unless the borehole is in the immediate vicinity of the tunnel. Hence, covering a large area is not feasible at an early stage in the hunt for the tunnel.

Sounding arrays are 1D depth soundings that produce a single apparent resistivity versus depth curve centered at the midpoint of the current and potential electrode. The data collected are all situated around a common point and

the electrodes are symmetrically placed away from the centre of the spread in order to give data directly underneath the middle of the spread. Such types of soundings have long been employed. This was the first type of technique used and even though it gives good vertical resolution it provides no information on lateral heterogeneities (Koefoed 1979). The 1D surveys require only 4 electrodes: 2 current and 2 potential that are moved separately for each station for each measurement. The depth of penetration depends on the electrode separation. As the electrodes are moved farther apart the depth of investigation increases, although more current must be injected into the ground in order that a sufficient voltage is recorded across the potential electrodes.

Similar to this method there are also induced polarization (IP) and spectral induced polarization (SIP) resistivity surveys which use alternating current. These methods are useful for detecting conductive materials but in general require a large amount of current.

2D imaging. surveys build on the 1D approach and were first introduced in order to obtain information on lateral variations of electrical resistivity. Such systems only came about with advances in digital data collection and instrument control as, to be practical, a new type of system was needed to acquire a large amount of data in a short time. This was done by using multiple electrodes and takeouts attached to a computer and a multiplexer to switch the electrodes for each measurement. This idea was first tested by Griffiths and Barker (Griffiths and Barker 1993) and Ramirez et al. (Ramirez et al. 1993). The system requires the electrodes to be connected to a "smart" cable which has multiple takeouts; the cable is then attached to a computer. A survey design that depends on the expected structure of the target is implemented to evenly sample the subsurface.

In the field the goal is to sample a uniform spread of information to display the gathered data into a pseudosection. The pseudosection is the data plotted along a transverse line showing the apparent resistivity as measured and calculated

immediately in the field (Edwards 1977). The data seen are not the true resistivity and cannot be directly interpreted for geology since each type of resistivity array changes the way the resistivity contours react. A pseudosection gives the general trend in changes in the subsurface and can be used to eliminate bad data (Loke 2002). Since there are multiple types of arrays, only the arrays used in modeling are discussed in detail. The two types of surveys used were the Wenner array, which is more sensitive to vertical changes in the subsurface, and the dipole-dipole survey which is more sensitive to lateral changes in the subsurface.

The Wenner array is the most popular type of resistivity imaging geometry. This survey requires two current electrodes and two potential electrodes. The current electrodes are the outermost electrodes and are used to inject the current; the inner two electrodes then receive the current and measure the potential which is then digitally recorded. Figure 5-1 shows the layout of a Wenner array and how the measurement will change if the electrode locations are varied. In the Wenner array all 4 electrodes are evenly spaced. Hence, for each station level we just move over 1 electrode, thus instead of electrode 1, 2, 3, 4 being used we have 2, 3, 4, 5. This is done until the electrodes hit the end of the array spread when electrodes 22, 23, 24, 25 are used. After this there is an increase in separation distance to 2a, thus using electrodes 1, 3, 5, 7 and continuing until 19, 21, 23, 25 are used. This procedure is iterated until there is no equal separation to fit all 4 electrodes on a spread cable. This can be seen in Figure 5-1; looking at station 23 we can see what electrodes are used to obtain the data point. This process is continued until the distance between the electrodes is greater than that of the electrode spread. The Wenner array gives a trapezoidal array of data of the subsurface. At the largest electrode separation we then have the largest depth of penetration but the lowest lateral resolution. The depth of penetration depends on the electrode spacing and the electrical conductivity, and since conductivity cannot be changed, only spread length can change how deep the survey is. The reason Wenner arrays are sensitive to vertical changes in the subsurface is due to the sensitivity of how the electrodes

react. Since the spacings between the electrodes are the same, with injection of current at the first electrode, the potential measured at the first potential electrode has a horizontal sensitivity contour. Injection at the second current electrode shows the same response at the second potential electrode. Since the current travels through the ground horizontally at each measurement, any horizontal feature is averaged out and looks like a vertical change in a pseudosection.

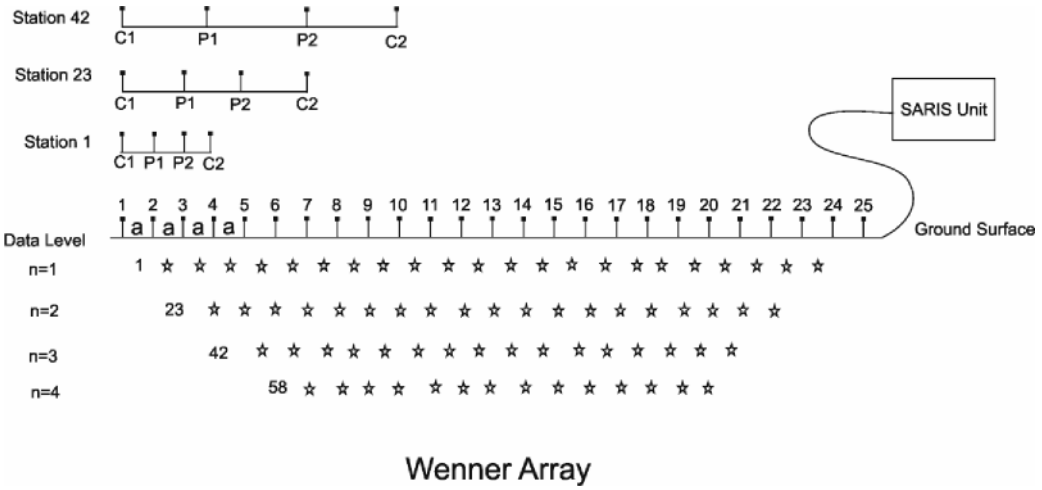

Figure 5-1 Wenner array configuration and arrangement of data points gathered in the subsurface. A trapezoidal shape which progressively gets thinner at larger depths is produced with larger electrode spacings. The resistivity system used in the figure is a Scintrex SARIS ERT imaging system using a 25 electrode smart cable. Surveys obtained in the field used either 25 or 50 electrodes.

In contrast to the Wenner array that is sensitive to vertical variations in electrical resistivity, dipole-dipole surveys are sensitive to lateral changes in the subsurface. As for most geoelectrical surveys, the dipole-dipole array uses four electrodes, again, two current and two potential. The main difference is that the two current electrodes are adjacent to one another as are the potential electrodes. For example, in an a imaging survey the current electrodes start as 1, 2 and the potential electrodes as 3, 4, as seen in Figure 5-2. For a dipole-dipole survey each level of measurements maintains the same electrode spacing while the separation between the current and potential electrode pairs is varied. Continuing the example, the second measurement would have current electrodes at 1, 2 with the potential electrodes at positions 4, 5. If enough current can be put into

the ground this will continue until the end of the spread where the current electrodes are at positions 1, 2 and the potential electrodes are at 24, 25 (Figure 5-2). The next data level then increases the electrode spacing and the same process is repeated. Unlike the Wenner array, a large amount of data can be collected with this method so the subsurface is measured at a higher sampling rate. The key aspect is: since the electrodes are so far apart a large amount of current is needed for the potential to be measurable at the far end of the spread. As stated before, the dipole-dipole array is sensitive to lateral changes in the subsurface. This is true because of the spacing between the current and potential electrodes. The current that is received is detected after going through vertical changes in the subsurface. The sensitivity contours at larger offsets then average the vertical changes that go though the subsurface; as a result, changes in the vertical direction such as layering are averaged out and not detected. The large amount of measurements gathered with the dipole-dipole array leads to better sampling of the subsurface and gives ideas about local lateral heterogeneity better then the Wenner array. For more information about sensitivity functions and graphing geoelectrical measurements, a good reference is Furman, Ferre, and Warrick (Furman, Ferre and Warrick 2003).

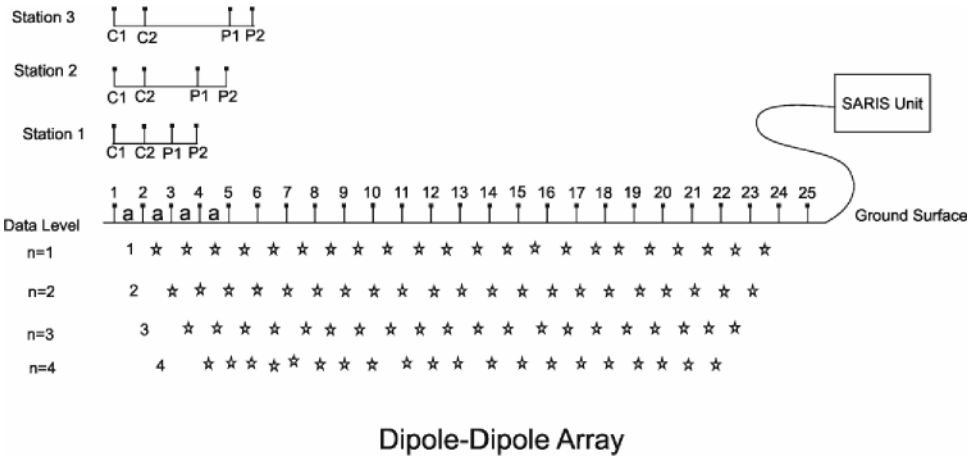

Figure 5-2 Geometry of a dipole-dipole array showing locations of the measured apparent resistivity values in the subsurface. Three sample configurations are given above the diagram to show which electrodes were used to get measurements. The resistivity system used above is a Scintrex SARIS ERT imaging system using a 25 electrode smart cable. Surveys calculated in the field used either 25 or 50 electrodes.

5.3 INVERSION

The inversion of electrical data takes the measured apparent resistivity and puts the data into blocks of calculated apparent resistivity. Once this is done the image can be viewed as a 2D grid and displayed as a "pseudosection." Geophysical inversion inverts the observed apparent resistivities in the field into a mapping of the variations in resistivity of the subsurface. This is done by defining a set of model parameters obtained from the measured data; the model response is the synthetic data calculated from mathematical relationships to resemble the subsurface. The model data and the response is related in the software RES2DINVTM using a finite difference technique (Dey and Morrison 1979), or for higher accuracy a finite element method (Silvester and Ferrari 1990). The forward modeling of the model and model response solves for apparent resistivity values in cell blocks which can be related to the observed measured resistivity data. The measured apparent resistivity values gathered from our imaging survey can be put into column format and described as **y**. The model response **f** is a column vector similar to the observed values and is calculated from forward modeling. The difference between the measurements is the relative error of the measurements and is given by the discrepancy vector g.

$$\boldsymbol{g} = \boldsymbol{y} - \mathbf{f} \tag{5.7}$$

The discrepancy vector **g** can be minimized to best fit the subsurface by summing the square of the discrepancy vector g,

$$G = \boldsymbol{g}^{\boldsymbol{t}}\boldsymbol{g} = \sum_{i=1}^{n} \mathbf{g}_{\mathrm{i}}^{2}. \tag{5.8}$$

By solving for the square of the discrepancy vector the RMS error can be minimized by iteratively updating the model to attempt to fit the real data. The initial model is changed to minimize these errors. After the iteration, if the error is worse than that of the previous model the model will be rejected. The more iterations done on the inverse problem, the closer the inversion comes to the

real subsurface model. To reduce error, a Gauss-Newton equation is used to solve for the inversion in order to limit the least squares error (Lines and Treitel 1984).

$$\mathbf{J^T J \Delta q_i = J^T g} \tag{5.9}$$

Where,

$$\boldsymbol{J_{ij} = \frac{\partial f_i}{\partial q_j}}, \tag{5.10}$$

J is the Jacobian of the partial derivative relating the model response to the model parameters. The vector $\boldsymbol{q}$ holds the model resistivity values known as the model parameters. The model parameters update after each iteration and the vector $\boldsymbol{q}_i$ is the model perturbation vector, this acts as a kick in the inversion to change the model values and find the optimum model.

More details about the inversion of such electrical data can be found in Loke (Loke 2002). However, it is worth commenting on some aspects of the inversion. Equation (5.9) is known as a basic least squares inversion and is useful for "well posed" inversions, but in general it is not practical for use in real cases. The reason for this is that problems can arise when the solution of the Jacobian vector is singular or nearly singular making it impossible to solve for the model perturbation vector accurately. This happens when the initial model that is used is far from an optimal model. To solve for this generally, an identity matrix is added to the data creating a smoothing function to create a well defined inversion, this is done by adding a damping/Marquardt factor (Lines and Treitel 1984). Without this the inversion can create sharp inversion artefacts. RES2DINVTM uses a similar type of damping parameter but the damping parameters can change for both horizontal and vertical values. The inversion is known as a smoothness-constrained least squares method and is shown in equation (5.11) (Sasaki 1992).

$$\left(\boldsymbol{J}^{\boldsymbol{T}}\boldsymbol{J}+\mu\boldsymbol{F}\right)\Delta\mathbf{q_i}=\boldsymbol{J}^{\boldsymbol{T}}\boldsymbol{g} \quad \text{Where,} \qquad \boldsymbol{F}=\boldsymbol{f_x}\boldsymbol{f_x}^{\boldsymbol{T}}+\boldsymbol{f_z}\boldsymbol{f_z}^{\boldsymbol{T}} \tag{5.11}$$

The value $\boldsymbol{f_x}$ is known as the horizontal flatness filter and $\boldsymbol{f_z}$ is the vertical flatness filter. These values make it possible to change the application of the damping to the inversion process giving more ability to adjust for different surveys. The inversion parameters can be changed in the program but for information about the inversion or how the parameters change the inversion process see the resistivity tutorial notes in Loke (Loke 2002).

The inversion of the apparent resistivity data takes the observed data and forward models it so it will look similar to the measured results; it can then can be inverted to obtain the true apparent resistivity. The first step is to divide the subsurface into rectangular blocks (for finite differences) or trapezoids (for finite elements) within which the observed values are assigned. The blocks of data are then forward modeled to resemble the original data. This is done to get a continuous spectrum of resistivity data and not just blocks of resistivity values which would give spiky inversion results. Once a continuous spectrum of a 2-D pseudosection can be calculated, this value will be inverted to obtain the true apparent resistivity. This is done by looking at the difference between the calculated and measured apparent resistivity. The residual between these measurements is used to update the inverted resistivity pseudosection. How close the apparent resistivity is to the modeled resistivity gives you the RMS error of the inversion. The lower the RMS error, the closer the modeled data is to the original data. This inversion process is iterated and continually updates the model until the RMS error stops decreasing, if the RMS error starts increasing you then start creating over-inversions and false anomalies in the data. The ERT tomograms shown below will have only the original dataset and the inverted true apparent resistivity section. The forward modeled resistivity section is useful for quality control of the results but is not mandatory for interpretation.

5.5 Oxford, MS

The field sites in Oxford, MS, are described in detail in the Appendix; since there are multiple sites with similar characteristics, not all tunnel sites will be discussed. The goals of this study are (1) to see if tunnels can be detected with resistivity tomography and (2) to determine the limitations and weakness of resistivity tomography in the detection of tunnels. Data from the individual test sites are presented and information about the test sites is discussed. Voids could not be detected at all of the sites tested; this indicated a limitation of the technique that was to be used to detect a clandestine tunnel in the Arizona test site. The data gathered in Oxford were postprocessed in Edmonton, so no further surveys could be performed after the initial surveys.

The Dam site was the most unique test site in this project; it had different subsurface geology and probably the most competent surface soils. The dam site was largely comprised of rich clay soils. The test site was an earthen man-made dam situated just off the University of Mississippi campus. The dam was constructed in order to control excess water run-off from an up-river dam. The culvert in the dam was placed using a cut and cover technique, and the surrounding material was a brownish clay which was water saturated at the surface. Clay creates a cap to limit water infiltration through the dam. The electrical surveys performed on this site employed a 25 m, 50 m, 100 m electrode dipole-dipole array. The survey included 1 m, 2 m, and 4 m electrode spacings centered around the 13th electrode that was placed directly over the middle of the tunnel location. The 2 m electrode spaced dipole-dipole array is shown in Figure 5-3 and the 4 m electrode spaced dipole-dipole survey can be seen in Figure 5-4. The results show a strongly conductive anomaly.

The electrical data shown in Figure 5-3 show a low resistivity anomaly around 8 m depth and 24 m offset. The inversion has 3.3% RMS error with 5 iterations. The first thing that was considered was that the anomaly was related to the ground going from the cut and fill to native laminated sandstones. The main issue with this assumption is that in Figure 5-4 the resistivity increases past 12 m depth. Figure 5-4 shows a 4 m electrode spaced dipole-

dipole array which is inverted with 5 iterations and a 1.26% RMS error. The anomalies seen on the edge of the data in Figure 5-4 are due to over-inversion and are in no way part of the subsurface. When the data are iterated over time, the edge effects are extenuated and cause false artefacts known as edge effects (Loke and Barker 1996). The approximate locations of the tunnels are shown in Figure 5-3 and Figure 5-4; the tunnel is over-estimated and is seen at 7 m in both figures. This is due to a resistive surface with a conductive anomaly. The synthetic data in chapter 4 showed that a high resistivity anomaly of air should give a small resistive zone seen in the data. In the case of the dam site there were a large amount of low resistivity soils and a concrete pipe in which water had infiltrated from the stagnant water in the dam. The water running through the pipe gives the electrical current a fast way to transfer. In addition to this there was water traveling through the culvert.

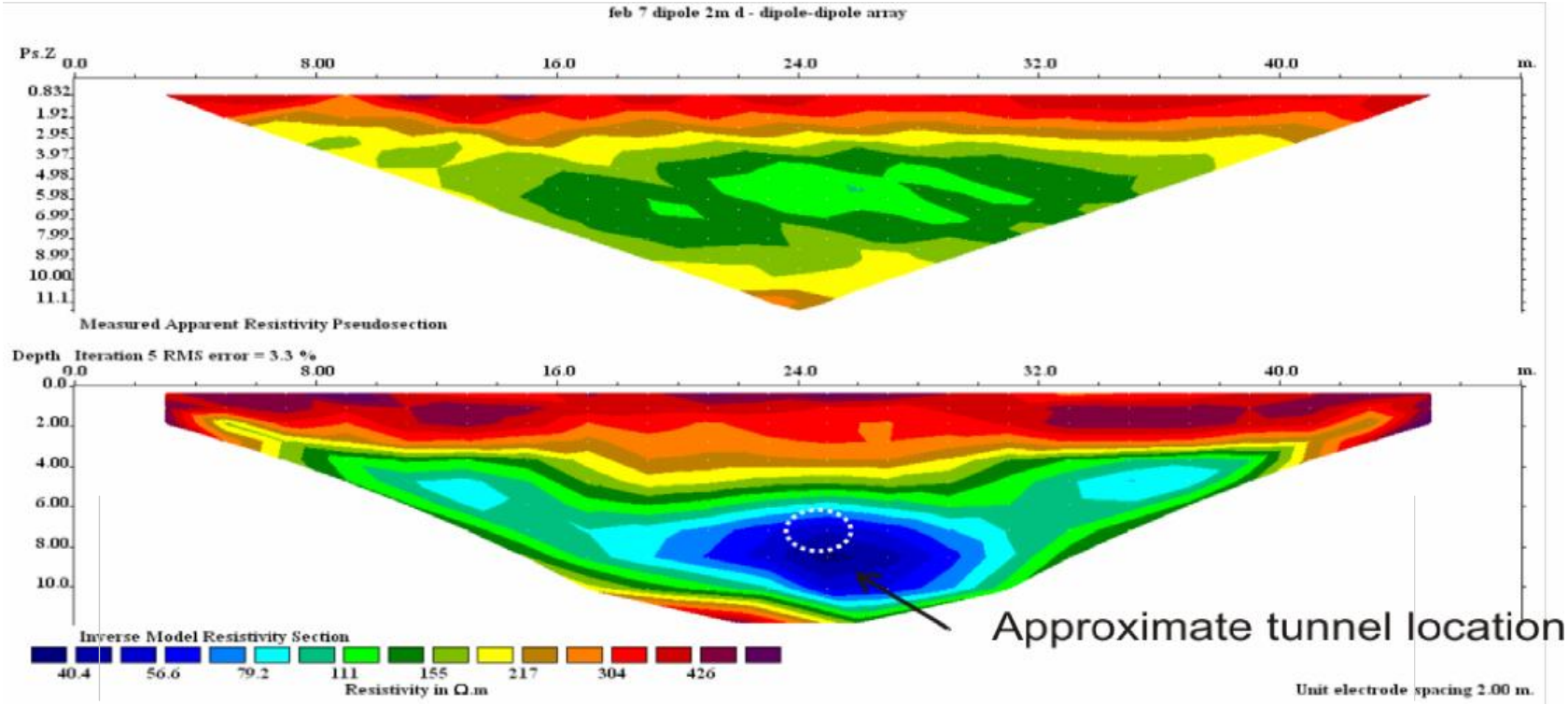

Figure 5-3: Top: The pseudosection for the apparent resistivity section. The dipole-dipole array has 2 m electrode spacing. Bottom: The inverted apparent resistivity pseudosection; around 26 m offset and 8 m depth there is a low conductivity zone. The final section has 3.3% RMS after 5 iterations. The estimated location of the tunnel was around position 24 m and at 6.5 m depth. In the top section a high conductivity anomaly appears around 5–7m depth and 22–27m offset; the inversion causes the high conductivity anomaly to be estimated deeper than its true position. The low conductivity is associated with water infiltration around the concrete acting like a salt double layer.

.

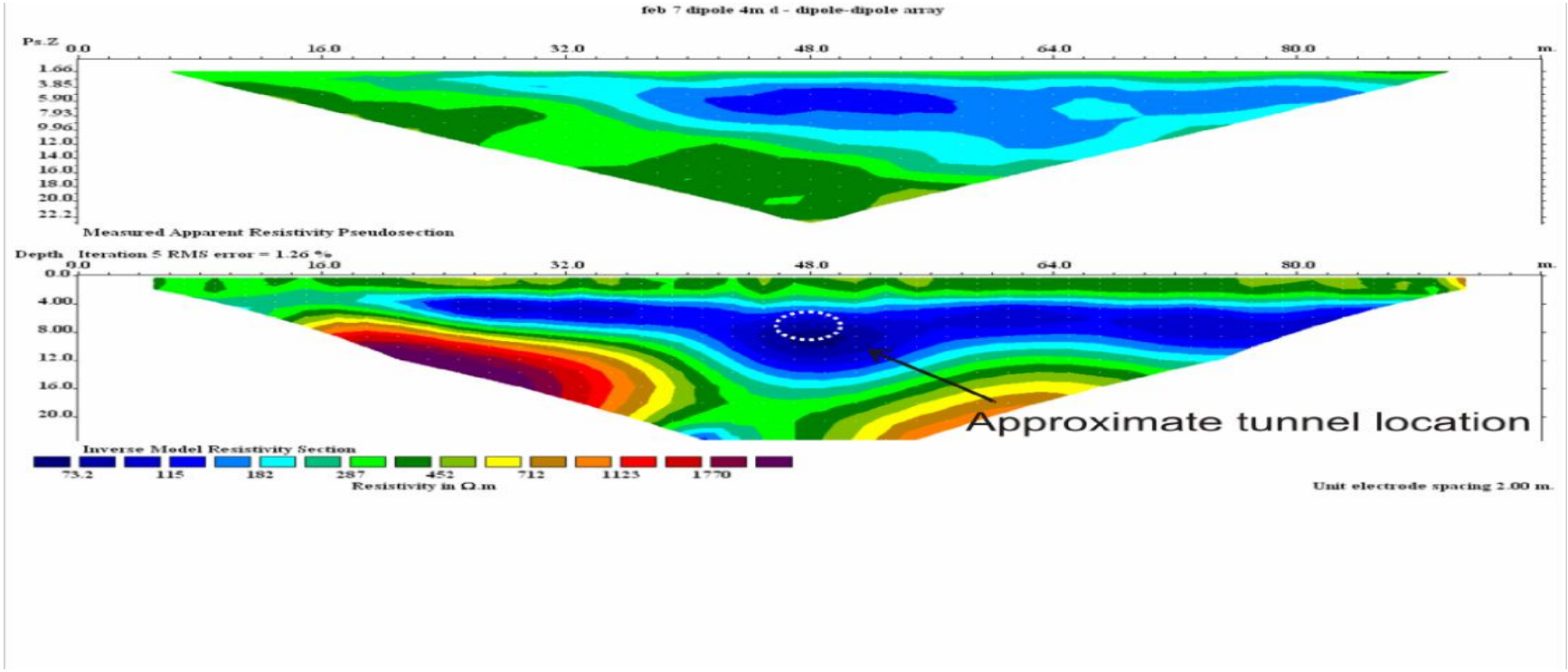

Figure 5-4 Top: Thepseudosection for the apparent resistivity section. The dipole-dipole array has 4 m electrode spacing. Bottom: The inverted apparent resistivity pseudosection; around 48 m offset and 8 m depth there is a low conductivity zone. The final section has a 1.26% RMS error after 5 iterations. The estimated tunnel location is higher than what is seen in the inverted section. The low conductivity zone is in the region where the tunnel should be located and is where the water is infiltrating into the subsurface. In the top section a concentration of low resistance appears around the location of the tunnel.

Similar to what was seen in the dam site, tunnel site 3 shows a conductive anomaly. But unlike the dam site this was a metal pipe culvert. The metal culvert was estimated to be 4–5 m deep and approximately only 0.5 m wide. The survey collected 190 data points over a 50 m dipole-dipole array with 2 m electrode spacing. The inversion included a finite element forward model with trapezoid grid blocks; due to some very large standard deviation differences some data were removed from the edge of the survey and from some of the bottom layers. The two resistive edge anomalies have been over-inverted creating a layering effect that could lead to incorrect interpretation. From the measured apparent resistivity pseudosection in Figure 5-5, we see a boundary of quite low resistivity values imprinted by a resistive region. This region is most likely the location of where they excavated to place the tunnel into the subsurface. The overall quality of the data is still fairly good, since after 5 iterations there was a 15.7% RMS error that was nearly all associated with the edge anomalies. The culvert in this case was not directly seen in the spread, but evidence of changes in the natural rock can be seen. To get more accurate results, a tighter spread length would be needed.

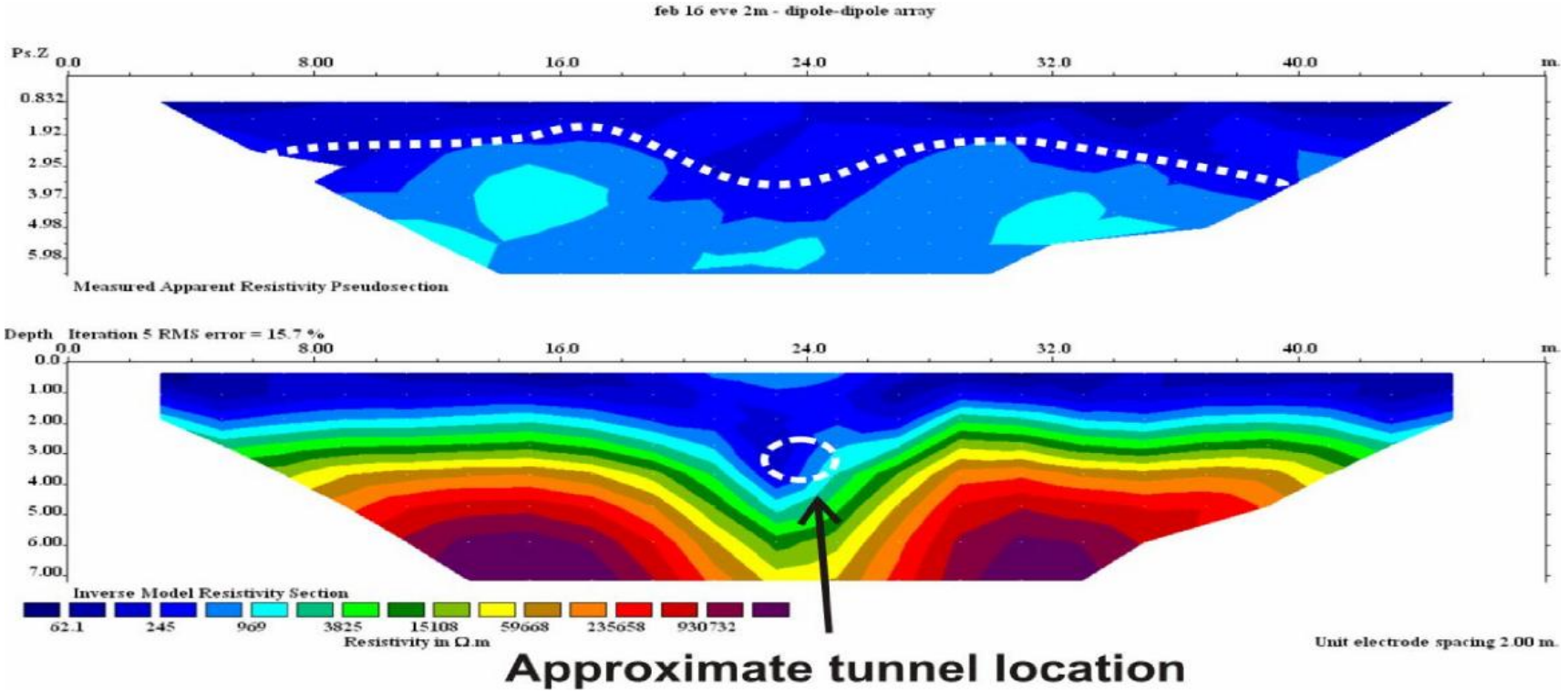

Figure 5-5 Top: The measured apparent resistivity section of a 50 m dipole-dipole array over the Oxford, MS, tunnel 3 site; the electrode spacing is 2 m. A finite element with trapezoid blocks were used for inversion; the only editing done was to remove a bad data point on the edge of the data. The data needed to be removed due to the inversion causing unrealistic values. Bottom: The inverse model resistivity section; there is a slight dip at 24 m offset, above the approximate location of the tunnel. The RMS error is 15.7% after 5 iterations; the large resistive edge anomalies are inversion related and have nothing to do with the data.

Due to the resolution of the technique, tunnel detection will not succeed if the tunnel is too deep. The reason for this is that the source signal will eventually be smoothed out making it no longer possible to detect the void. A high degree of heterogeneity in the near surface can also make it difficult to detect the tunnel as the electrical conductivity results may be too scattered.

In Oxford, MS, we tried doing both electrical and seismic arrays on tunnels as shallow as 1–2 m. Figure 5-6 shows a shallow concrete culvert about 2–3 m deep and approximately 0.4 × 0.4 m wide. This survey used 1 m electrode spacing on a 25 m dipole-dipole spread. A resistive zone at 12 m offset is seen near the surface at approximately 1 m depth. This zone spreads from 8–14 m offset and 1–3 m depth and is simiar to what was seen in chapter 4 where synthetic models of resistive anomalies were expanded. The inversion took 5 iterations and the RMS error was only 3.8%; the error was associated with fitting the conductive subsurface underneath the resistive anomaly. The dipole-dipole array has 232 data points with some of the data removed from the bottom layers (i.e., farthest offsets); a lack of current strength caused false artefacts. The inversion shows two strong anomalies and the approximate tunnel location is indicated in Figure 5-6. Although the resistive zone is spread over the tunnel, the location of the air filled void is still overestimated and looks a lot larger in the inversion; the depth is also not estimated correctly.

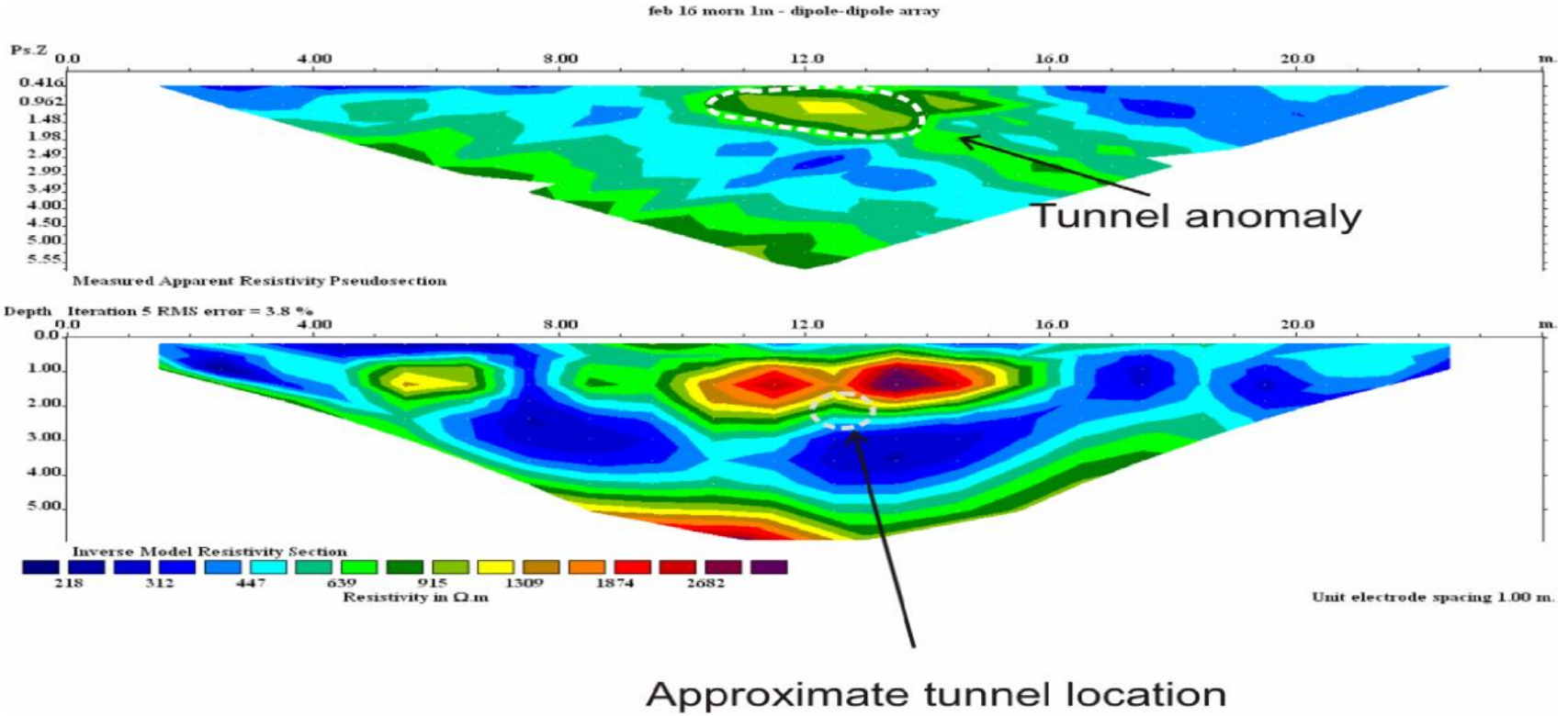

Figure 5-6 Tunnel 5 of the Oxford, MS, test site culverts; the tunnel is approximately 2–3 m deep and 0.4 × 0.4 m in dimensions. Top: the measured apparent resistivity pseudosection; there are 232 data points on a 25 m dipole-dipole array with 1 m electrode spacing. The section had some very minor editing done on the bottom few layers; these were removed because they were so resistive they masked some of the signal closer to the surface. Bottom: the inverse model resistivity section where the approximate location of the tunnel is indicated.

The following tunnels of larger depth and size resembled what was expected at Douglas, AZ. Tunnel 6 was an interesting test site because the depth was approximately 8–10 m deep and the culvert walls were made up of concrete blocks rather than solid concrete. This change causes the way water drains in the tunnel as the blocks do not act as barriers for the water. In contrast, metal pipes and solid concrete culverts can fully restrict the movement of water. A dipole-dipole survey was performed with 4 m electrode spacing and 100 m spread length. The day this survey was performed was very windy causing the seismic data to be quite bad, thus is was hard to compare the results. The resistivity noise resulting from wind is little to none, only the movement of the wires can cause a small distortion. Since the tunnel was so deep the goal of the survey was to see if the anomaly could be seen with such a large electrode spread, since using smaller electrode spacing would not give enough depth penetration. The data were processed using a finite element and trapezoid block forward model configuration giving the inverted resistivity pseudosection a 4.1% RMS error after 7 iterations with no data editing. Figure 5-7 shows that the inversion hints at the estimated location with a local increase in the resistivity. The inversion appears to further suggest that the tunnel lies in between two geological layers of differing electrical conductivity. The actual apparent resistivity indicates that the most conductive zone is still somewhat resistive at nearly 60 Ω.m, giving an indication of sedimentary rock. The resistive zone above this region is higher, around 500–1000 Ω.m, giving the impression of very loosely packed gravel with little to no water saturation. Though this anomaly does not give a defined location of the tunnel, it is reasonable to think that the tunnel could be detected with shorter electrode spacing and a similar spread length. This site had only 4 m electrode spacing,

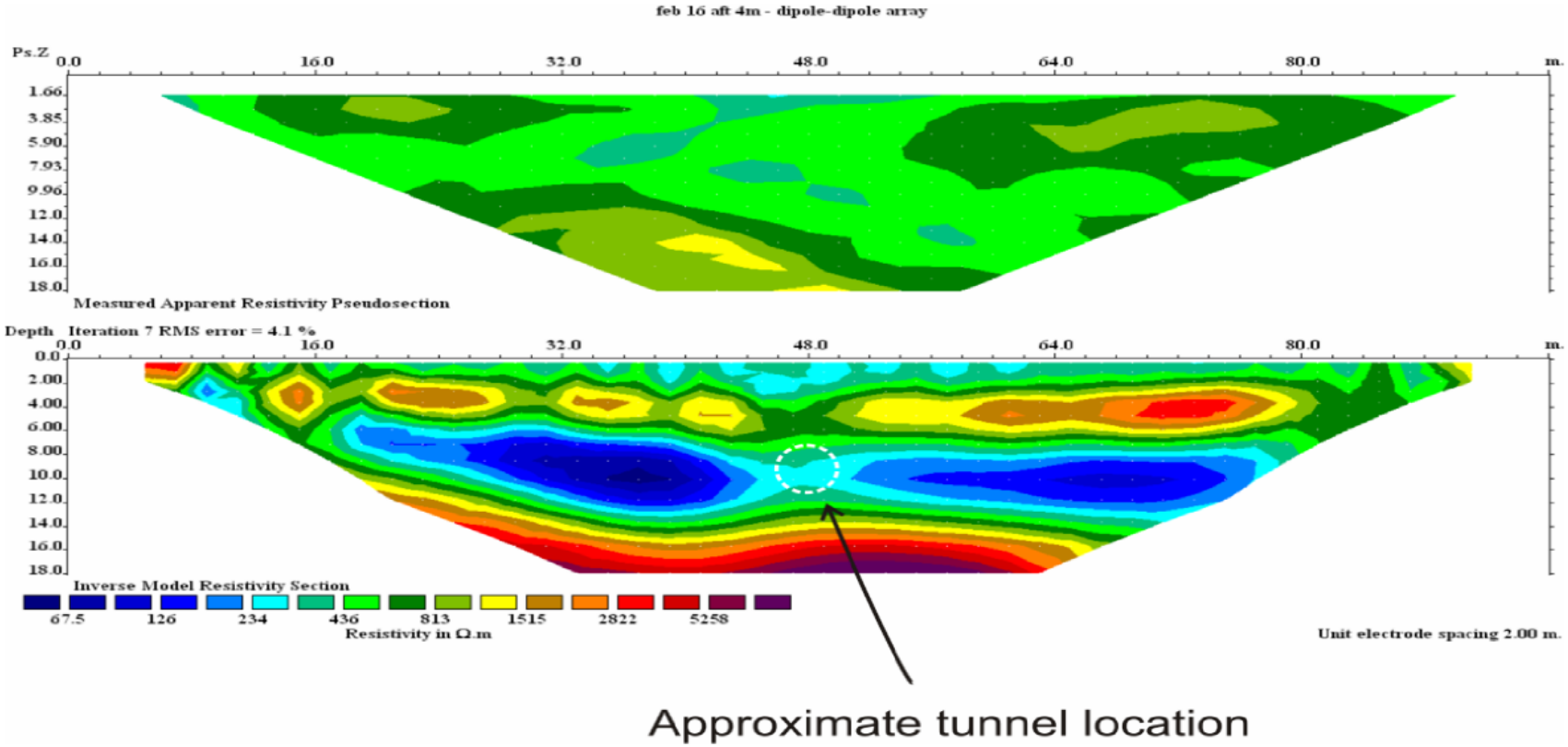

Figure 5-7 The Oxford, MS, test site culverts; the tunnel is approximately 8–10 m deep and approximately 1 m wide and 0.5 m tall. Top: the measured apparent resistivity pseudosection; there are 232 data points on a 100 m dipole-dipole array with 4 m electrode spacing. Bottom: the inverse model resistivity section; the approximate location of the tunnel is indicated. The tunnel site is not detected by the electrical array, most likely due to the large electrode spacing and smoothing of the pseudosection. The data are of excellent quality as after 7 iterations only a 4.1% RMS error was found

The first survey examined the deepest but also the largest tunnel site. Both Wenner and dipole-dipole arrays were performed at this site. The dipole survey had a power outage so the last few data points were not obtained and do not add to the final interpretation. The dipole-dipole survey that was performed had 2 m electrode spacing and a 96 m spread length. This is a longer spread length due to the depth of the tunnel. The tunnel was constructed of concrete blocks and was used as a drainage culvert. Figure 5-8 shows the resistivity pseudosection. The tunnel location is approximately halfway through the spread, at around 10–12 m depth. The tunnel anomaly is not seen well in the pseudosection, possibly because of the large amount of heterogeneity above the tunnel location. A slight perturbation is observed above the tunnel location, but a tunnel was not detected. The inversion ran with 4 iterations but still had 19.7% RMS error; thus the layering and near surface effects are related to inversion related artefacts.

The other ERT survey performed was a Wenner array. The goal of this survey was to see if doing a Wenner array would give any indication of the tunnel site. After inversion and interpretation it was noticed that the low resistivity zone seen in Figure 5-9 shows that the railway track may have been replaced with other material (possibly after damage). This is important in the next chapter where we see a similar anomaly c causing none of the seismic energy to be imaged properly.

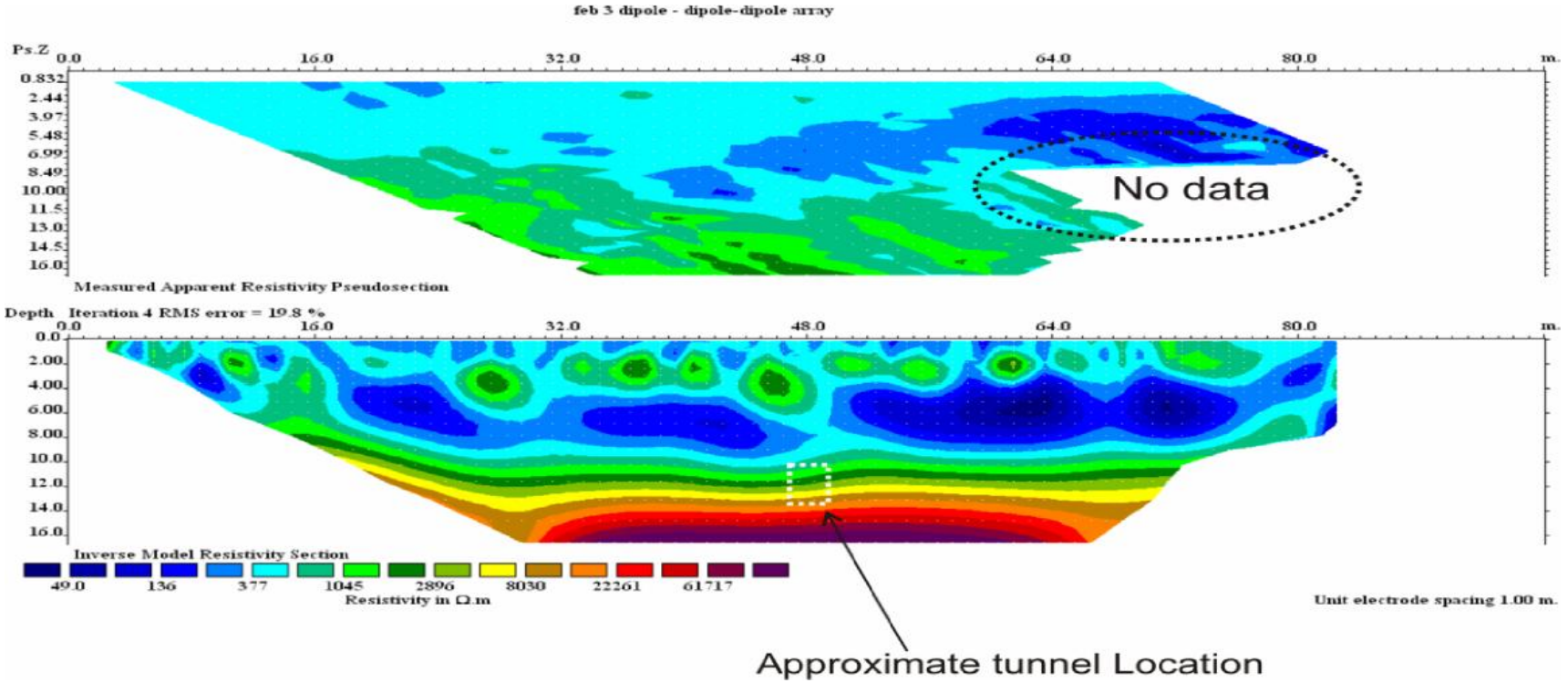

Figure 5-8 The first and largest survey site performed in Oxford, MS. The survey has 2 m electrode spacing with a 100 m dipole-dipole array. The survey was not completely finished due to a power shortage while running the survey. There are 753 data points with many poor data points removed. Top: raw data collected over the first tunnel site. The tunnel is approximately 12 m deep. Bottom: the inverted pseudosection of true apparent resistivity. The approximate location of the tunnel is displayed. There is a 96 m spread length with 2 m electrode spacing; the inversion iterated 4 times and had an RMS error of 19.7.

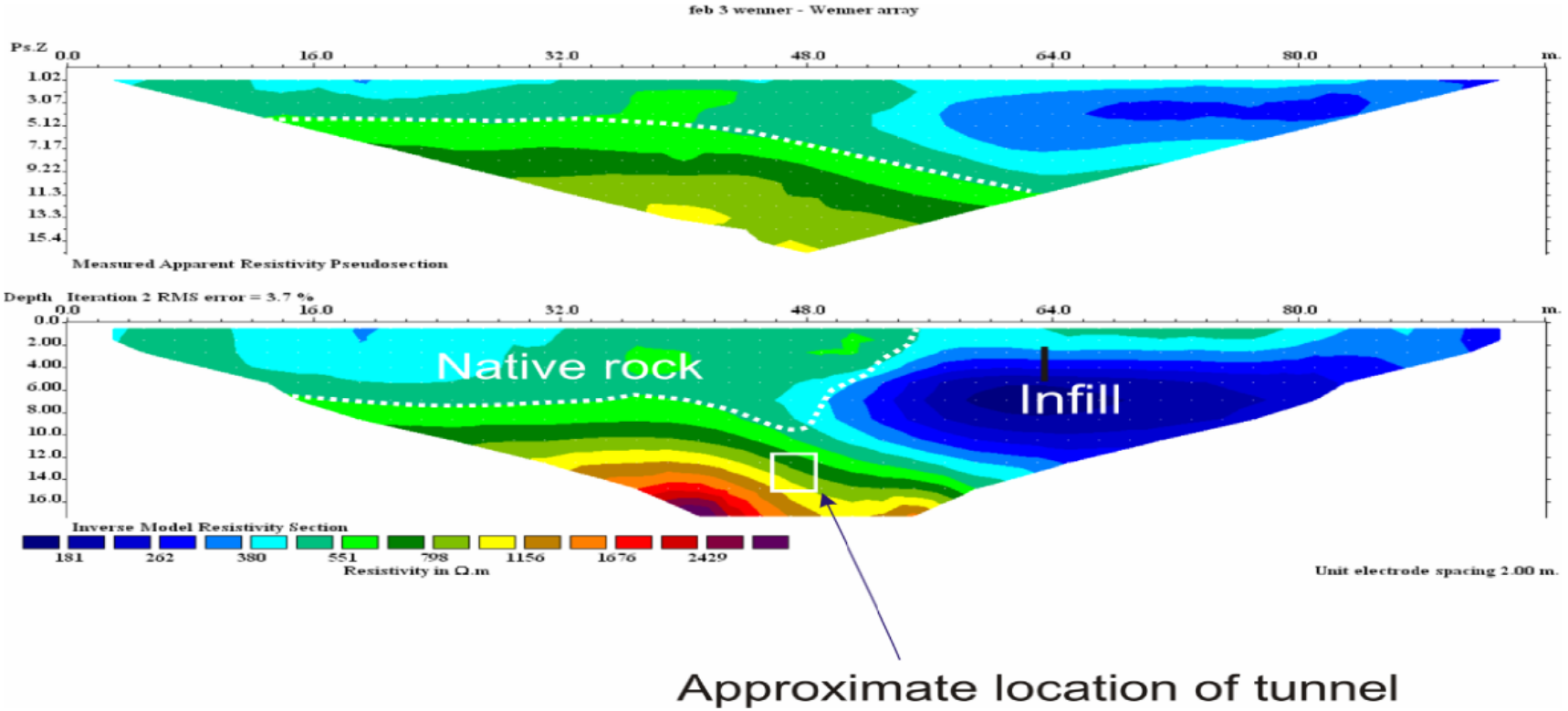

Figure 5-9 The first and largest survey performed in Oxford, MS. The survey has 2 m electrode spacing with a 100 m Wenner array. Top: raw data collected over the first tunnel site. The tunnel is approximately 12 m deep. There are 375 data points with 16 data levels and 1 data point removed. Very severe edge effects were applied. Bottom: The inverted pseudosection of true apparent resistivity. The approximate location of the tunnel is displayed. There is a 96 m spread length with 2 m electrode spacing; the inversion iterated 2 times and had an RMS error of 3.7 %.

5.6 DOUGLAS, AZ

The Douglas, AZ, test site had two surveys performed but due to a large amount of surface heterogeneity and a metal fence only one of these produced reliable results. Figure 5.10 shows the ditch data with little to no processing. Figure 5-11 shows the ditch data with some editing done to improve both the RMS error and also limit the false resistivity values seen. Since there was a large RMS error, very little parameter changes were done to the inversion. The modeled apparent resistivity section is also shown in Figure 5-11 to show the effects of the large RMS error and how random error can compound the error. E1 and E2 (Figure 5-10) are two high resistivity anomalies in the approximate location of the tunnel. Since the tunnel was built at the level of the water table and there was no water in the tunnel itself, we can expect a higher resistivity anomaly for the tunnel than for the surrounding materials. There was a large amount of surface heterogeneity but the actual subsurface should be fairly homogeneous, this assumption is based on the side wall in the ditch.

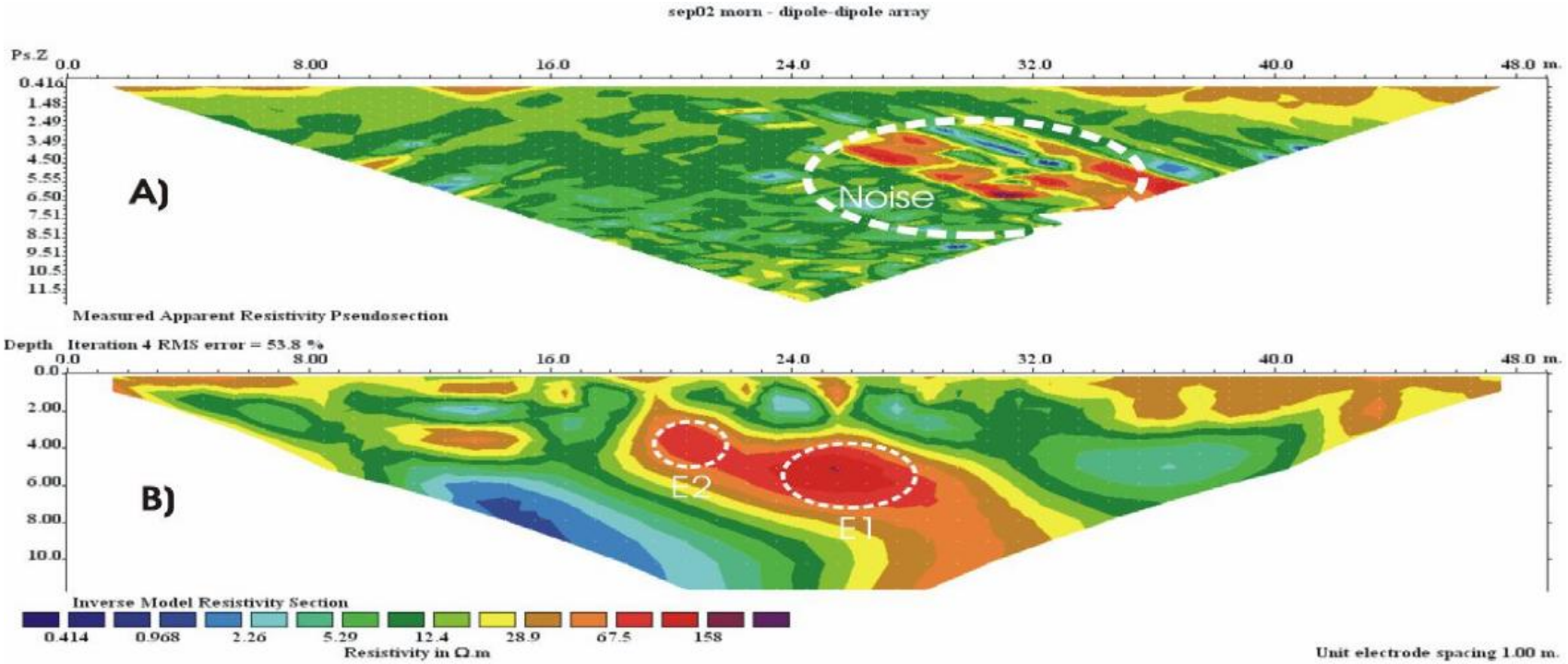

Figure 5-10 The electrical resistivity tomography of the ditch data in Douglas, AZ. The data have 1 m electrode spacing with a 50 m dipole-dipole spread. The tunnel location is approximately 6 m deep and the tunnel was estimated to be approximately in the center of the spread. There are only 3 data points removed in a finite element inversion. A): raw dataset gathered over 1000 data points. The data have a large amount of noise in the circle area. B): the inverse modeled resistivity section; the dataset has two anomalies in the section showing the possible location of the tunnel. There were 4 iterations with a large 53.8% RMS error.

The data were further processed to try to enhance the anomaly and also to try to decrease the RMS error. First, some of the noisy data on the far end of the spread were removed. Since the electrode contacts were loose because of the dry sand, at larger electrode offsets the current was not high enough to measure the resistivity of the subsurface. Second, the model spacings were halved in an attempt to increase lateral resolution. This usually increases lateral resolution but can also result in additional inversion anomalies (Loke 2002). The calculated apparent resistivity section in Figure 5-11 shows lineations and sporadic noise being compounded. This is the cause of the large RMS error. To resolve this problem, higher voltages need to be injected during the survey. The anomaly that is seen in the apparent resistivity is split into two anomalies around the estimated location of the tunnel. The RMS error for the newer inversion was 45.0% which is still high, this was after 2 iterations, and all iterations after this just enhanced the lineations in the calculated apparent resistivity section compounding the sporadic noise more. The survey was in loose sand where water was used to increase coupling with the ground, but by the end of the survey the water had dried up. The ground in this region had a resistivity of around 15 Lm and the inverted anomaly for the tunnel had only around 80 dm. At the roadside site the second resistivity survey was parallel to a metal fence that essentially short-circuited the measurements.

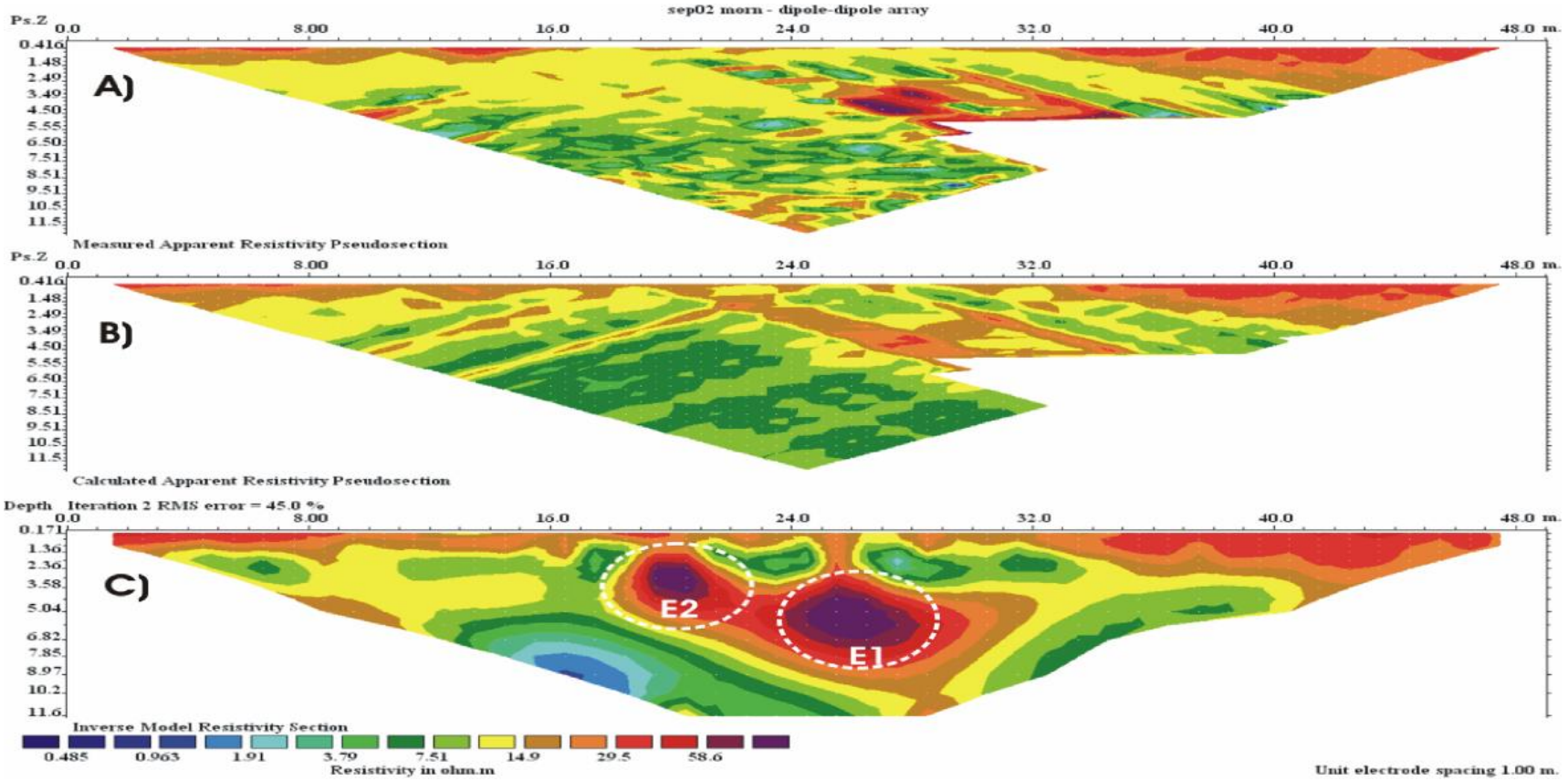

Figure 5-11 Electrical resistivity tomography of the ditch data in Douglas, AZ. The data have a 1 m electrode spacing with a 50 m dipole-dipole spread. The tunnel location is rectangular, approximately 6 m deep and approximately 1 m wide. A): the apparent resistivity section with many data points removed. B): the calculated apparent resistivity pseudosection; the lineations indicate low voltage and are sources of error. C): the inverse modeled resistivity section; the dataset has two anomalies in the section showing the possible location of the tunnel. There were 4 iterations and 45.0% RMS error.

5.7 DISCUSSION

The use of electrical methods for finding subsurface tunnels had mixed results. In general, a survey can detect a tunnel if the tunnel is fairly shallow and there is enough injected current capacity to produce measureable electrical potentials. The main problem with using electrical methods is that in urban environments many man-made near surface conducting features divert the current. The theory of electrical resistivity tomography and how it was used to detect tunnels was described in this chapter. The experiences gained here suggest that natural and/or cultural heterogeneity in the subsurface make it difficult to interpret tomography data. In the Oxford, MS, test sites the expected anomaly was detected at only four of eight sites surveyed.

This disappointingly low success rate included surveys that suffered from poor injected current. Consequently, the electrode-ground coupling was taken more seriously at the Douglas, AZ, sites so less current would be dissipated at the near surface. Despite this, the tunnel was detected only in the survey carried out in the ditch at the site. The roadside site in Douglas, AZ, had a large metal fence beside it so there was little hope of void detection.

In Oxford, MS, some of the sites, such as tunnel 5, displayed resistive anomalies while others were conductive, such as the dam site and tunnel 3. This suggests that some care must be taken in the interpretation of the tomograms; a tunnel is not necessarily associated with a highly resistive anomaly in the tomogram.

During the synthetic modeling of the surveys, we felt that the casing around the tunnel would not affect the resistivity and the air in the tunnel would provide a large resistivity contrast. What was seen was that the casing could provide paths for water to flow, making the anomaly conductive. The Douglas, AZ, test site showed a large amount of surface heterogeneity causing data acquisition problems, but it was the problem of getting enough current into the electrodes that held us back. Due to an increasing resistivity with depth, some of the current got trapped near the surface where it was easier to move. This caused poor

signal at larger depths and the noise could be quite large. We conclude that electrical methods can be used to detect tunnels if other techniques are employed to ratify the results. Although other studies have reported finding near surface voids, due to the large amount of surface changes in urban environments, we experienced mixed results. The tunnel anomaly was seen in only 4 out of 8 possible tunnel locations in Oxford, MS, and in 1 out of 2 locations in Douglas, AZ.

CHAPTER 6
6.0 SEISMIC REFRACTION TOMOGRAPHY

The goal of this chapter is to show how seismic first arrival waves and refracted waves can be used to image the subsurface in terms of its seismic velocities. This is done by first giving a brief overview of some of the basic seismic principles and following this with theory on refraction modeling and ray tracing. With this background, some practical aspects of data preparation, first arrival time picking, and theory of refraction inversion are presented. The chapter concludes with data examples from both Oxford, MS, and Douglas, AZ.

6.1SEISMIC OVERVIEW

6.1.1 SEISMIC WAVES

A seismic wave is an elastic wave that is caused by an excitation or source that causes the elastic energy to propagate through the earth. The energy transfer depends on the type of particle motion, which can be either parallel (longitudinal) or perpendicular (transverse) to the wave's propagation direction, with these two waves (in isotropic media) called the P- and S-waves, respectively. In most refraction studies we will be focusing on these two body waves. Surface waves also play a part in near surface studies and must be discussed because they always exist and cause problems for the analysis of the body wave refractions because of their strength.

There are two main types of body waves: P- (or also compressional, longitudinal, primary) waves or S- (or also transverse, shear, and secondary) waves. The speed of transmission depends on the density and the stiffness (i.e., elastic moduli) of the material it travels through. When travelling through the earth, the shear wave depends on the rigidity of the material, if the material is a fluid and has no rigidity, then there is no shear wave propagation as is the case for all

fluids. The velocities of the body waves for isotropic media can be described as:

$$Vp = \sqrt{\frac{\left(k+\frac{4}{3}\mu\right)}{\rho}} \qquad (6.1)$$

And,

$$Vs = \sqrt{\frac{\mu}{\rho}}, \qquad (6.2)$$

where Vp is the compressional velocity or the P-wave, and Vs is the shear velocity or the S- wave. The parameters k and μ are the effective bulk and shear moduli, respectively, and ρ is the density. The bulk modulus is a measure of the compressibility of a rock; that is, the degree to which the material changes volume under a change in applied hydrostatic pressure. The shear modulus, or the rigidity, is a measure of the distortion produced by the application of a constant shear stress. A major difference between the bulk and shear moduli is that there is no change in shape with the former (only volume) and only change in shape (no volume) with the latter. A compressional wave travels though rock with the particle motion in the same direction as the direction of the wave. Shear waves travel through rock with the particle motion perpendicular to that of the direction of the wave. The body waves are faster than the surface waves and the primary wave is faster than the shear waves as can be seen in Eqn. 6.2.

Surface waves travel in the top layer along the surface; there are multiple types of surface waves but for this study I considered only Rayleigh waves. The Rayleigh wave is made of both compression and transverse waves and it depends on the same elastic parameters and density. The speed of the Rayleigh wave is slower than the speed of the shear wave and for a Poisson solid (where shear and compressional moduli are the same) can be estimated as $v_{rayleig\ h} \approx 0.91 v_s$ (Sheriff and Geldart 1985). Rayleigh waves travel along the surface with a retrograde elliptical motion. In practice they can be considered low frequency low speed waves that travel in the top layer of the earth. In the context of the current study, surface waves are essentially noise and often called “ground roll” in most seismic surveys. Using spectral analysis and transferring the seismic signal into the frequency ray parameter domain, the Rayleigh wave can be used as a

signal for some near surface studies (Park, Miller and Xia 1999) and in tunnel detection (Miller et al. 2006). We did not use surface wave techniques in this study because we did not have geophones sensitive to low enough frequencies to image enough of the fundamental mode that will penetrate to sufficient depth (Xia, Miller and Park 1999).

When the elastic wave energy propagates from the source into the subsurface and intersects a boundary of changing impedance, then the seismic waves will reflect or, depending on the angle of incidence, critically refract. The acoustic impedance is defined as a product of the velocity and the density for a given material. The transmission and reflection of elastic waves through a boundary depends on the contrast in impedance across it. The ray paths that the wave follow are described by Snell`s law where $\theta_1$is the angle of incidence,θ_2 is the angle of refraction; the angles depend on the ratio of the velocities between the layers $\frac{v_1}{v_2}$:

$$\frac{\sin\,\theta_1}{\sin\,\theta_2} = \frac{v_1}{v_2}. \qquad (6.3)$$

As known from elementary physics principles, the angle of refraction depends on the angle of incidence and is controlled by the difference in wave speed between two media. Further, Snell's law states that at a certain incidence angle the wave will critically refract at a refraction angle of 90°. At this point the wave follows along the boundary and as it goes it leaks back up to the surface. Figure 6-1 shows the transmission of a wave through the subsurface, and the different situations possible. The blue ray highlights the situation where the incident wave is incident at the critical angle of refraction; the subsequent blue paths show the wave following along the boundary interface and radiating energy back toward the surface as it goes. The red ray shows the situation when the wave energy transfers through the first boundary being again refracted within the third layer. The red ray path shows a true primary reflection that reflects back to the surface. In this study we were interested in how the seismic wave is affected by a subsurface void and in Figure 6-1 we see that a possible tunnel location that is air filled causes the wave to refract off the tunnel due to its slow speed. The energy around the tunnel goes to the surface leaving a blackout zone with no rays going through. This will give a zone of

low coverage and indicates a low velocity zone. Snell`s law states that as the seismic wave travels through the subsurface, the angle that it travels depends on the velocity of the material it is traveling through. This means that eventually the energy will either attenuate or it will reach the surface and be detected.

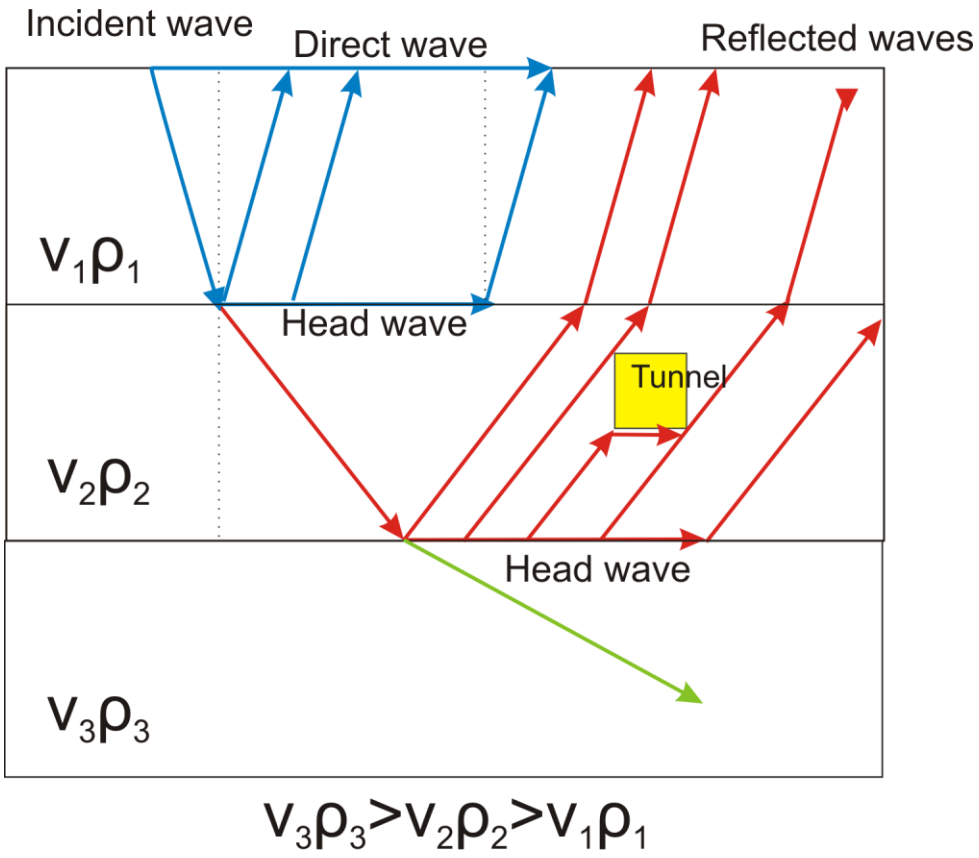

Figure 6-1 Seismic waves travelling through the subsurface through a three layer model with increasing impedance. The tunnel shows how an air filled void of small wave velocity is displayed.

In a seismic survey we have a "controlled" source, which in our case is either a sledgehammer or an accelerated weight drop. The seismic waves are detected with an array of receivers laid out in a straight line radiating from the source. We consider the location of the source to be a point from which energy radiates equally in every direction. The receivers, in our case, geophones, are sensitive to the vertical component of the particle velocity of the ground surface; as the wave passes, the geophone transduces this particle velocity to an analog voltage time series. In modern practice, this time series is digitally recorded, and in geophysical practice the record of the particle motions commences with the

triggering of the source and continues for a set period of time (usually influenced by instrumental sampling rates and memory). This record is called a "trace" and the surface distance between each geophone and the source is called the "offset." The offset-ordered ensemble of all the traces of a given shot is called a field record or a common shot gather (CSG).

The collection of various shot gathers with the source at different locations is the basic data collected in a seismic survey. To record a seismic survey we start recording the receivers' analog output as the sledgehammer hits the ground. The shot gather is displayed as offset vs. time where the offset is just the relative distance from the shot to the receiver. An example of a CSG can be seen in Figure 6-2; the figure shows how surface waves and primary waves are displayed, the reflections are much weaker and are masked due to the large amount of energy of the surface waves and the first refraction. To increase the energy and limit the random noise, multiple field records will be recorded at a given location and stacked (summed) to increase the signal to noise (S/N) ratio. The field record should be the same at the same location and gives the results repeatably, this has been tested (Knapp and Steeples 1986). Stacking at a single location should decrease the random noise encountered in a survey. Noise is anything that is not considered as signal, this can include other types of seismic waves, random noise, or correlated noise. Random noise is noise that varies on a field record to field record basis; examples are a footstep or wind blowing on the receivers. Correlated noise is noise that is seen in all shots and is stacked when stacking different field records; examples are other seismic waves, or a running engine on the accelerated weight drop.

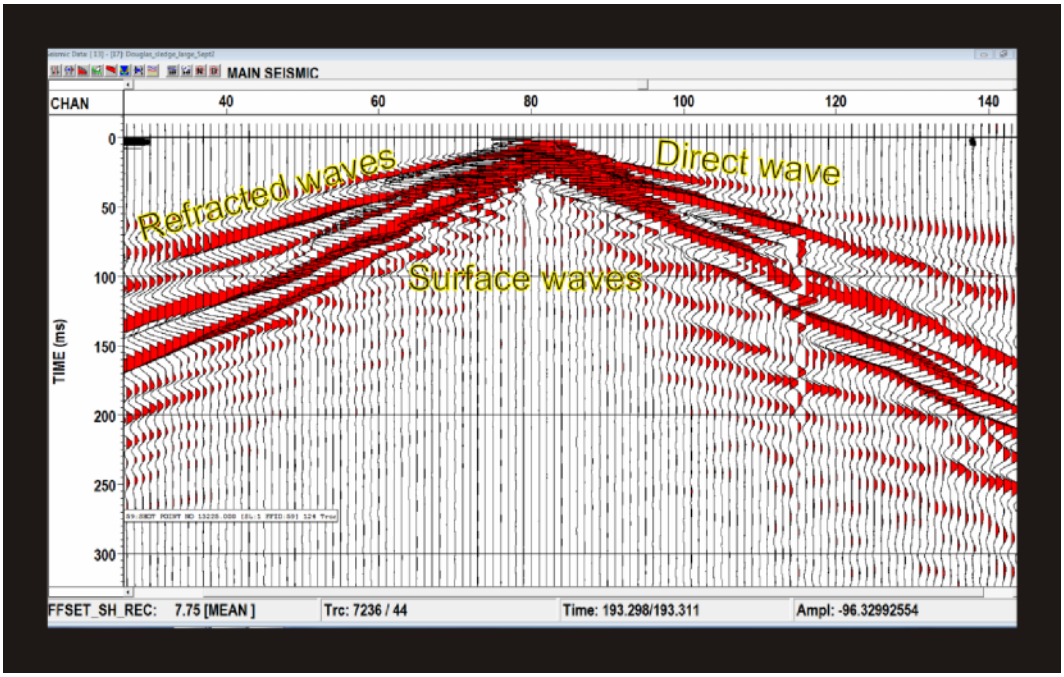

Figure 6-2 Example of an ensemble of seismograms (a common shot gather) from the Douglas, AZ, test site. Direct, refracted, and surface waves are shown.

The other type of survey that can be acquired in the near surface employs a downhole geophone package; in this case the travel times of waves travelling down from the surface can be directly measured. This type of data acquisition is known as vertical seismic profiling (VSP). The main difference from a survey employing geophones above ground is that since the receiver is down in the ground the seismic waves that travel toward it are one-way and direct, thus giving exact velocity information about the material they traveled through. This type of survey was carried out at only one survey site, but can be useful in getting exact wave velocities in the subsurface.

6.1.2 Resolution

Before details are given about the modeling of the seismic wave field for tunnel detection, the concepts of seismic resolution need to be introduced; to some degree seismic resolution remains difficult to quantify. Classically, resolution limits are defined as being the minimum distance apart that two independent objects can be such that they can still both be individually identified. These limits depend on the wavelengths involved, and Rayleigh considered 1/4 wavelength separation to

be the limit. This concept becomes less clear once we deal with real seismic pulses that have a broad range of wavelengths.

When dealing with tunnel detection the main concern is that for data acquisition we are setting up a survey that has a theoretical chance of being able to image a tunnel. Resolution can be either vertical or horizontal. Vertical resolution depends on the wavelength of the incoming wave and the ability to discriminate individual layering and horizontal structures. Horizontal (or lateral) resolution depends on the dominant incoming frequency of the wave field and the depth of the target. These values determine the size of the Fresnel volume which is a circular zone that controls the area from which an observed anomaly will come. Advanced processing techniques such as deconvolution and migration can help increase both vertical and horizontal resolution (Yilmaz 2001), but this chapter focuses on the resolution of the unprocessed seismic wave.

As stated above, vertical resolution is how close two objects can be placed to be distinguished separately. The oncoming wave has a dominant wave length in which anything smaller than this wavelength will cause tuning and not image each feature independently. The dominant wavelength **λ** can be calculated from the velocity of the wave **v** and the dominant frequency of that wave **f**.

$$\lambda = \frac{\vec{v}}{f} \tag{6.3}$$

For the case of tunnel detection, we can assume that the first arrival wave speed should be in the range of 600–2000 m/s and the dominant frequencies produced by a sledge hammer or the weight drop striking a plate on the ground are on the order of 20–60 Hz. Given that the wave speeds in the near surface are on the order of 300 to 2000 m/s the seismic wavelengths will range from 5–100 m, which is drastically greater than the dimensions of the tunnel. For most cases you can still resolve an anomaly in the range of λ/4; this depends on the S/N ratio, and in some cases anomalies up to λ/8 can be resolved (Widess 1973) where constructive interference occurs between the top and the bottom of the reflector. These considerations are for seismic thin beds but the theory also applies to small anomalies.

Horizontal resolution is the ability to see two separate laterally offset events and distinguish each independently. For a wave field to adequately detect the presence of a tunnel, we need to be able to resolve a single object. We will assume that the only way to distinguish a horizontal object is that it must be larger than half of the Fresnel zone width (Yilmaz 2001). The Fresnel volume width is the region over which a reflected wave will interfere constructively and thus we will not see two independent events. The size of the Fresnel zone depends on the frequency and velocity of the incoming wave and also the velocity and depth of the reflector.

In tunnel detection it is generally assumed that we are trying to image only one structure and that is the void of the tunnel itself; but in reality the "tunnel" is more than this—the first item being the void in the ground that is filled with water or air and the second item being the tunnel casing; the casing is usually a thin layer comprised of wood planks, concrete, or other support material surrounded by native rock. The final zone (usually not discussed) is the damage zone in the vicinity of the tunnel. In weak soils this could be produced by the boring of the tunnel and also by the stresses concentrated in the vicinity of the void. Considering all of this and taking vertical resolution into account, we need to figure out what the seismic wave field is seeing when entering a possible tunnel location.

6.1.3 RAY LIMIT APPROXIMATION

The other resolution consideration is related to the ray limit theory. The limit of resolution in travel time tomography is based on the ray approximation where we can assume that the ray tracing will generally break down when the scale of the anomaly is on a size similar to the wavelength (Williamson 1991).

$$r_{min} \approx \sqrt{L\lambda}, \qquad (6.4)$$

where r_{min} is the radius of the first Fresnel volume, L is the propagation distance,

and λ is the wavelength of the seismic wave. This means there will be higher resolution at higher frequencies and lower resolution with longer wave propagation. The resolution of travel time tomography also depends on ray tracing theory and the reliability of ray tracing in image sharp contrasts or diffractions

and postcritical wave behaviours. Studies using ray tracing programs have been performed to see how sharp boundaries are handled. The ray tracing programs assume constant velocity in the vertical direction, generally, and thus will smear a sharp boundary into a gradient or an area (Sheehan et al. 2006b). The reasoning for this is that the wave resolution and the regularization algorithms used assume constant horizontal velocity distributions which cause the smear.

6.2 REFRACTION THEORY

Seismic refraction tomography images the subsurface by inverting the observed travel-times of the first arrivals of the direct and the refracted waves to produce an accurate velocity structure of the subsurface. This is done by inverting the travel time data for both the refracted and direct arrival P-waves into a 2D grid whose cells are to be populated with the wave speeds. Since in most refraction methods we are measuring the velocity of a single source receiver pair, the image that is gathered can change laterally as well as horizontally.

Refraction methods in the past were used to find the base of the weathering layer; this information is important when correcting for near surface effects (static corrections) in reflection seismic imaging. Methods of carrying out such analyses include the intercept-time method (Edge and Laby 1931), the delay time or Gardner method (Gardner 1939), the plus-minus method (Hagedoorn 1959), and the generalized reciprocal method (Palmer 1981). These techniques all assume rather simple geometries of the near surface materials; as they are based on systems of linear equations they are able to solve for vertical changes in the subsurface, but they will not be able to distinguish horizontal features. The goal of linear methods is to image the base of weathering and apply that static corrections to normal moveout (NMO) corrected seismic reflection data.

A linear inversion that tries to synthetically trace the seismic wave as it would propagate through the subsurface was first developed by Hampson and Russell (Hampson and Russell 1984) and is known as generalized linear inversion (GLI). This method is a layered base method that inverts the subsurface as continuous layers and does not truly model horizontal variations. This method works by ray

tracing through an initial model, constructed either using prior knowledge of the subsurface or by educated "guessing" to provide a series of traveltimes that are compared to those picked (observed) in the seismograms. GLI assumes that the seismic velocity within the layer is constant and thus the depths of the refractors can be calculated. However, this method also suffers from not being able to truly distinguish lateral variations in seismic wave speeds.

The basic premise for tomographic inversion is similar to GLI methods, except the velocity model is now gridded into a 2D mesh instead of layered. Ray tracing methods have four requirements: (1) an initial model to begin the calculations, (2) a forward model solver for the ray paths in order to obtain theoretical traveltimes (synthetic picks), (3) a regularization scheme, and (4) an inversion method to solve for both velocity and depth. The initial model does not have to be indicative of the true geological model, but can help reduce the number of iterations that are needed; the modeling should eventually give comparable results (Lanz, Maurer and Green 1998). This being said, use of a completely wrong geological model can lead to a bias in the inverted model (Kissling et al. 1994). The forward modeling program needs to be able to create synthetic picks, and be able to compare them to the original picks. The inversion needs to be able to calculate the difference between the first signal arrivals and to update the velocity model according to the residual of the travel time file. The inversion then iterates this procedure until a predetermined stopping criterion is encountered. The inversion must converge to comparable results despite using different initial models.

6.2.1 REFRACTION INVERSION

Two tomographic modeling programs were used in this study. The Rayfract™ (Intelligent Resources Inc.) program uses a wavepath eikonal traveltime (WET) inversion based on the work of Schuster and Quintusbosz (Schuster and Quintusbosz 1993). SeisOpt® ProTM software (provided by Optim Software and Data Solutions, USA) is a generalized simulated annealing approach based on the work of Pullammanappallil and Louie (Pullammanappallil and Louie 1993). Both programs were used for inverting the tunnel data but due to the

large computational cost of simulating annealing, SeisOpt Pro was not employed at all tunnel sites. The Rayfract software license resides at the University of Mississippi in Oxford, MS, and the tomographic calculations were done by our collaborators, Dr. Craig Hickey and his associates. The two inversion programs are described briefly below. Both tomographic programs use a finite difference approach to solve for the ray path location, but the inversion and updates of the velocity model differ significantly. The results of the tomography are then displayed with depth on the y-axis and the surface location on the x-axis; the velocity is displayed as a color bar and each grid location is filled in with a color that designates its velocity. Smoothing is applied to the data to make the model look continuous.

6.2.1.1 Rayfract

Rayfract™ models rays using a finite difference back propagation method. The finite difference modeling program is based on back propagating the rays and calculating the travel times (Vidale 1988), these travels times then are used to solve the wave eikonal equation (Qin et al. 1992). This inversion was then made faster and just as accurate using the WET technique (Schuster and Quintusbosz 1993). This back propagation technique uses a Fresnel volume approach which incorporates the finite wavelength of the real waves and the influence of adjacent ray paths up to half of the period of the fastest waveform. This program uses the following procedure.

(1) The first arrival travel times (either of the refracted or of the direct wave) are picked from the seismograms.

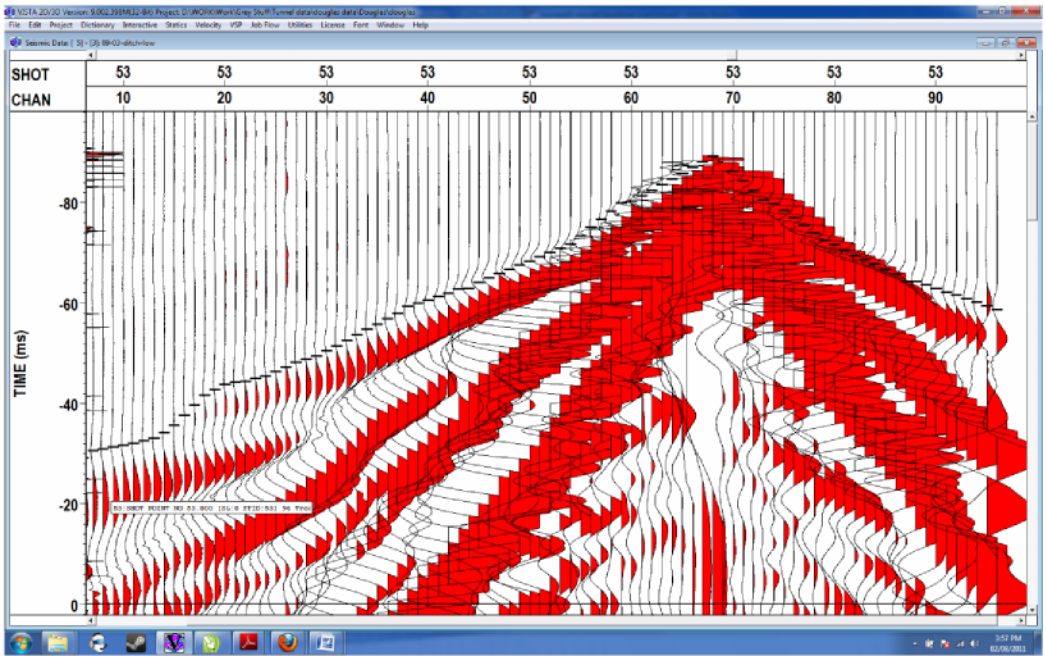

Figure 6-3 Seismogram with first arrival waves displayed in black; amplitudes are normalized using a mean scale. This was a 96 m spread length.

(2) The initial velocity model is proposed; in our case a 1D gradient model was used. The eikonal equation is solved using a finite difference method (Qin et al. 1992) to obtain the finite difference travel times. The travel time residual is calculated by subtracting the observed first arrival travel times and finite difference calculated synthetic ray traced travel times.

(3) A weighting function is solved for all points in the model to give a source misfit value. This misfit is a function related to the slowness; it is used as the velocity update.

(4) The slowness model is updated and these steps are iterated until convergence. This scheme can be seen in more detail in Schuster and Quintusbosz (Schuster and Quintusbosz 1993).

6.2.1.2 SeisOpt

SeisOpt® ProTM software is an algorithm that inverts the first arrival travel times using a nonlinear optimization technique called generalized simulated annealing (Pullammanappallil and Louie 1993). The technique uses a simple

simulated annealing and does not go into major details of statistical measures. The program splits the subsurface into numerous rectangular blocks of equal size; the dimensions are user dependent. The smaller the grid blocks the higher the resolution but the larger the cost of computation. The travel times have the ray tracing calculated by finite difference modeling based on the work of Vidale (Vidale 1988). The simulated annealing approach tries to determine an optimized model using a statistical approach and trying to find the global minimum least squares error. The algorithm proposed by seismic imaging (Pullammanappallil and Louie 1993) is presented below.

1) Pick the first arrivals in the observed data set.
2) Using finite difference modeling, the synthetic first arrivals are picked for the proposed initial model.
3) An error function is calculated comparing the observed travel times and the calculated first arrival times, using a least squares approach. This can be seen in the equation below,

4) $$E_i = \frac{1}{n}\left(\sum_{j=1}^{n}\left(t_j^{obs} - t_j^{cal}\right)^2\right) \qquad (6.5)$$

where E is the error function, n is the amount of travel time per shot record location, j is the actual travel time, and t^{obs} and t^{cal} are the observed and calculated travel times, respectively.

5) The current model velocity field is perturbed by randomly adding constant velocities in different neighbouring boxes in the model. This procedure is statistically random and the change can be any velocity within a range that is given. The new model has new travel times calculated and thus a new error calculation, E1. The purpose of this step is to avoid local minima of error (Eqn 6.5).

5) The new model is accepted if the error is less than that of the previous model $E_1 \leq E_0$, and when $E_1 > E_0$ is accepted; sometimes the model is accepted provisionally based on an annealing probability cooling function (Pullammanappallil and Louie 1993). This probability is used as a kick function to prevent the model from stopping in local minima in the search for the global minima. The probability can be seen below:

$$P_c = \exp\left(\frac{(E_{min} - E_1)^q \Delta E}{T}\right), \qquad (6.6)$$

where $\Delta E = E_0 - E_1$ the change in error, T is the temperature for annealing, q is an empirical parameter, and E_{min} is the least squares error at the global minimum, usually close to 0. This probability can "kick" the inversion out of local minima, but in later iterations and when the model approaches the global minimum it decreases the probability of a new model being accepted. The rate of cooling is the process of decreasing the value T; T is quite a large number in the beginning to help get to a good model. This large T increases the probability that a new model will be accepted even though the RMS error is high, to help kick the model out of local minimas. As the iterations increase, the value of T is lowered as it approaches a global minimum; eventually T is so low a new model cannot be accepted (Pullammanappallil and Louie 1993).

6) This process is iterated until the inversion reaches a predetermined error criterion. The convergence conditions require the difference in the least square model between consecutive models to be minimal and the probability to be very low that a new model will be accepted.

6.2.2 METHOD

The data collected in the field went through a similar processing scheme in both refraction tomography programs. A common processing scheme was used because the data were being processed at two different locations. The procedure is outlined below.

1) The shot gathers that are in SEG-2 format are imported as a single project with all the shot gathers that were used for inversion. To do this, vertical stacking at each shot location of common shots needs to be done to get unique shot records or only one shot gather at each location is inserted.

2) The shot-receiver geometry is checked and additional header information is inserted for each case. Since the geometry is only inserted for shot records, additional information such as source receiver offset, field station numbers, etc., is needed to see the seismic data in other domains. The geometry is then subjected to

quality control where the headers and seismic data are compared to field record notes. Bad traces are removed and traces that can't be properly picked are removed to avoid contamination of the solution.

3) The first arrivals are initially picked automatically as shown in Figure 6-3. To do this an amplitude gain is applied ranging from 0–12 dB in order to boost the visibility of the attenuated arrival at far offsets relative to those on traces near the source. A general mean normalization is performed to obtain consistent wave fields for easier picking. No automatic gain control (AGC) or other processing is performed during the first break arrival process.

4) First breaks are calculated from an automated picked an are checked for consistency and picked manually if they are bad. If no energy of the first arrival can be seen then it is ignored (i.e., not included in the calculation of error).

5) These picked first arrival times are then inverted for the velocity tomogram using one of the algorithms shown above. Most models were processed with Rayfract™ due to time constraints but some were done with SeisOpt® ProTM. The initial models were used as a 1D gradient model for Rayfract™ and a homogeneous layer for SeisOpt® ProTM. Default parameters are generally used with 20 iterations for Rayfract™, and around 50,000 for SeisOpt™, corresponding to about 10 minutes and 4 days, respectively.

6) The velocity and ray tracing image are then displayed. The ray tracing is compared to the velocity model to check for consistency and geological accuracy. The number of iterations could either be increased if the RMS error still shows substantial decay, or decreased if the model is too smooth and horizontal features are not resolved.

6.3 Oxford, MS

Seismic data were first collected over the tunnel sites in Oxford, MS, where we tried to detect the presence of culverts on an abandoned railway tunnel. The test sites that are going to be shown use the program Rayfract™ and both the refraction tomogram and ray tracing coverage will be shown. The refraction tomography that uses Rayfract™ was done by Dr. Craig Hickey and his colleagues at the National Center of Physical Acoustics (NCPA). Similar to what was seen in electrical studies, the ray tracing gives us an idea of the forward modeling and

how well the inversion will be able to resolve the features. The ray tracing and velocity image of the subsurface change due to differences in elastic parameters (Baker 2002). The elasticity of the soil is dependent on the cohesion, degree of cementation, and water content. These parameters are what are considered when interpreting the subsurface. The seismic surveys carried out in Oxford, MS, had refraction tomography applied to the first arrivals of the seismic waves. As will be seen below, a velocity and/or ray density anomaly at the location of the tunnel was detected in six out of the nine surveys conducted. The results from three tunnels are presented to illustrate cases: (i) the tunnel was not detected (failure), (ii) the tunnel was detected easily, and (iii) the tunnel was located only after additional processing.

6.3.1 TUNNEL 4

Tunnel 4 is constructed of small concrete blocks and is approximately 5–6 m in depth. The tunnel site had loose gravel on the surface but most geophones could get good contact. The seismic spread laid out had a 1 m geophone spacing and was 96 m in length, roughly centred on the tunnel. The shot spacing was 1 m. The source was an accelerated weight drop 1.5 m laterally offset from the line of geophones and so was within 2 geophone intervals. The general rule of thumb is that the shot has to be within 2 geophone spacings in order that one may still safely assume that the ray paths fall within a vertical plane and 3D effects can be ignored. There was an elevation difference of only 0.6 m from the start to the end of the line so a horizontal datum was assumed. The waves arriving first from the weight drop produced enough energy that all first arrivals could be picked in the spread. In refraction tomography the depth of investigation is approximately 1/4 the size of the spread length. Figure 6-4 shows that the tomogram images down to about 40 m (that is how deep the ray paths interrogate the earth) but the good data were seen only up to about 25 m, we see this since very few rays are going past the 25 m mark. The spread length was 96 m so the data is getting down to 1/3 of the depth vs. spread length ratio. The only anomalies that are considered are the ones that should be within the Fresnel volume of the rays; anything outside the ray coverage of most rays will be ignored.

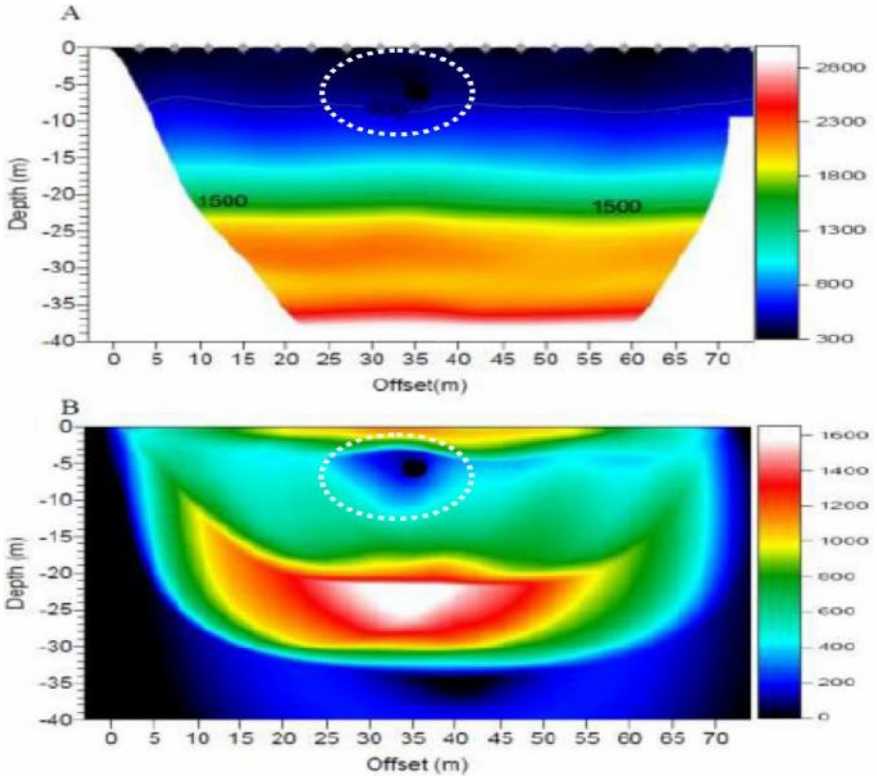

Figure 6-4 Seismic refraction result for tunnel 4. (A) Refraction velocity image. (B) Ray coverage map. The black dots are the approximate location of the tunnel. The highlighted region indicates the anomaly. The inversion used a 1D gradient initial model and 20 iterations.

Data were inverted for the entire dataset of first arrival waves; there were approximately 7000 rays in this region. The high resolution spread was then inverted with 20 iterations using the WET tomography from Rayfract™ where we assumed a vertical gradient mode. The initial model was based on the linear move out (LMO) velocity which is the velocity taken to flatten the first arrivals, this is just the arrival speed of the direct wave. The gradient model is a vertical change in velocity that assumes constant horizontal velocity. Figure 6-4 shows both the velocity tomogram and the ray density coverage from the finite difference modeling. Looking at the velocity structure we can see some perturbations and some long wavelength changes in the horizontal direction but only a slight drop down in the velocity structure. This is similar to what was seen in other subsurface void test sites (Cardarelli et al. 2010, Belfer et al. 1998, Karaman and Karadayilar 2004); realistically, it is difficult to show the existence of the tunnel from this tomogram alone. What is more interesting, however, is the ray density coverage image that has a region of low ray coverage in the vicinity of the tunnel. This is anticipated

because, as discussed in the earlier theoretical sections, the velocity of the air in the tunnel (-P343 m/s) is substantially lower than that of the surrounding materials (-P600 m/s), and as such the first arriving rays cannot pass through the tunnel. The low ray coverage does give an indication of a tunnel. However, similar to what was seen by Sheehan et al. (Sheehan et al. 2006b), the region sensed in the tomogram is actually much larger than the tunnel itself, likely due to the disruptive influence of the regularization program.

6.3.2 TUNNEL 6

Tunnel 6 at a depth of 6.5 m, had similar dimensions and construction to tunnel 4, but was not detected with the initial survey geometry and processing. The spread length used was the same as for tunnel 4, 96 m with 1 m geophone spacing, but in this case, because of the differing velocity conditions, most of the rays penetrated at least to 15 m which was below the level of the tunnel. The tunnel anomaly is technically there but, due to the masking of velocities by the color map, the small change in velocity and ray coverage made it impossible to see the tunnel at first glance. To get around this, the tomography used only stations 32–72 with the corresponding shots. This was just a perception issue and was used to be able to see the tunnel anomaly with the naked eye. We can see this in Figure 6-5 where the refraction tomography for tunnel 6 and the ray coverage is shown. If we take the rule of thumb that 1/4 the spread length is equal to the depth of investigation, then the data are still good to 10 m and the tunnel location is 6 m. Figure 6-5 shows that the velocity anomaly has a significant drop down in velocity to the other layer and the surface seismic velocities are on the order of 400 m/s. This is why we don't see the tunnel clearly, since the surrounding rocks have a similar velocity. Looking at the ray tracing map we see that there are vanishingly few traces going through the approximate location of the void while the rays bend around it both on top and below. Therefore both refraction and ray coverage show the presence of a slower velocity and thus indicate the presence of a tunnel.

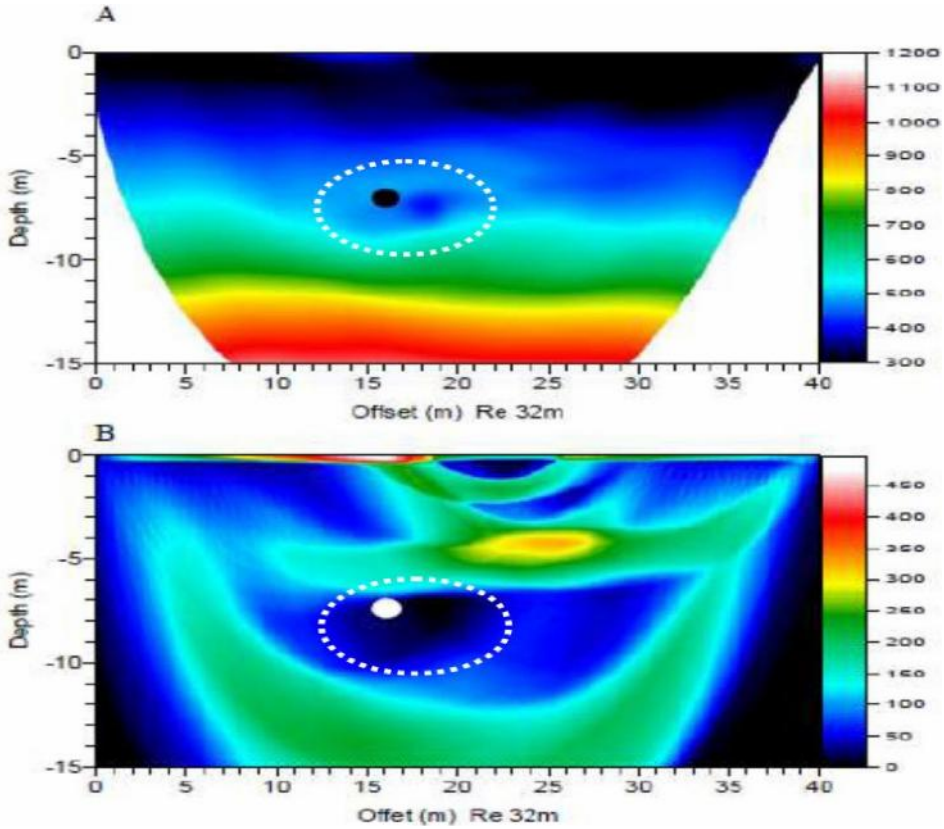

Figure 6-5 Refraction tomography of tunnel 6 where (A) is the refraction tomogram and (B) is the ray coverage of the plot. The tomography has had its spread shortened to zoom in on the site. Most rays were going in past 15 m so the spread was shortened to stations 32–72. The white and black circles are the approximate location of the tunnel. The inversion used a 1D gradient initial model and 20 iterations.

6.3.3 TUNNEL 1

The tunnel 1 site was the deepest and tunnel 1 was one of the largest tunnels at the Oxford, MS, site. The spread length used was 120 m with 1 m geophone spacing and 1 m shot spacing. The accelerated weight drop was used in this survey and had enough energy to produce acceptable first arrival waves across the entire spread with a low gain applied. The first arrivals were clean and only a minor batch of bad geophones had to be killed for the tomography. Figure 6.6 shows the approximate velocity tomogram and the ray coverage plot for this tunnel location; the black dots indicate the approximate location of the tunnel. There is no significant drop down in velocity around the tunnel location, actually, many rays are traveling through the tunnel location. The near surface

velocities range from 400–800 m/s which is faster than the velocity in air and the rays in the trace nearly all go at least 15 m deep. Looking at the ray coverage we can see a reliable inversion down to about 30 m and an acceptable solution all the way to 45 m in some parts. This test shows that the seismic image here has passed the ray limits for this survey site and was not able to detect the tunnel. The velocity model shows some slight horizontal variations, but mostly only a general increase in velocity with depth is calculated. With postprocessing the same result was found when trying to lower the spread size since the rays around the tunnel indicate a faster anomaly there, not a slower one. The interpretation is that the resolution of the seismic wave cannot detect the presence of a tunnel; this tunnel is just too deep to be detected in this environment. The combination of loose gravel and slow near surface materials results in steeply propagating waves that travel to deeper depths with the result that the ray path coverage through the tunnel is limited. The data collected were good and the first arrival waves that were used were consistent and had very few poor picks.

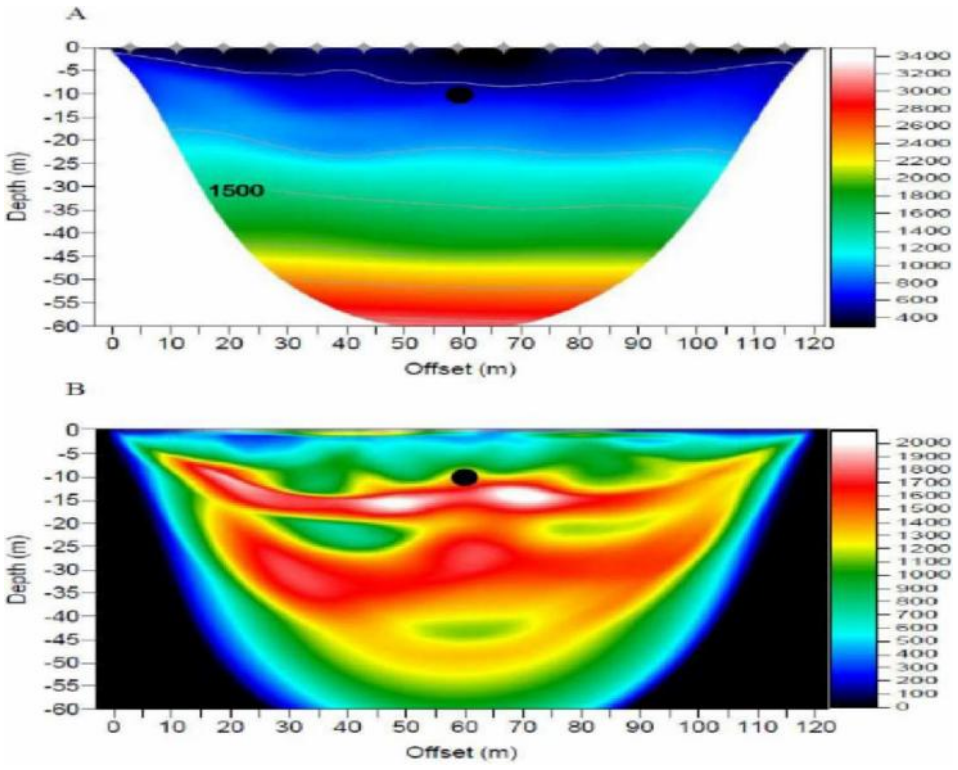

Figure 6-6 The tunnel 1 location. This site has an approximate tunnel depth of 10–12 m and is a approximately 1 m wide. (A) Refraction tomography of the subsurface of depth up to 60

m. (B) Ray coverage plot showing how the rays traveled through the subsurface. The inversion used a 1D gradient initial model and 20 iterations.

6.3.4 DISCUSSION

Nine different test sites were measured at Oxford, MS (see the Appendix for details of each site). Tunnels 1 and 8 and the dam site could not be detected. Although some of the remaining sites required additional processing, the existence of a tunnel, or more precisely the zone of disturbed materials surrounding a void, was detected. The most important finding of this investigation is that the ray coverage density maps highlighted the location of the tunnel much more effectively than the velocity tomogram.

Additional processing was not successful at the tunnel 1 site and the dam site, probably because the near surface conditions did not allow sufficient refracted energy to be detected.

This study has not produced a definitive indication of tunnel existence. Even in some of the "successes" the evidence for the tunnel, known to exist in reality, was tenuous; and complementary schemes to reduce detection failure (both false positives and negatives) are necessary and will be discussed in chapter 7. The experiences gained at the Oxford, MS, site were used at the Douglas, AZ, site to increase the chance of finding an existing tunnel. The key factors that were changed in data acquisition at the Douglas, AZ, site were:

1) Use of a sledge hammer as the source to limit the effect of lateral ray tracing of the seismic waves.
2) Use of a sledge hammer as the source to decrease the noise produced by the engine used to operate the hydraulics of the weight drop source.
3) Use of broader band geophones with lower frequency cutoff geophones to increase the sharpness of the detected refracted pulse.
4) Geophone spacing was decreased to increase lateral resolution and allow for denser ray path sampling.

6.4 DOUGLAS, AZ

At the Douglas, AZ, site at the U.S.-Mexico border, urban barriers like fences, paved roads, ditches, and the significant barriers at the border itself only allowed for surveys of the roadside and a ditch to be carried out.

The roadside data site was along a road parallel and adjacent to a high wire metal fence. The surface consisted of hard gravel that made the proper planting of geophones difficult. The geometry of the paved streets forced the centre of the geophone profile to be offset from the tunnel. Nearby traffic noise was a minor irritant at this site. The roadside site was interesting in that a number of shallow boreholes had been emplaced by earlier researchers who had hoped to use cross well tomographic methods to image the tunnel; to our knowledge this work is not available to the public.

The other data site was a deep ditch running parallel to the road; the ditch had been dug recently to provide an additional barrier to crossing the U.S.-Mexican border and, fortunately, had not yet been paved with concrete. This site, too, was contaminated with traffic noise on a busy parallel road immediately across the fence in Mexico, although the depth of the tunnel appeared to reduce this problem.

At the Douglas, AZ, site, refraction tomography was performed at the roadside borehole tunnel site by SeisOpt® ProTM software (provided by Optim Software and Data Solutions, USA) due to the capabilities of the program to handle borehole tomography. The seismic refraction data along the surface was processed by Dr. Craig Hickey of National Center of Physical Acoustics at the University of Mississippi using Rayfract™ software. The seismic data were collected using both 14 Hz and 40 Hz geophones and both surveys used swinging hammer blows as the main seismic source.

6.4.1 DITCH DATA

Seismic data collected in the ditch consisted of two surveys in which the 14 Hz or the 40 Hz geophones were used. As indicated in the last section, this was just a test to see if the seismic refraction wave arrivals did indeed depend on the frequency of the geophone and if our results were skewed. Both geophones gave very

similar results and the tomography was nearly identical. The higher frequency phones had less ground roll but the signal amplitude was comparable to that obtained with the 14 Hz geophones. The ditch profile was a 48 m seismic spread with 96 geophones spaced at 0.5 m; the tighter sampling was used to increase resolution as recommended on the basis of the earlier Oxford, MS, surveys.

Another difference between the Oxford, MS, and Douglas, AZ, surveys was that in the former the locations of the tunnels or culverts were unambiguously known as they could be easily seen. As the tunnel was completely buried at the Douglas, AZ, site, and because no exact information was available on its location, we could not guarantee that the observing geophone profiles were centered. The advantage of this is that this was closer to a true blind survey.

Examples of two shot gathers are shown in Figure 6-7 with the source either near the end or at the center of the spread; this result has a mean scale applied and a slight gain attached. The desired first arriving refracted signal is good but there is substantial surface wave energy. No reflections can be seen in the data; any reflections that would come off the tunnel would be in the top 100 ms.

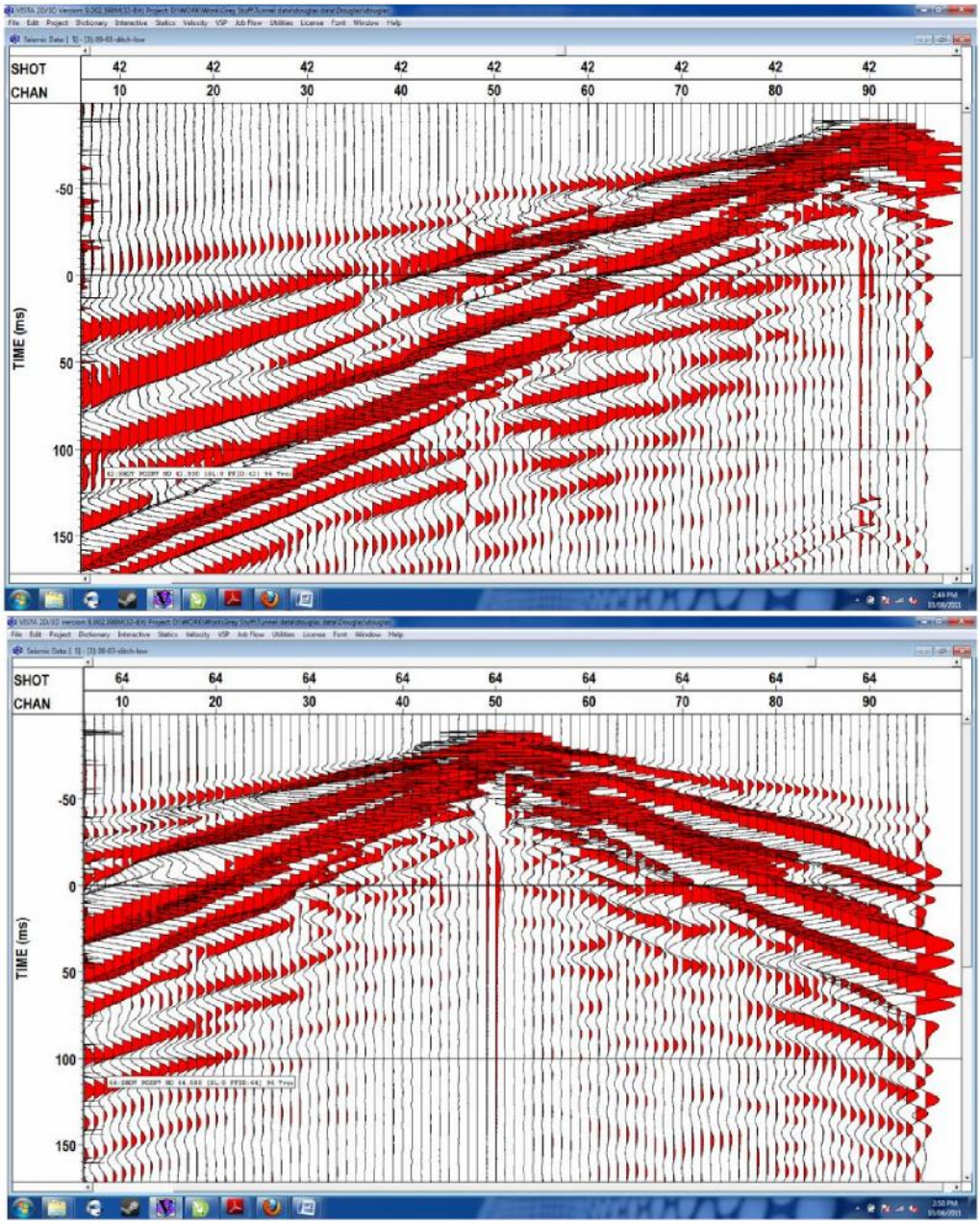

Figure 6-7 Sample shot gather for the Douglas, AZ, ditch site using 14 Hz geophones. Top: Shot record 42 with the shot at the 90th channel or 3 m into the spread. Bottom: The middle of the spread where the shot is at channel 50, or 25 m into the spread. The first arrivals can be seen clearly; only a gain and a mean scaling were applied.

The seismic data initially had the first signal arrivals automatically picked and then the bad ones were manually picked to the correct times. Overall, this set consisted of 97 shots with the 96 receivers that resulted in 9312 first break time picks deemed acceptable for the inversion. The starting model was the 1D gradient

model and an initial 20 iterations were done for the ditch data. The result can be seen in Figure 6-8 where the velocity tomogram is displayed with two anomalies located on it. These anomalies come from the ray coverage plot where we see a zone of low ray coverage. The approximate velocity of this tunnel site is significantly higher than what was seen in the Oxford, MS, test sites; at around 1000 m/s the ray coverage plot shows that most rays are traveling through around 10m down and very few rays go below this point. The two anomalies are label S1, which is around the center of the spread, and S2, which is on the end of the spread. Both these anomalies were marked since the result could indicate another tunnel

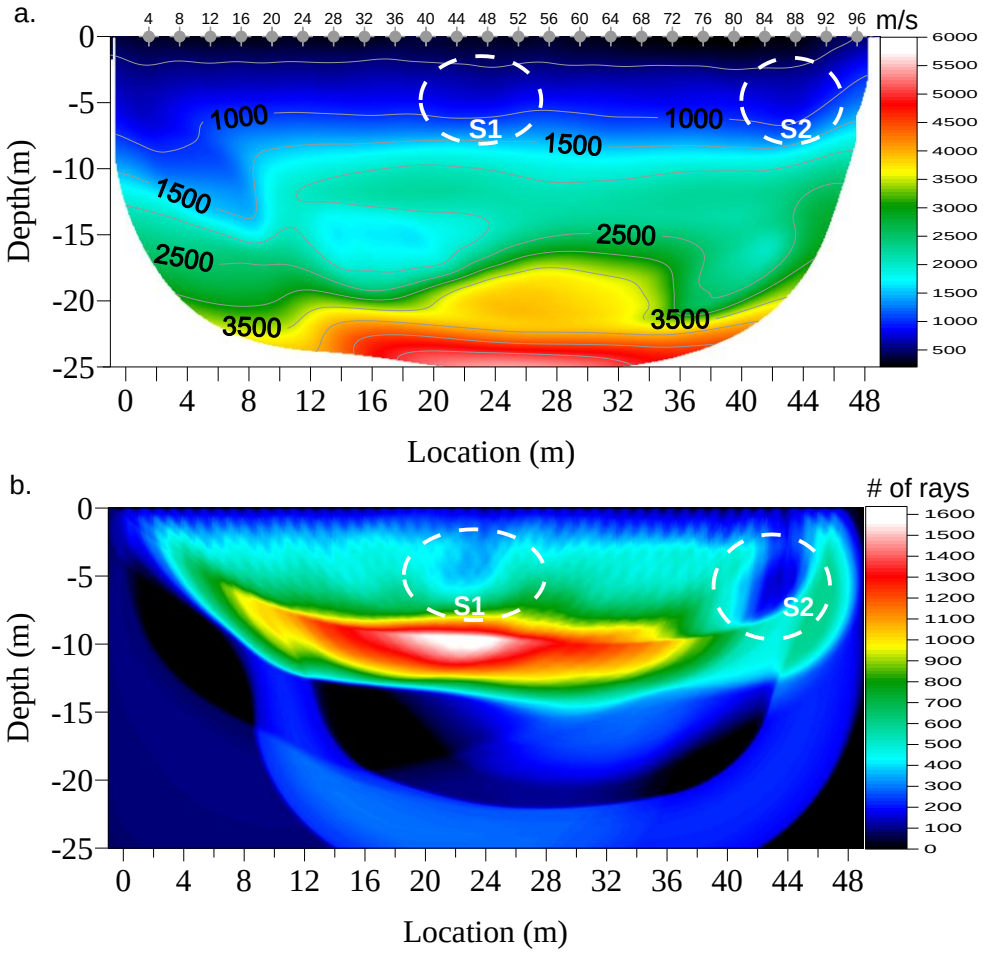

Figure 6-8 Refraction tomogram of the ditch at the Douglas, AZ, site. Top: The velocity tomogram which is a vertical cross-section of depth vs. surface location. Bottom: A ray coverage plot of how the waves traveled through the subsurface. S1 is labelled as a low velocity zone and is indicative of where the tunnel is; S2 is an unknown anomaly.

S1 in Figure 6-8 represents the tunnel location we were looking for. The location is slightly off the center of the refraction tomogram but approximately at the right depth, around 5 m in the ground. The seismic data were reprocessed using a shortened spread length that focused around the S1 anomaly. This is a perception issue so we can see the ray coverage, similar to what was done for tunnel 6 in Oxford, MS, using smaller offsets. To look at this we used only stations from 12 m–36 m giving ample coverage to see the anomaly. With this reduced data set, at 20 iterations the anomaly was detectable but the image continued to improve with every additional iteration. The final result at 50 iterations is shown in Figure 6-9 where the top figure shows the velocity tomogram, the middle figure shows the ray coverage plot, and the bottom figure shows the threshold ray coverage plot to better delineate the paucity of ray density at the tunnel location. The tunnel anomaly can be seen 1.5 m off the center of the spread, the velocity image shows a drop down at about 6 m depth. The ray coverage takes a banana shape with an elongated circle in the middle. The threshold ray coverage plot is used to better delineate the tunnel for easy referencing. This is done by setting a maximum number of rays that can go though; the minimum threshold should be reached in the region of the tunnel. The data show the approximate location of a low velocity zone which is around the tunnel location; the next site at the roadside has the tunnel quite a bit deeper and the surface conditions are substantially more problematic.

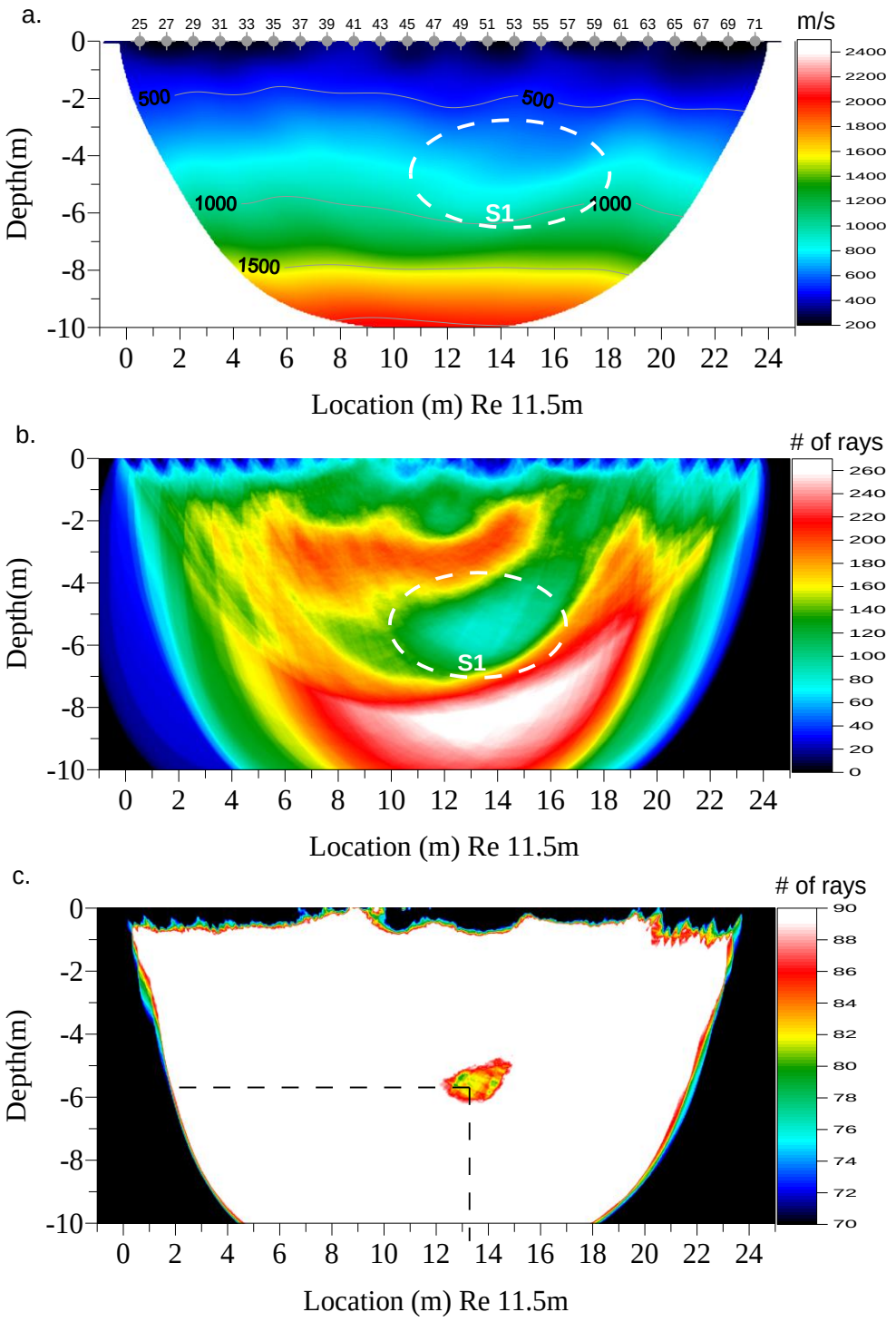

Figure 6-9 Refraction tomography for the Douglas, AZ, ditch site with reprocessing to enhance the S1 anomaly seen in Figure 6-8. Top: The refraction velocity tomogram showing the approximate location of the S1 anomaly and the dropdown in velocity observed. Middle: A ray coverage plot of where the rays traveled in the subsurface. Bottom: A threshold ray coverage plot showing the location where the fewest rays traveled. The hot spotting technique makes a bull's eye around the tunnel.

6.4.2 ROADSIDE SURVEY

The roadside survey was much more difficult than the ditch survey to implement. The near surface of the roadside was more heterogeneous than that of the ditch and there was substantially more traffic noise at the roadside site. In particular, the necessary first arrival signals were highly attenuated at distances greater than about 40 m from the shot point, primarily because wind and traffic noise amplitudes were comparable to the signal. The seismic data could be obtained only 18 m to the west side of the spread due to the presence of a paved concrete road.

A number of shallow boreholes were drilled for cross bore tomography, and during the surveys a downhole geophone package was placed in them to assist in characterizing the site. The downhole tool consists of three geophones mounted on a weighted gimbal system that allowed one vertical and two horizontal components of the wavefield to be obtained. When a seismic shot was taken we got a direct 1–way travel time and thus the results gave accurate velocity information. The seismic profile was 60 m long with a 0.5 m geophone spacing; the tunnel was located approximately 18 m from the west end of the spread. The borehole in which the geophone was emplaced was approximately 12 m into the spread. Multiple shots for purposes of stacking were taken every 1 m. As noted, the energy transmitted across the array was significantly attenuated due to poor coupling of the geophones to the hard ground and due to the low energy source employed. Consequently, not all of the first arrival signals could be reliably time picked on the eastside of the dataset.

The seismic survey carried out for seismic refraction tomography shown in Figure 6-10 used 14 Hz geophones, and the seismic data were inverted commencing with a 1D gradient and 20 iterations. Refraction results show that nearly all the rays are traveling through to 5 m of depth with, regrettably, few going any deeper. The velocity tomogram does not show the same anomaly; it shows an increasing velocity with depth, following the initial model. The few rays that go through cause the model to not be updated and thus we cannot get a good idea how the velocity changes at this test site. This reduction in depth of investigation could be a result

of a zone of better cemented sands and soils as were seen in the drainage ditch walls. This tunnel most likely will not be detected using seismic refraction techniques or using the first arrival signals; other techniques are needed to detect the tunnel.

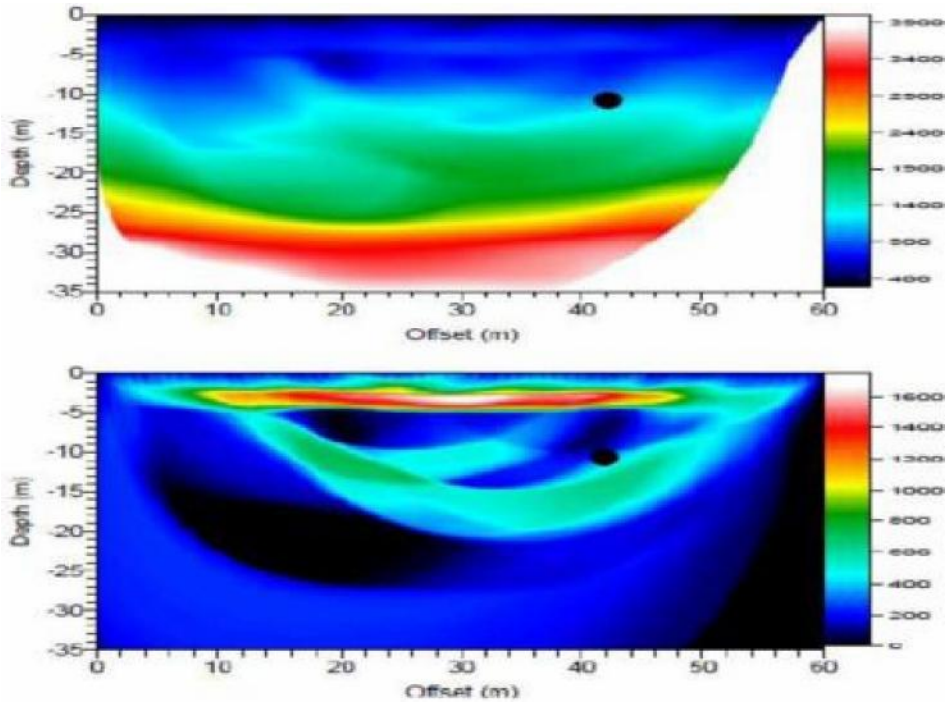

Figure 6-10 Results of the roadside refraction tomography using 20 iterations and a 1D gradient. Top: Velocity image showing the location of the tunnel at around the 42 m offset range and 10 m depth. Bottom: Ray coverage plot for the seismic signals that were recorded. Most the rays are trapped at around 3 m depth and thus the tunnel was not imaged.

Borehole data were also collected at this site using a 1 station walkway seismic survey, a technique known as vertical seismic profiling (VSP). In VSP the receiver location is constant and the source location changes. The goal was to see if the direct arrival of the seismic wave could detect the presence of the void and to see if the wave bends around the tunnel. The little amount of data and small geometry made it possible to use SeisOpt™. We used an initial constant velocity of 1000 m/s and iterated the procedure until the tomography converged on a result. Although there were only 100 first arrivals to fit, the inversion took around 2 days to run on one Windows computer, with a dual core Pentium 4, 2.0 Ghz processor and 4 Gb of RAM. The results can be seen in Figure 6-11 where the borehole and the approximate tunnel location are specified. The tunnel is

approximately 10 m in depth and 18 m on the surface. The length of the spread is large since some far offset data were acquired for this result. The borehole shows that some of the rays are curving around the tunnel and are actually traveling at a faster velocity. No rays passed underneath the tunnel except some from the far offsets, so the tunnel location is not truly seen. The results show that if another downhole tool were place in a borehole on the other side of the tunnel, solid evidence for the tunnel might be obtained. There is a change in velocity from about 400 m/s to 800 m/s at about the 7 m mark in the subsurface, this could be the velocity change that was seen in the surface seismic data. Thus, lots of holes and false artefacts in the data are observed with the simulated annealing approach.

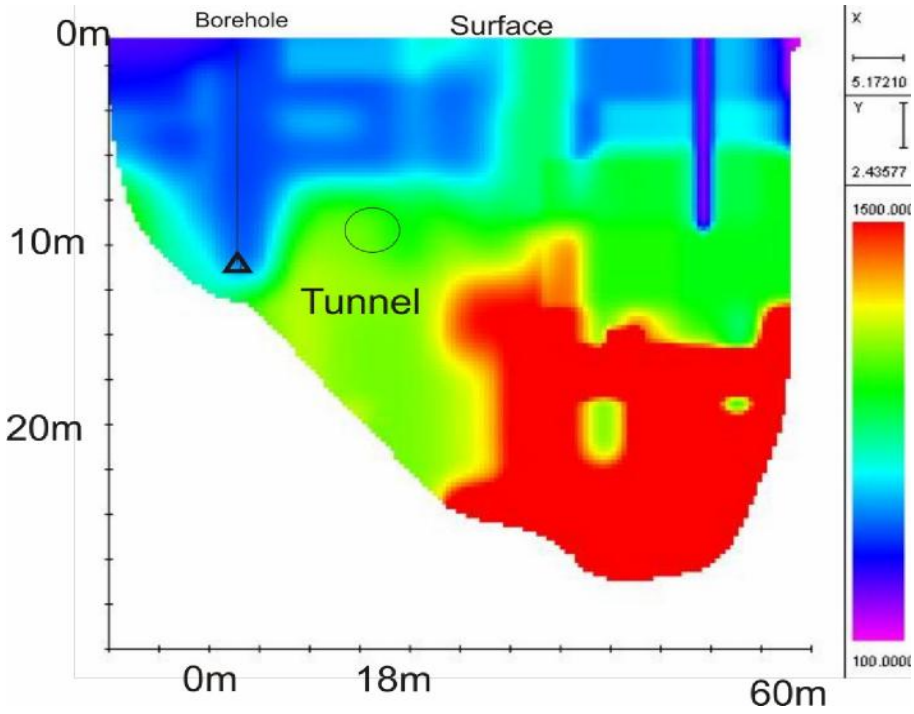

Figure 6-11 Borehole tomography using far offsets in the model. The tomography is zoomed in onto the length of the spread. The approximate location of the tunnel is shown and the velocity of rays bending around the tunnel can be seen. The rays are all above the tunnel location and very little data were retrieved from below the tunnel site. Only some of the far offset rays go around the tunnel and the red velocities do not represent real rays.

6.4.3 DISCUSSION

The results in Douglas, AZ, showed that refraction methods can be used to detect tunnels if the conditions are appropriate, but they also illustrate the limitations of the technique and the influence of noise, depth, and the actual geological

velocity structure. A good analogy is sonar, where submarines can use the low velocity SOFAR subsea channel to avoid interrogating ray paths and hence detection. Using smaller geophone spacing increased the resolution of the survey and increased the number of travel time picks. In the tests here, using different geophones had little to no effect and the seismic traces gathered were quite similar. Shortening the spread improved the identification of the tunnel as it made the window smaller, but a large survey is still needed, especially in cases where the actual location of the tunnel is unknown. The velocity drop down seen was minimal but using the ray threshold coverage plot helped to eliminate zones of low velocity.

6.5 SUMMARY

Seismic refraction tomography has proved to be a useful technique in identifying subsurface voids; the methods of data analysis were discussed in this chapter. Compared to what was seen in the modeling, the refraction method showed a reduction in velocity around the tunnel. Because the rays bend around the low velocity range of the tunnel, a ray coverage plot can indicate the presence of a tunnel. This was seen in the seismic ray tracing and was particularly evidenced by regions of low ray density coverage and, to a lesser extent, as zones of decreased signal velocity in the tomogram. The seismic wave does "see" the tunnel as in most cases it is below the resolving limits at the wavelengths employed. In Oxford, MS, the tunnel was detected in six out of nine sites and in Douglas, AZ, in one out of two sites using surface refraction tomography. Failures were a result of: (1) ray trapping in slow near surface materials that do not allow lower sections to be properly interrogated (e.g., the Douglas, AZ, roadside site), (2) ray trapping in slow near surface materials due to velocity gradients that force most of the ray paths to go deeper than the tunnel (e.g., Oxford, MS, tunnel 1), (3) high levels of cultural noise, and (4) the tunnel being too small and too deep. At some sites the anomaly was so small that additional processing was needed to ensure that the "detection" was not a false positive artifact. Very few surveys detected the tunnel distinctly. The reliability of the survey depended critically on the quality of the data acquired.

CHAPTER 7
7.0 JOINT INTERPRETATION AND FUTURE WORK

The previous two chapters discussed how seismic methods and electrical methods can be used to detect clandestine tunnels. The goal of this chapter is first to show how using both electrical and seismic methods can be used to delineate artefacts and improve detection, and second to discuss future work and how other methods could be used to detect tunnels on the U.S.-Mexico border. Third, some of the key issues associated with this study, such as repeatability and tunnel detection criteria for future work, are considered, and suggestions about how to resolve these issues are made.

7.1 JOINT INTERPRETATION

This chapter illustrates how seismic and electrical methods can be used to jointly delineate anomalies and how these methods can be used more effectively. One crucial issue is that both ERT and seismic refraction tomography methods detect most anomalies as highly resistive zones for ERT and low velocity zones for SRT, but knowing whether these zones are actually tunnels or whether they are false positive indicators is difficult. A low velocity localized tomographic image may or may not represent a subsurface tunnel. In situations of poor data this can be problematic as experimental errors in the travel times could result in false anomalies in the final tomogram. In a ray density coverage plot we should see very few rays in the presence of a low velocity zone, but the zone can be quite large. Further, depending on the local velocity structure, sometimes the rays are trapped by a high velocity zone, and don't go near the tunnel location. In electrical methods a subsurface void filled with air, which is highly resistive, suggests the anomaly may be a tunnel, but a water filled void might be missed because of the conductivity of salts in the water.

In near surface studies the amount of near surface heterogeneity (difference in the physical properties of the surface materials) can change quite drastically due to different levels of cementation and water saturation. The factors that will change the resistivity in partially saturated near surface rocks are the

ionic concentration, porosity surface conduction, tortuosity, and connectivity of fluid or conductive solid phases (Gueguen and Palciauskas 1994). For seismic methods the main factors that will change velocity in the subsurface are the lithology, porosity, fluid saturation, pressure, and temperature. (Yilmaz 2001). Both methods are sensitive to porosity and fluid saturation, but in addition, seismic methods are sensitive to the elastic parameters of the rock frame. Electrical methods are sensitive to fluid motion and how fluids move through the subsurface. When these factors are taken into account, methods can be devised to discriminate between false and positive anomalies.

Seismic methods and electrical methods can be used to delineate subsurface features such as sinkholes (Dobecki and Upchurch 2006) or even cavities (Piro et al. 2001), (Cardarelli, Fischanger and Piro 2008). Furthermore, electrical and seismic methods for joint inversion can improve the chances of tunnel detection (Cardarelli et al. 2010). All these studies found that the use of multiple geophysical methods increases the reliability of detecting subsurface voids. The electrical methods are very popular for void detection because of the contrast in resistivities between air (in the void) and near surface soils (van Schoor 2002). Electrical methods do not work well in zones of very resistive materials as it is difficult to get enough current through the rock. Zones of very resistive rock are generally indicative of stiff and fast velocity rocks where seismic methods can work as the void filled with air will be a low velocity zone. (Cardarelli et al. 2010). Data from both electrical and seismic methods were collected in this study to increase our confidence that the anomalies detected were subsurface voids.

To illustrate how the two methods complement each other, seismic and electrical results are discussed in detail for the Douglas, AZ, ditch site, and Oxford, MS, tunnels 1 and 5. The Douglas, AZ, ditch site is discussed to compare the tunnel related anomalies that were seen in both SRT and ERT images. The Oxford, MS, tunnel 5 site is discussed because two anomalies were seen in the dipole-dipole array and as such it is good to contrast this result with the SRT images to see if the image actually represents a tunnel. The Oxford, MS, tunnel 1 site illustrates a case in which neither of the methods were able to find an anomaly related to the known tunnel.

The Douglas, AZ, test site was already discussed in previous chapters but what we need to remember for this section is that both electrical and seismic methods were performed 3 m laterally offset from each other and both had similar spread arrays. Briefly, the seismic tomography had 0.5 m geophone spacing and a 48 m spread while the electrical method was a 50 m dipole-dipole array with 1 m electrode spacing as seen in Figure 7-1A. The electrical anomaly that was seen was inverted and two anomalies E1 and E2 were observed in Figure 7-2C. E1 is the approximate location of the known tunnel, but anomaly E2, which is slightly shallower and 6 m laterally offset, is very similar. The inversion creates both these anomalies so both have a legitimate chance to be the tunnel and if the location of the tunnel were unknown then confidence in the presence of the tunnel would be low.

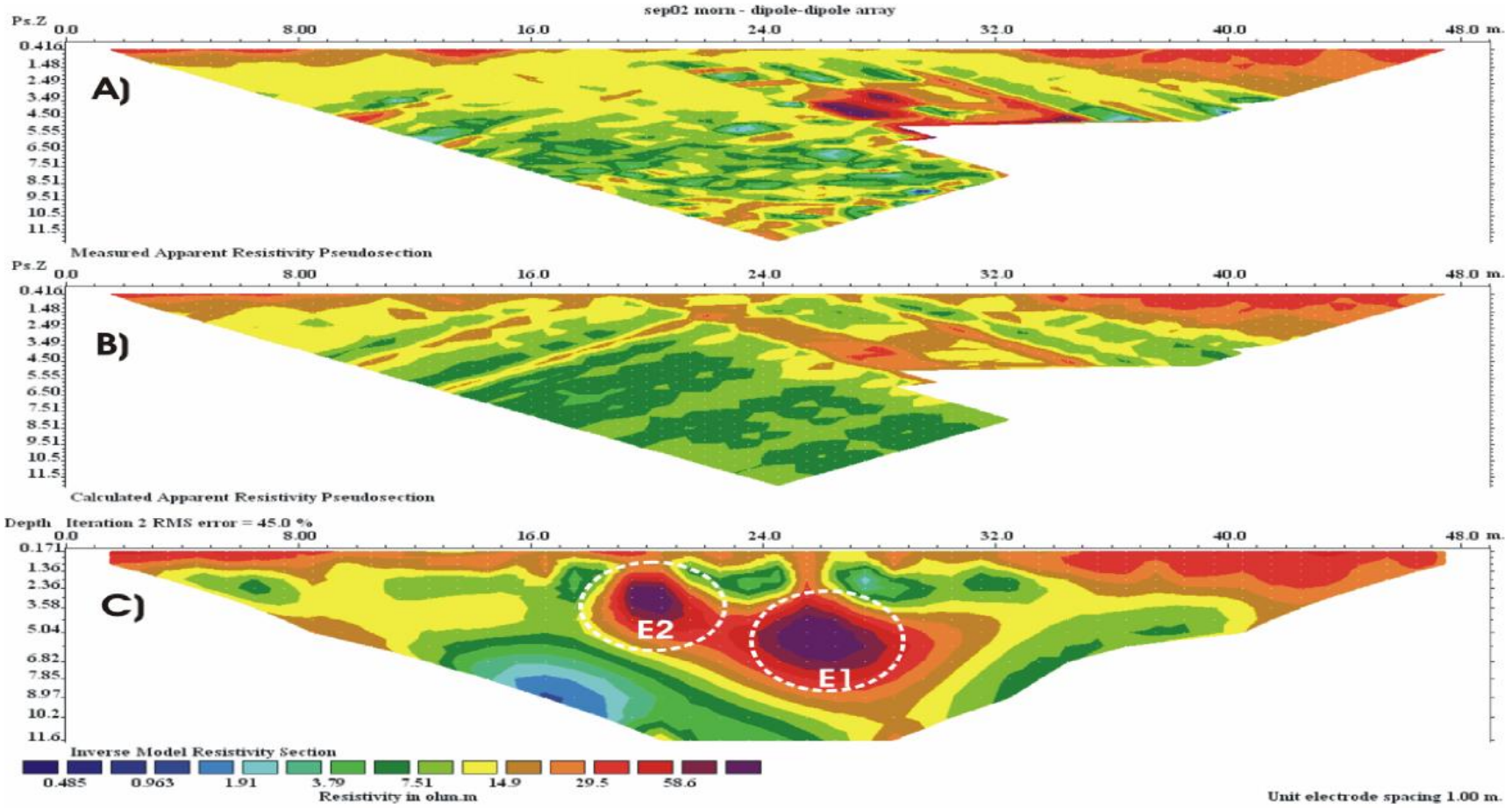

Figure 7-1 ERT image for the dipole-dipole array in Douglas, AZ. (A) The measured apparent resistivity pseudosection. (B) The calculated apparent resistivity pseudosection. (C) The inverse modeled resistivity section. The tunnel analogies are highlighted as E1 and E2.

The seismic profile was acquired 3m laterally offset from the ERT line. The initial SRT displayed two possible anomalies S1 and S2 in Figure. 7-2. In this case the two anomalies were both approximately 5m in depth but were laterally offset by 20m. Additional processing was carried out over the S1 anomaly but not at the S2 which was at the end of the spread. Looking at Figure 7-2 we can see the velocity image with the anomalies S1 and S2, these anomalies are seen as a lack of ray coverage but display only a slight drop down in velocity. The ray coverage shows a small amount of rays not going through the tunnel area, the confidence in this plot would be quite small if the location of the tunnel was not known.

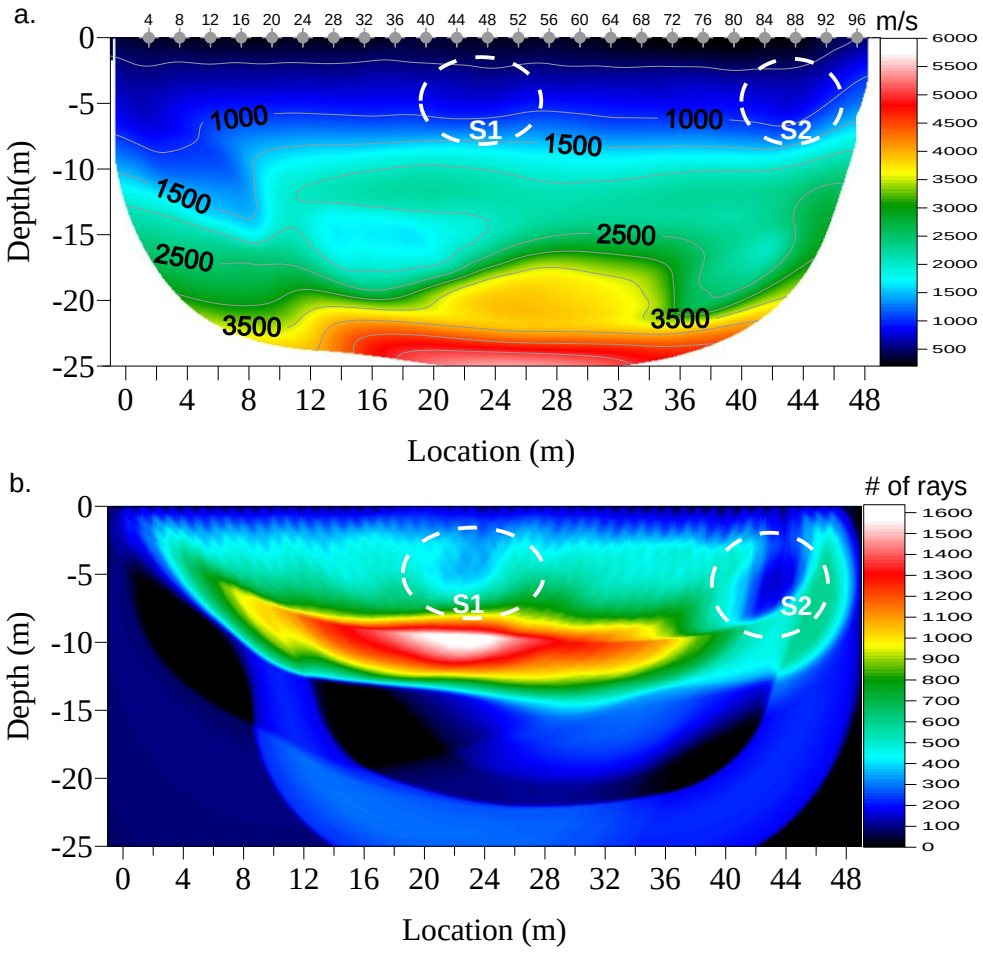

Figure 7-2 Refraction tomography for the ditch data in the Douglas, AZ, test site. Top: Velocity tomogram for the surface with both S1 and S2 anomalies present. Bottom: Ray coverage; the two zones of low ray coverage are the estimated tunnel anomaly sites.

Figure 7-1 and Figure 7-2 show that both methods provided a depth of investigation of approximately 12 m. The rock surrounding the tunnel had a resistivity of 10–30 ∼.m while the seismic velocities ranged from 200–1000 m/s. The resistivities are largest nearest the surface and decrease with depth which suggests increasing water content in the rock; around 10–15 m of depth the velocity is 1500–2000 m/s, indicative of fully saturated sandstones (Gueguen and Palciauskas 1994). The resistivity decreases with depth which may indicate increased fluid content in the sandstone, thus the location of the tunnel is in partially-saturated and relatively well consolidated material. Promisingly, the E1 (high resistivity) and S1 (low ray density) anomalies match the position well. In contrast, the E2 anomaly is resistive but there is no corresponding lowering of seismic velocity or ray coverage density in this location. The region around site S2 is fairly resistive compared to other areas but shows no resistive anomaly at this location. Use of both electrical and seismic methods has increased the confidence in detecting this tunnel location.

Oxford, AZ, tunnel 5 was an interesting site since the culvert was only 2 m deep and most of the other survey sites were a lot deeper. The electrical array used was 3 m laterally offset from the seismic array, and the seismic survey was only 24 m long. Figure 7-3 shows a 25 m dipole-dipole electrical array with 1 m electrode spacing; the electrical survey shows 2 resistivity anomalies where the approximate location of the tunnel is in the middle of these tunnel sites. We saw in chapter 5 that the electrical array shows the presence of an anomaly but the anomaly is quite large for a tunnel of only 0.4 x 0.4 m.

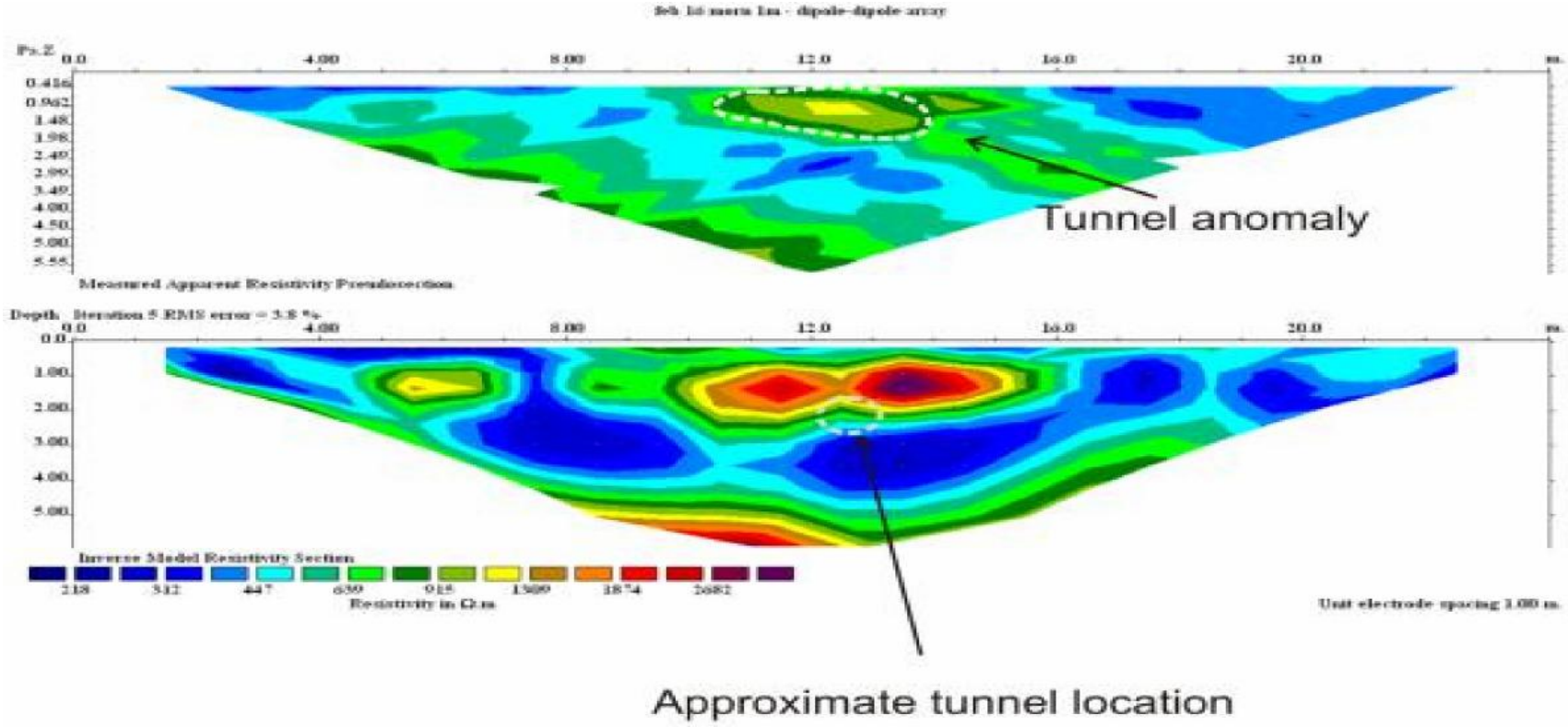

Figure 7-3 Tunnel 5 of the Oxford, MS, test site culverts; the tunnel is approximately 2–3 m deep and 0.4 × 0.4 m in dimensions. Top: The measured apparent resistivity pseudosection; there are 232 data points on a 25 m dipole-dipole array with 1 m electrode spacing. Bottom: Inverse model resistivity section where the approximate location of the tunnel is indicated.

The seismic data from tunnel 5 was not discussed in Chapter 6 so a brief overview will be given for the tunnel 5 test site. The seismic data were gathered from a 28.8 m long spread with 0.6 m geophone spacing and 0.6 m shot spacing. The seismic refraction arrivals had good energy throughout the whole spread; the velocity tomogram and ray coverage can be seen in Figure 7-4. The tunnel anomaly is indicated by the low ray coverage; however, there is only a slight velocity perturbation and it is not apparent at the approximate location of the tunnel.

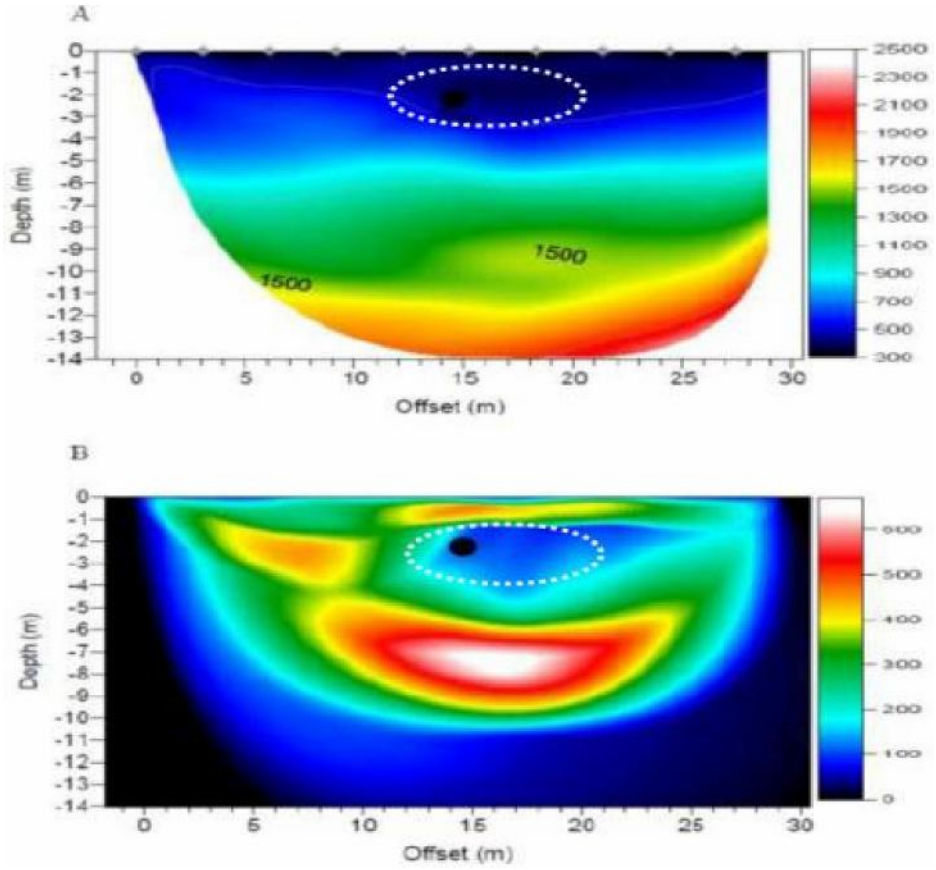

Figure 7-4 Refraction tomography for tunnel 5. (A) Velocity tomogram for the site; the tunnel is approximately 0.4 × 0.4 m and is only 2 m deep. (B) Ray coverage of the seismic site.

The tunnel anomaly seen in Figure 7-4 shows a large zone of low ray coverage and, in comparison to Figure 7-3, this is near the same position as the resistive anomaly. The tunnel site in this location was only 0.4 × 0.4 m in dimensions and it was partially filled with debris. This might be the reason why the anomaly that is seen is so large and why this whole region responded with low signal velocity. The velocity barely changes in this region because the velocity around the tunnel is

approximately 200–500 m/s, which is similar to that of air; thus the velocity model did not change. The low ray coverage indicates that most of the energy is traveling along the surface and then to the competent material below the tunnel. Looking at the resistivity model we can see that the resistivity of the tunnel anomaly is quite large and the resistivity of the surrounding rock is around 200–500 Lm. This is evidence that the anomaly cannot be partially saturated with water; the anomaly zone is probably filled with loosely consolidated sands with little to no water in this region. The area is still disrupted so the tunnel site is predicted to be quite large and could have been constructed recently or has been worked on recently. The survey showed low signal velocity, a low ray coverage zone, and a highly resistive region, however, the tunnel anomaly could not be detected confidently.

Tunnel 1 in Oxford, MS, was the deepest tunnel site and also one of the few sites that a team of seismic and electrical methods could not find any indication of a tunnel. The reason for this makes more sense when looking at both the electrical and seismic methods. Figure 7-5 shows the velocity tomogram for tunnel 1 site. The location responded with signals of fairly consistent velocity and the approximate location of the tunnel had a large amount of rays traveling through it.

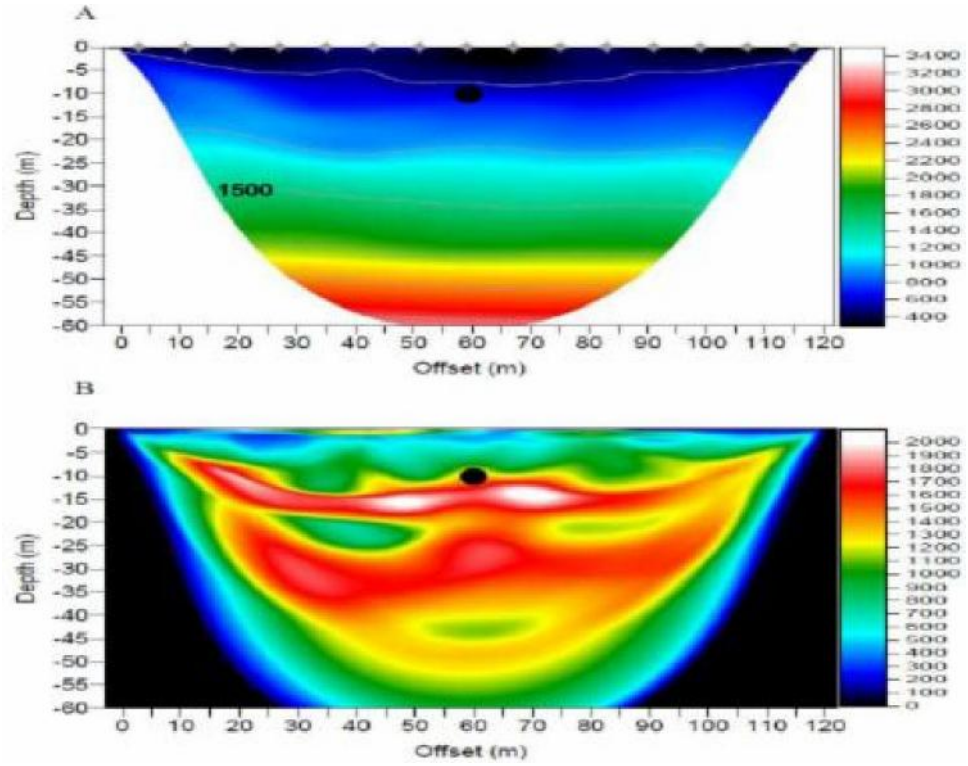

Figure 7-5 Refraction tomography for tunnel 1 in Oxford, MS. (A) Velocity tomogram. (B) Ray tracing plot. The black dot indicates the approximate tunnel location.

Tunnel 1 in Oxford, MS, was one of the few sites where the Wenner array and a dipole-dipole array were both done over the seismic profile. The electrical array was 100 m, similar to that of the seismic array which was 120 m. In the Wenner array shown in Figure 7-6, we see that on the left hand side of the array we have a resistive material and on the right hand side we have a region which is more conductive. The region on the left is fairly resistive with an approximate resistivity of about 750 Lm and the right side has an approximate rock resistivity of 200 dm.

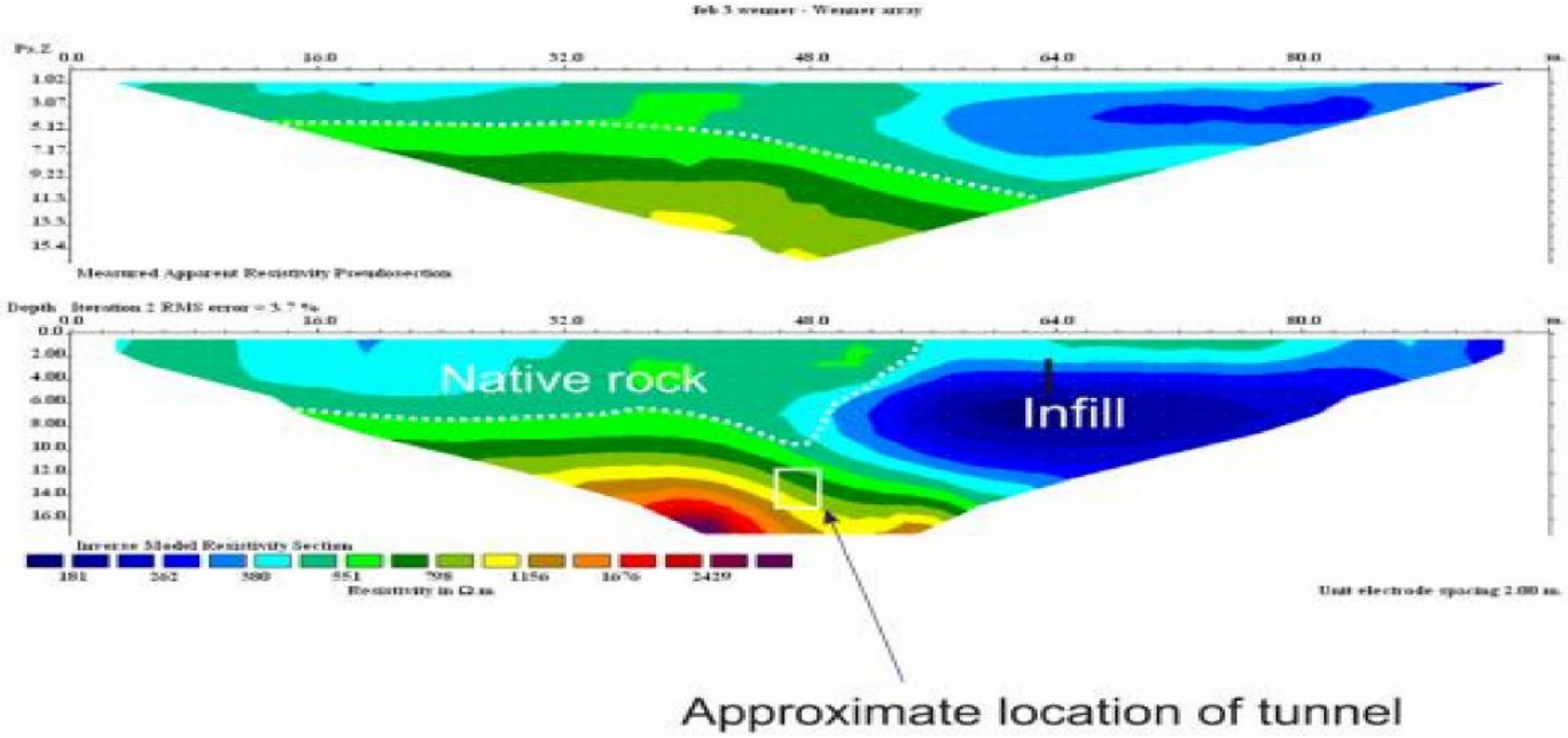

Figure 7-6 First survey performed in Oxford, MS, and also the largest. The survey has 2 m electrode spacing with a 100 m Wenner array. Top: Raw data gathered over the tunnel 1 site. Bottom: Inverted pseudosection to obtain true apparent resistivity.

Both the SRT and ERT methods could not detect the presence of a tunnel at the tunnel 1 site in Oxford, MS., although the tunnel was quite large. Figure 7-6 shows two regions of differing resistivity, indicative of two different materials. In contrast, the seismic image (Figure 7-5) is more laterally uniform with a consistent velocity. The ray coverage plot shows that most of the rays travel beneath the tunnel to about 12–15 m depth and then come back to the surface. The ray coverage shows a consistent number of rays traveling at least 15 m deep but some go as deep as 30 m. The change of resistivity of the different sides of the tunnel site can be seen in the Wenner array, but the seismic tomography does not take that into account. The site was believed to have had some repairs done to it after the insertion of the tunnel, but the material used for fill must have been the same material used in the construction. The interesting thing is that the construction appears to have happened all the way from the tunnel to a point past the seismic line. The seismic refraction method provides very little evidence for this and thus other seismic methods or electrical methods are critical. Other techniques that don't use the first arrival signal energy or techniques that use surface waves might be more beneficial in detecting some of these tunnel sites.

We have been able to show that seismic refraction and electrical methods can help to delineate some artefacts seen in the data. The use of multiple geophysical techniques also increases the likelihood that the anomaly detected is a true subsurface void and can also help us understand why the method did not work. Electrical and seismic tomography data were compared at all the tunnel sites to see if the tunnel was truly detected and also to see if any intricacies could be used to improve the interpretation.

7.2 FUTURE WORK

The goal of this thesis was to test the ability of seismic refraction and electrical resistivity tomography to find subsurface tunnels. While using refraction methods other seismic methods were entertained and tried to see if we could detect the presence of the tunnel. Other seismic methods were tested but could be taken further to get a better idea of their utility.

The first method used for tunnel detection was reflection profiling. A conventional processing scheme was used but the noise removal removed the actual reflection data. As no reflection energy could be seen the method could not be used. In the modeling chapter we showed that the tunnel should be able to diffract energy; that is, impinging energy should be reflected or diffracted from a tunnel surface. Numerous studies have used reflection profiling to detect abandoned mines (Yancey et al. 2007, Curro, Cooper and Ballard 1981) or delineate karst cavities. More advanced processing techniques in which the reflection profile is migrated to collapse diffractions have shown some promise in detecting voids. (Grandjean and Leparoux 2004). The main problem with using the reflection method to detect tunnels is that the tunnels are small relative to the wavelengths of the seismic energy and thus they cannot be properly imaged. Another problem is that reflections coming from a tunnel are usually swamped by the much stronger direct refractions and surface waves that arrive at the detector at the same time.

An alternative approach may be to attempt to image the diffracted seismic energy scattered by the tunnel. The full elastic wave modeling of Chapter 4 showed two strong diffractions: a P-wave diffraction and a P-SV diffraction. These diffractions are caused by the large variation in impedance between the tunnel and the surrounding earth material that acts, by Huygens's principle, as a new point source. The incoming wave could possibly diffract and create both a shear and a compressional component (Meier and Lee 2009). Knowing this studies have used the diffracted wave to help delineate a void (Keydar et al. 2010) or to gather the velocity and depth of a diffraction (Xia et al. 2007). Referring back to the models of Figure 4-7 we see the P-SV wave diffraction later than the surface wave and the first refracted arrival, hence in principle it should not be as easily masked as the pure P-wave diffraction. To enhance the diffraction methods, radon transforms are used to separate the surface and primary wave energies and also the diffraction (Bansal and Imhof 2005). Once the diffraction is enhanced then the image can be defined using the migration techniques to collapse the diffraction to a point (Keydar et al. 2010) along a seismic profile.

The methods of Xia et al. (Xia et al. 2007) were tested and it was found that from the P-SV diffraction seen in the synthetic data (e.g., Figure 4-7) the depth of the tunnel and the seismic wave velocity around the tunnel could be determined. When used in the data we collected and multiple ranges of velocity were used to estimate the diffractor velocity, the tunnel could not be imaged. This was done by Xia himself and the results proved to be inconclusive for the Oxford, MS, tunnel 1 data set. This data set was used since it was the deepest and the diffraction had a better chance of not being overwhelmed by the primary and surface waves. The reasoning was that the surface waves were so strong that even with processing they masked the diffraction energy and could not image the tunnel. Unfortunately, the use of diffraction techniques did not delineate tunnel 1.

Up to now we have completely ignored the seismic surface waves assuming they are no more than noise relative to refracted and reflected waves. However, the surface wave as a source has been used for some time in near surface studies (Park et al. 1999) and has even been applied in cavity detection (Karray and Lefebvre 2009, Xu and Butt 2006, Gelis et al. 2005). Surface waves differ significantly from body waves in that the former are usually highly dispersive, that is the phase velocities that make up the surface wave packet are dependent on frequency. As such, this dispersion can be studied to better understand the velocity structure of the subsurface. The method requires a spectral transformation of the surface wave and the frequency vs. velocity component of the Rayleigh wave is analysed. The Rayleigh wave velocity is dispersive, so when put into the spectrum, the velocities of the Rayleigh can be picked and inverted to give an S-wave tomography (Xia et al. 1999). The required frequency is usually from 4.5–20 Hz since that is the dominant range of frequencies in ground roll. The reason surface wave techniques are so useful is that since there is a shear component in the presence of air, the velocity goes to zero and thus the tunnel can significantly influence the surface waves. The problem is that in near surface studies it can be difficult to distinguish a tunnel site from other heterogeneities. The advantage of the method is that since the surface wave amplitudes are usually the strongest they allow for detection of concrete covered cavities or voids in noisy urban environments (Karray and Lefebvre 2009). This method was not used for our tunnel sites since the 40 Hz

geophone frequency used at the Oxford, MS, test sites was quite high and in the sites where 14 Hz geophones were used, the surface wave energy could not have each mode picked very well. The data acquisition for a survey using surface wave studies is different but should be investigated to see if data from surface waves in conjunction with traditional P-wave tomography data could enhance near surface void detection.

Using the different wave components of the seismogram can help us image the subsurface, but each method has its own limitations and benefits. To truly image the near surface the entire waveform needs to be taken into account, particularly dispersion and attenuation must be considered. Methods such as full waveform inversion (FWI) can be used to image the subsurface (Lee et al. 2010, Brossier 2011). The method tries to image the subsurface by modeling the entire wave field spectrum and iterates until the original seismic gather is similar to that of the synthetic gather. This method is highly labour intensive and computationally expensive. The technique also requires high quality data that must be processed to minimize differences in source point characteristics. The full frequency spectrum is needed to image the waves so broadband data is required. To our knowledge this method is not used for near surface modeling but this technique has some potential and should be attempted in the future.

Two major considerations that were ignored for most of this report need to be looked at in greater detail before larger studies can be pursued. The first is repeatability—the ability to have different groups of contractors able to detect the same void using the same technique. The second is the establishment of criteria of that makes the anomaly a tunnel in regions where a tunnel is not known. The test for repeatability should be easy enough to approach: different groups without prior information can run similar surveys over a given tunnel site. Since the anomalies are quite small, the time lapse between surveys should be small to make sure local changes of weather and season don't affect the results. For instance, changing water table levels could drastically change the interpretation of a tunnel anomaly. The harder issue is to classify a tunnel anomaly in a global sense. To establish detection criteria for everyone to use will require multiple geophysical techniques (Cardarelli et al. 2010) using joint inversion. Correlations between multiple

different methods would need to be done to look at the relative anomaly for multiple different sites.

7.3 SUMMARY

The use of both seismic and electrical methods can help improve the interpretation of tunnel sites by eliminating possibly false artifacts. The joint interpretation was found useful to both detect the actual location of a tunnel, to confirm the presence of a tunnel, and to describe why the method(s) did not work. Seismic diffraction techniques were shown to detect tunnels but in situations of loose gravel and sand the surface wave energy was too great and masked the diffractor energy. The next methods discussed were surface wave techniques such as MASW; they were not used in this study as their low frequency was incompatible with our equipment and experience. The final area that was talked about was using the full waveform to image the subsurface using techniques such as full waveform inversion, but the code is not readily available.

CHAPTER 8
8.0 CONCLUSION

Clandestine tunnels that cross the U.S.-Mexico border make it difficult to control illegal immigration and transportation of goods. The use of noninvasive techniques to detect these tunnels is critical when other methods such as intelligence don't work. The work presented here uses seismic refraction and electrical resistivity tomography to detect such subsurface voids. The project was split into two different test areas. The first was in Oxford, MS, where surveys were conducted over an area containing culverts that acted as surrogate tunnels. Culverts of various shapes, compositions, and depths were tested to establish practical methods that could be applied to detect a real clandestine tunnel in Douglas, AZ. The survey site in Douglas, AZ, is a tunnel that crosses the U.S.-Mexico border. It was discovered in 1990 and is now used as a test site for the U.S. Department of Homeland Security and U.S Customs and Border Protection. The goal was to determine the feasibility of using seismic and electrical methods for the detection of clandestine voids. The principal involved was that the contrast in physical properties of a tunnel and the surrounding rock should be susceptible to imaging by these methods, revealing the near surface void.

Equipment for the project was acquired from the University of Alberta, and the National Center of Physical Acoustics at the University of Mississippi. The research involved the acquisition, processing, and interpretation of seismic and electrical data. Different acquisition parameters and survey arrays were used to optimize techniques and determine which were appropriate for the detection of near surface voids. Tunnel detection procedures and geophysical techniques that have been used to detect tunnels are described as necessary.

Before data were collected, synthetic data was used to simulate what would be seen in the test sites. To simulate how electrical data would be used to detect a tunnel, sample resistivity spreads for both Wenner and dipole-dipole arrays were prepared. The initial model was a homogeneous layer with an air filled void in the middle of the model. The test showed that the casing around a model had little to

no affect on the inversion of the data. The inversion of a test array showed that using a dipole-dipole array could detect a high resistivity anomaly around the location of the tunnel. The use of a Wenner array showed little evidence for detecting the tunnel. Similar to the electrical data, synthetic seismograms for individual shots were used to help simulate how the seismic wavefield is affected by a tunnel. The shot gathers showed little evidence for changes in the direct and refracted wave, unless a significantly large tunnel was the object. The seismogram showed that both P and P-SV waves were diffracted back to the ground surface from the tunnel. The synthetic data collected showed that a dipole-dipole array could be used to detect a tunnel. The synthetic seismogram data showed that only a large tunnel could be detected with direct and refracted waves.

The Oxford, MS, test site was an abandoned railway track that is now used as a walking path; along the path culverts are placed with various depths. The culverts that were placed in the railway had different compositions ranging from metal pipes to concrete to sandstones blocks. The depths of the culverts also changed ranging from 1.5–10 m. The size of the array that was used depended on the perceived depth of the tunnel. The deeper the tunnel the larger the spread length, for both electrical and seismic surveys. There were nine tunnel sites in total that had both electrical and seismic data recorded. The seismic data and electrical data were processed at the University of Alberta, and at the NCPA. Taking the information gathered at the Oxford, MS, site, data were collected at the U.S.-Mexico border at the Douglas, AZ, test site. The test site is on the border and both seismic and electrical data were collected at two survey sites. The tunnel was concrete lined and varied from 5–10 m in depth depending on the location in the spread. The seismic data were collected from a surface array and from a geophone placed in one of the boreholes. Electrical data were acquired from both Wenner and dipole-dipole arrays. The data were postprocessed and interpreted later in the University ofAlberta.

Electrical data were processed using electrical resistivity tomography (ERT) where the measured apparent resistivity taken at the site is inverted to produce a 2D image of the true resistivity. Since the difference in resistivity

between surface rocks and air is quite large, it was expected that an air-filled void would be detected with the ERT method. The ERT pseudosection should display the tunnel anomaly as a highly resistive zone. What was seen was that there could be resistive or conductive anomalies present at the approximate locations of a tunnel. In Oxford, MS, a tunnel anomaly was detected at only four of eight sites. Some sites showed areas of conductive anomalies which were interpreted as zones where water could flow easily due to the presence of the tunnel. Water flowing inside or just outside the tunnel would create a pathway for ions to move and the area would be detected as an anomaly. This was different from what was expected in modeling since the motion of ions was not taken into account. The main source of error and why most tunnel sites could not be detected was attributed to the contact of the electrodes causing the current to stay near the surface. At the Douglas, AZ, test site, an anomaly was detected in one out of two test areas; only the dipole-dipole array detected this anomaly. The anomaly was highly resistive. The inversion showed two possible anomalies around the approximate location of the tunnel. The site where there was no anomaly detected had a metal fence that soaked up the current. Overall, the electrical method proved to be successful in detecting subsurface voids, but information about the subsurface was important to the interpretation.

The seismic data were processed and imaged using refraction tomography. The refraction method tries to image the near surface using direct and refracted waves. The velocities of signals in an air-filled tunnel are similar to velocities in air and signals should travel in the surrounding rock at a higher velocity compared to the velocity in air. The seismic data has its first signal arrivals picked and the data were inverted using ray tracing to give a velocity tomogram and a ray coverage plot. The velocities should drop down around the tunnel and the ray coverage should show a zone of fewer rays traveling through it. In the Oxford, MS, site nine tunnel sites were imaged and six out of nine tunnels showed the presence of a tunnel anomaly. Similar to what was seen in the modeling, the velocity tomogram showed very little evidence of the tunnel and at best showed a small velocity drop down. The ray coverage that characterized the tunnel as a low ray coverage zone proved to be the best method to detect the tunnels. At the Douglas, AZ, test site, refraction

tomography was performed on the surface and beneath the surface using a geophone in a borehole. The refraction method found the tunnel location at the same spot as the dipole-dipole array showing a drop down in velocity and low ray coverage around the approximate location of the tunnel. The borehole showed ray bending around the tunnel as seen in the velocity tomogram at the site where the electrical and seismic methods could not detect the tunnel. The seismic data could not detect the tunnel along a site with large surface heterogeneity. Other seismic reflection and diffraction techniques could not image the tunnel due to the strong heterogeneity in the near surface and the large amount of surface wave noise.

We found that both electrical and seismic methods could detect the presence of a tunnel. The anomaly that was seen in both methods was not distinct and the use of both electrical and seismic methods is thought to be critical for the interpretation of a tunnel site. In a situation where the tunnel location is not known, the use of multiple geophysical techniques could be crucial to eliminate false tunnels sites. In conclusion, the use of high resolution seismic and electrical methods can help detect the location of a clandestine tunnel in an urban environment.

REFERENCES

ANON. 1981. PROCEEDINGS OF THE SECOND TECHNICAL SYMPOSIUM ON TUNNEL DETECTION. GOLDEN, COLORADO.

ANON-. 1988. PROCEEDINGS OF THE THIRD TECHNICAL SYMPOSIUM ON TUNNEL DETECTION. GOLDEN, COLORADO.

BAKER, G. S. 2002. NEAR-SURFACE SEISMIC REFRACTION TOMOGRAPHY TUTORIAL.

BANSAL, R. & M. G. IMHOF (2005) DIFFRACTION ENHANCEMENT IN PRESTACK SEISMIC DATA. *GEOPHYSICS,* 70, V73-V79.

BELFER, I., I. BRUNER, S. KEYDAR, A. KRAVTSOV & E. LANDA (1998) DETECTION OF SHALLOW OBJECTS USING REFRACTED AND DIFFRACTED SEISMIC WAVES. *JOURNAL OF APPLIED GEOPHYSICS,* 38, 155-168.

BENSON, A. K. (1995) APPLICATIONS OF GROUND-PENETRATING RADAR IN ASSESSING SOME GEOLOGICAL HAZARDS - EXAMPLES OF GROUNDWATER CONTAMINATION, FAULTS, CAVITIES. *JOURNAL OF APPLIED GEOPHYSICS,* 33, 177-193.

BISHOP, I., P. STYLES, S. J. EMSLEY & N. S. FERGUSON. 1997. THE DETECTION OF CAVITIES USING THE MICROGRAVITY TECHNIQUE: CASE HISTORIES FROM MINING AND KARSTIC ENVIRONMENTS. IN *MODERN GEOPHYSICS IN ENGINEERING GEOLOGY,* EDS. D. M. MCCANN, M. EDDLESTON, P. J. FENNING & G. M. REEVES, 153-166. BATH: GEOLOGICAL SOC PUBLISHING HOUSE.

BOHLEN, T. (2002) PARALLEL 3-D VISCOELASTIC FINITE DIFFERENCE SEISMIC MODELLING. *COMPUTERS & GEOSCIENCES,* 28, 887-899.

BROSSIER, R. B. R. (2011) TWO-DIMENSIONAL FREQUENCY-DOMAIN VISCO-ELASTIC FULL WAVEFORM INVERSION: PARALLEL ALGORITHMS, OPTIMIZATION AND PERFORMANCE. *COMPUTERS & GEOSCIENCES,* 37, 444-455.

BUTLER, D. K. (1984) MICROGRAVIMETRIC AND GRAVITY GRADIENT TECHNIQUES FOR DETECTION OF SUBSURFACE CAVITIES. *GEOPHYSICS,* 49, 1084-1096.

CARDARELLI, E., M. CERCATO, A. CERRETO & G. DI FILIPPO (2010) ELECTRICAL RESISTIVITY AND SEISMIC REFRACTION TOMOGRAPHY TO DETECT BURIED CAVITIES. *GEOPHYSICAL PROSPECTING,* 58, 685-695.

CARDARELLI, E., E. FISCHANGER & S. PIRO (2008) INTEGRATED GEOPHYSICAL SURVEY TO DETECT BURIED STRUCTURES FOR ARCHAEOLOGICAL PROSPECTING. A CASE-HISTORY AT SABINE NECROPOLIS (ROME, ITALY). *NEAR SURFACE GEOPHYSICS,* 6, 15-20.

CERJAN, C., D. KOSLOFF, R. KOSLOFF & M. RESHEF (1985) A NONREFLECTING BOUNDARY-CONDITION FOR DISCRETE ACOUSTIC AND ELASTIC WAVE-EQUATIONS. *GEOPHYSICS,* 50, 705-708.

CHAMBERLAIN, A. T., W. SELLERS, C. PROCTOR & R. COARD (2000) CAVE DETECTION IN LIMESTONE USING GROUND PENETRATING RADAR. *JOURNAL OF ARCHAEOLOGICAL SCIENCE,* 27, 957-964.

CURRO, J. R., S. S. COOPER & R. F. BALLARD (1981) CAVITY DETECTION-DELINEATION IN KARST AREAS - AN INVESTIGATION USING SEISMIC AND ACOUSTIC METHODOLOGY. *GEOPHYSICS,* 46, 452-452.

DAILY, W., W. LIN & T. BUSCHECK (1987) HYDROLOGICAL PROPERTIES OF TOPOPAH SPRING TUFF - LABORATORY MEASUREMENTS. *JOURNAL OF GEOPHYSICAL RESEARCH-SOLID EARTH AND PLANETS,* 92, 7854-7864.

DAILY, W., A. RAMIREZ, A. BINLEY & B. LABRECQUE. 2005. *ELECTRICAL REISISTANCE TOMOGRAPHY-THEORY AND PRACTICE*.

DEBEGLIA, N. & F. DUPONT (2002) SOME CRITICAL FACTORS FOR ENGINEERING AND ENVIRONMENTAL MICROGRAVITY INVESTIGATIONS. *JOURNAL OF APPLIED GEOPHYSICS,* 50, 435-454.

DEY, A. & H. F. MORRISON (1979) RESISTIVITY MODELING FOR ARBITRARILY SHAPED TWO-DIMENSIONAL STRUCTURES. *GEOPHYSICAL PROSPECTING,* 27, 1020-1036.

DOBECKI, T. L. & S. B. UPCHURCH (2006) GEOPHYSICAL APPLICATIONS TO DETECT SINKHOLES AND GROUND SUBSIDENCE. *THE LEADING EDGE,* 25, 336-341.

DOLL, W. E., J. R. SHEEHAN, W. A. MANDELL & D. B. WATSON. 2006. *SEISMIC REFRACTION TOMOGRAPHY FOR KARST IMAGING*. MONMOUTH JUNCTION: SCIENCE PRESS USA INC.

EDGE, A. B. & T. H. LABY. 1931. THE PRINCIPLES AND PRACTICE OF GEOPHYSICAL PROSPECTING. 339-341. CAMBRIDGE UNIVERSITY PRESS.

EDWARDS, L. S. (1977) MODIFIED PSEUDO-SECTION FOR RESISTIVITY AND IP. *GEOPHYSICS,* 42, 1020-1036.

EL KHAMMARI, K., A. NAJINE, M. JAFFAL, T. AIFA, M. HIMI, D. VASQUEZ, A. CASAS & P. ANDRIEUX (2007) COMBINED GEOELECTRICAL-GPR MAPPING OF UNDERGROUND CAVITIES IN THE ZAOUIT ECH CHEIKH CITY (MOROCCO). *COMPTES RENDUS GEOSCIENCE,* 339, 460-467.

ENGELSFELD, T., F. SUMANOVAC & N. PAVIN (2008) INVESTIGATION OF UNDERGROUND CAVITIES IN A TWO-LAYER MODEL USING THE REFRACTION SEISMIC METHOD. *NEAR SURFACE GEOPHYSICS,* 6, 221-231.

FURMAN, A., T. P. A. FERRE & A. W. WARRICK (2003) A SENSITIVITY ANALYSIS OF ELECTRICAL RESISTIVITY TOMOGRAPHY ARRAY TYPES USING ANALYTICAL ELEMENT MODELING. *VADOSE ZONE JOURNAL,* 2, 416-423.

GARDNER, L. W. 1939. AN AEREAL PLAN OF MAPPING A SUBSURFACE BY REFRACTION SHOOTING. GEOPHYSICS.

GELIS, C., D. LEPAROUX, J. VIRIEUX, A. BITRI, S. OPERTO & G. GRANDJEAN (2005) NUMERICAL MODELING OF SURFACE WAVES OVER SHALLOW CAVITIES. *JOURNAL OF ENVIRONMENTAL AND ENGINEERING GEOPHYSICS,* 10, 111-121.

GRANDJEAN, G. & D. LEPAROUX (2004) THE POTENTIAL OF SEISMIC METHODS FOR DETECTING CAVITIES AND BURIED OBJECTS: EXPERIMENTATION AT A TEST SITE. *JOURNAL OF APPLIED GEOPHYSICS,* 56, 93-106.

GRIFFITHS, D. H. & R. D. BARKER (1993) 2-DIMENSIONAL RESISTIVITY IMAGING AND MODELING IN AREAS OF COMPLEX GEOLOGY. *JOURNAL OF APPLIED GEOPHYSICS,* 29, 211-226.

GUEGUEN, Y. & V. PALCIAUSKAS. 1994. *INTRODUCTION TO THE PHYSICS OF ROCKS*.

HAGEDOORN, J. G. 1959. THE PLUS-MINUS METHOD OF0 INTERPRETING SEISMIC REFRACTION SECTIONS. 158-182. GEOPHYSICAL PROSPECTING.

HALIHAN, T. & J. E. NYQUIST. 2006. DETECTION OF VOIDS, TUNNELS AND COLLAPSE FEATURES. IN *PHILADELPHIA ANNUAL MEETING OF THE GEOLOGICAL SOCIETY OF AMERICA*. PHILADELPHIA, PA.

HAMPSON, D. & B. RUSSELL. 1984. FIRST-BREAK INTERPRETATION USING GENERALIZED LINEAR INVERSION. 40-50. CANADIAN JOURNAL OF EXPLORATION GEOPHYSICS.

HICKEY, C. J. & W. B. HOWARD. 2006. REFRACTION TOMOGRAPHY FOR TUNNEL DETECTION. IN *US ARMY WORKSHOP ON THE REAL-TIME DETECTION OF CLANDESTINE SHALLOW TUNNELS*. OXFORD, MS.

JETSCHNY, S., T. BOHLEN & D. DE NIL (2010) ON THE PROPAGATION CHARACTERISTICS OF TUNNEL SURFACE-WAVES FOR SEISMIC PREDICTION. *GEOPHYSICAL PROSPECTING,* 58, 245-256.

KARAMAN, A. & T. KARADAYILAR (2004) IDENTIFICATION OF KARST FEATURES USING SEISMIC P-WAVE TOMOGRAPHY AND RESISTIVITY ANISOTROPY MEASUREMENTS. *ENVIRONMENTAL GEOLOGY,* 45, 957-962.

KARRAY, M. & G. LEFEBVRE (2009) DETECTION OF CAVITIES UNDER PAVEMENTS BY MODAL ANALYSIS OF RAYLEIGH WAVES (MASW). *CANADIAN GEOTECHNICAL JOURNAL,* 46, 424-437.

KELLER, G. V. & F. C. FRISCHKNECHT. 1966. *ELECTICAL METHODS IN GEOPHYSICAL PROSPECTING*. PERGAMON PRESS.

KETCHAM, S. A., J. R. MCKENNA, R. J. GREENFIELD & T. S. ANDERSON. 2006. SEISMIC PROPAGATION FROM ACTIVITY IN TUNNELS. IN *HPCMP USERS GROUP CONFERENCE (HPCMP-UGC'06)*. DENVER, CO.

KEYDAR, S., D. PELMAN & M. EZERSKY (2010) APPLICATION OF SEISMIC DIFFRACTION IMAGING FOR DETECTING NEAR-SURFACE INHOMOGENEITIES IN THE DEAD SEA AREA. *JOURNAL OF APPLIED GEOPHYSICS,* 71, 47-52.

KHAIDUKOV, V., E. LANDA & T. J. MOSER (2004) DIFFRACTION IMAGING BY FOCUSING-DEFOCUSING: AN OUTLOOK ON SEISMIC SUPERRESOLUTION. *GEOPHYSICS,* 69, 1478-1490.

KISSLING, E., W. L. ELLSWORTH, D. EBERHARTPHILLIPS & U. KRADOLFER (1994) INITIAL REFERENCE MODELS IN LOCAL EARTHQUAKE TOMOGRAPHY. *JOURNAL OF GEOPHYSICAL RESEARCH-SOLID EARTH,* 99, 19635-19646.

KNAPP, R. W. & D. W. STEEPLES (1986) HIGH-RESOLUTION COMMON-DEPTH-POINT REFLECTION PROFILING - FIELD ACQUISITION PARAMETER DESIGN. *GEOPHYSICS,* 51, 283-294.

KNEIB, G. & A. LEYKAM (2004) FINITE-DIFFERENCE MODELLING FOR TUNNEL SEISMOLOGY. *NEAR SURFACE GEOPHYSICS,* 2, 71-93.

KNIGHT, R. L. & A. L. ENDRES. 2005. *AN INTRODUCTION TO ROCK PHYSICS PRINCIPLES FOR NEAR-SURFACE GEOPHYSICS*.

KOEFOED, O. 1979. *GEOSOUNDING PRINCIPLES 1 : RESISTIVITY SOUNDING MEASUREMENTS*. ELSEVIER SCIENCE PUBLISHINGCCOMPANY.

KORN, M. (1987) COMPUTATION OF WAVE-FIELDS IN VERTICALLY INHOMOGENEOUS-MEDIA BY A FREQUENCY-DOMAIN FINITE-DIFFERENCE METHOD AND APPLICATION TO WAVE-PROPAGATION IN EARTH MODELS WITH RANDOM VELOCITY AND DENSITY PERTURBATIONS. *GEOPHYSICAL JOURNAL OF THE ROYAL ASTRONOMICAL SOCIETY,* 88, 345-377.

KRUSE, S., M. GRASMUECK, M. WEISS & D. VIGGIANO (2006) SINKHOLE STRUCTURE IMAGING IN COVERED KARST TERRAIN. *GEOPHYSICAL RESEARCH LETTERS,* 33, 6.

LANZ, E., H. MAURER & A. G. GREEN (1998) REFRACTION TOMOGRAPHY OVER A BURIED WASTE DISPOSAL SITE. *GEOPHYSICS,* 63, 1414-1433.

LEE, H. Y., J. M. KOO, D. J. MIN, B. D. KWON & H. S. YOO (2010) FREQUENCY-DOMAIN ELASTIC FULL WAVEFORM INVERSION FOR VTI MEDIA. *GEOPHYSICAL JOURNAL INTERNATIONAL,* 183, 884-904.

LEE, T. K., S. O. PARK, J. W. RA & S. Y. KIM (1989) NEAR-FIELD DIFFRACTION PATTERN BY AN UNDERGROUND VOID OF CIRCULAR-CYLINDER. *MICROWAVE AND OPTICAL TECHNOLOGY LETTERS,* 2, 179-183.

LEGCHENKO, A., M. EZERSKY, C. CAMERLYNCK, A. AL-ZOUBI & K. CHALIKAKIS (2009) JOINT USE OF TEM AND MRS METHODS IN A COMPLEX GEOLOGICAL SETTING. *COMPTES RENDUS GEOSCIENCE,* 341, 908-917.

LEUCCI, G. & L. DE GIORGI (2010) MICROGRAVIMETRIC AND GROUND PENETRATING RADAR GEOPHYSICAL METHODS TO MAP THE SHALLOW KARSTIC CAVITIES NETWORK

IN A COASTAL AREA (MARINA DI CAPILUNGO, LECCE, ITALY). *EXPLORATION GEOPHYSICS,* 41, 178-188.

LEUCCI, G., S. MARGIOTTA & S. NEGRI (2004) GEOPHYSICAL AND GEOLOGICAL INVESTIGATIONS IN A KARSTIC ENVIRONMENT (SALICE SALENTINO, LECCE, ITALY). *JOURNAL OF ENVIRONMENTAL AND ENGINEERING GEOPHYSICS,* 9, 25-34.

LEVANDER, A. R. (1988) 4TH-ORDER FINITE-DIFFERENCE P-SV SEISMOGRAMS. *GEOPHYSICS,* 53, 1425-1436.

LINES, L. R. & S. TREITEL (1984) TUTORIAL - A REVIEW OF LEAST-SQUARES INVERSION AND ITS APPLICATION TO GEOPHYSICAL PROBLEMS. *GEOPHYSICAL PROSPECTING,* 32, 159-186.

LO MONTE, L., D. ERRICOLO, F. SOLDOVIERI & M. C. WICKS (2010) RADIO FREQUENCY TOMOGRAPHY FOR TUNNEL DETECTION. *IEEE TRANSACTIONS ON GEOSCIENCE AND REMOTE SENSING,* 48, 1128-1137.

LOKE, M. H. 2002. *TUTORIAL: 2-D AND 3-D ELECTRICAL IMAGING SURVEY*.

LOKE, M. H. & R. D. BARKER (1996) RAPID LEAST-SQUARES INVERSION OF APPARENT RESISTIVITY PSEUDOSECTIONS BY A QUASI-NEWTON METHOD. *GEOPHYSICAL PROSPECTING,* 44, 131-152.

MARION, D., A. NUR, H. YIN & D. HAN (1992) COMPRESSIONAL VELOCITY AND POROSITY IN SAND-CLAY MIXTURES. *GEOPHYSICS,* 57, 554-563.

MARKIEWICZ, R. D. & B. D. RODRIGUEZ (1986) DETECTION OF VOIDS BENEATH AN INTERSTATE HIGHWAY USING A REFRACTION SEISMOGRAPH. *GEOPHYSICS,* 51, 445-445.

MCKENNA, J. R. & S. A. KETCHUM. 2006. TUNNNEL DETECTION, MONITORING, AND MODELING. IN *NS21A, 2006 AGU, GSS, MAS, MSA, SEG, UGM JOINT ASSEMBLY*. BALTIMORE, MD.

MEIER, M. A. & P. J. LEE (2009) CONVERTED-WAVE RESOLUTION. *GEOPHYSICS,* 74, Q1-Q16.

MILLER, R., C. B. PARK, J. XIA, J. IVANOV, D. W. STEEPLES, N. RYDEN, R. F. BALLARD, J. L. LLOPIS, T. S. ANDERSON, M. L. MORAN & S. A. KETCHAM. 2006. TUNNEL DETECTION USING SEISMIC METHODS. IN *AGU FALL MEETING*. SAN FRANCISCO, CA.

MOURATIDIS, A., S. LAMBROPOULOS & E. SAKOUMPENTA. 2005. THE "COVER AND CUT" METHOD IN TUNNEL AND ROADWAY CONSTRUCTION. IN *PROC. 1ST CONFERENCE EARTHWORKS IN EUROPE*. PARIS.

NABIGHIAN, M. & J. MACNAE. 1991. *TIME DOMAIN ELECTROMAGNETIC PROSPECTING METHODS*. SOCIETY OF EXPLORATIONAL GEOPHYSCIS.

NASSERI-MOGHADDAM, A., G. CASCANTE, C. PHILLIPS & D. J. HUTCHINSON (2007) EFFECTS OF UNDERGROUND CAVITIES ON RAYLEIGH WAVES - FIELD AND NUMERICAL EXPERIMENTS. *SOIL DYNAMICS AND EARTHQUAKE ENGINEERING,* 27, 300-313.

NEGRI, S., G. LEUCCI & F. MAZZONE (2008) HIGH RESOLUTION 3D ERT TO HELP GPR DATA INTERPRETATION FOR RESEARCHING ARCHAEOLOGICAL ITEMS IN A GEOLOGICALLY COMPLEX SUBSURFACE. *JOURNAL OF APPLIED GEOPHYSICS,* 65, 111-120.

OCONNELL, R. J. & B. BUDIANSKY (1978) MEASURES OF DISSIPATION IN VISCOELASTIC MEDIA. *GEOPHYSICAL RESEARCH LETTERS,* 5, 5-8.

PALACKY, G. J. 1987. *RESISTIVY CHARACTERISTICS OF GEOLOGICAL TARGETS*.

PALMER, D. (1981) AN INTRODUCTION TO THE GENERALIZED RECIPROCAL METHOD OF SEISMIC REFRACTION INTERPRETATION. *GEOPHYSICS,* 46, 1508-1518.

PAPADOPOULOS, N. G., M. J. YI, J. H. KIM, P. TSOURLOS & G. N. TSOKAS (2010) GEOPHYSICAL INVESTIGATION OF TUMULI BY MEANS OF SURFACE 3D ELECTRICAL RESISTIVITY TOMOGRAPHY. *JOURNAL OF APPLIED GEOPHYSICS,* 70, 192-205.

PARK, C. B., R. D. MILLER & J. H. XIA (1999) MULTIMODAL ANALYSIS OF HIGH FREQUENCY SURFACE WAVES. *PROCEEDINGS OF THE SYMPOSIUM ON THE APPLICATION OF GEOPHYSICS TO ENGINEERING AND ENVIRONMENTAL PROBLEMS*, 115-121.

PIRO, S., P. I. TSOURLOS & G. N. TSOKAS (2001) CAVITY DETECTION EMPLOYING ADVANCED GEOPHYSICAL TECHNIQUES: A CASE STUDY. *EUROPEAN JOURNAL OF ENVIROMENTAL AND ENGINEERING GEOPHYSICS,* 6, 3-31.

PULLAMMANAPPALLIL, S. K. & J. N. LOUIE (1993) INVERSION OF SEISMIC-REFLECTION TRAVEL-TIMES USING A NONLINEAR OPTIMIZATION SCHEME. *GEOPHYSICS,* 58, 1607-1620.

QIN, F. H., Y. LUO, K. B. OLSEN, W. Y. CAI & G. T. SCHUSTER (1992) FINITE-DIFFERENCE SOLUTION OF THE EIKONAL EQUATION ALONG EXPANDING WAVE-FRONTS. *GEOPHYSICS,* 57, 478-487.

RAMIREZ, A., W. DAILY, D. LABRECQUE, E. OWEN & D. CHESNUT (1993) MONITORING AN UNDERGROUND STEAM INJECTION PROCESS USING ELECTRICAL-RESISTANCE TOMOGRAPHY. *WATER RESOURCES RESEARCH,* 29, 73-87.

RECHTIEN, R. D., R. J. GREENFIELD & R. F. BALLARD (1995) TUNNEL SIGNATURE PREDICTION FOR A CROSS-BOREHOLE SEISMIC SURVEY. *GEOPHYSICS,* 60, 76-86.

RIDDLE, G. I., C. J. HICKEY & D. SCHMITT, R. 2010. SUBSURFACE TUNNEL DETECTION USING ELECTRICAL RESISTIVITY TOMOGRAPHY AND SEISMIC REFRACTION TOMOGRAPHY: A CASE STUDY. IN *SAGEEP*, 11. KEYSTONE, CO.

ROBERTSSON, J. O. A. (1996) A NUMERICAL FREE-SURFACE CONDITION FOR ELASTIC/VISCOELASTIC FINITE-DIFFERENCE MODELING IN THE PRESENCE OF TOPOGRAPHY. *GEOPHYSICS,* 61, 1921-1934.

ROBERTSSON, J. O. A., J. O. BLANCH & W. W. SYMES (1994) VISCOELASTIC FINITE-DIFFERENCE MODELING. *GEOPHYSICS,* 59, 1444-1456.

SABATIER, J. M., G. M. MATALKAH & IEEE. 2008. *A STUDY ON THE PASSIVE DETECTION OF CLANDESTINE TUNNELS*. NEW YORK: IEEE.

SABATIER, J. M. & T. G. MUIR. 2006. WORKSHOP ON REAL-TIME DETECTION OF CLANDESTINE SHALLOW TUNNELS. NATIONAL CENTER FOR PHYSICAL ACOUSTICS, UNIVERSITY OF MISSISSIPPI.

SASAKI, Y. (1992) RESOLUTION OF RESISTIVITY TOMOGRAPHY INFERRED FROM NUMERICAL-SIMULATION. *GEOPHYSICAL PROSPECTING,* 40, 453-463.

SCHUSTER, G. T. & A. QUINTUSBOSZ (1993) WAVEPATH EIKONAL TRAVEL-TIME INVERSION - THEORY. *GEOPHYSICS,* 58, 1314-1323.

SENGLAUB, M., M. YEE, G. ELBRING, R. ABBOTT & B. N. 2010. SENSOR INTEGRATION STUDY FOR A SHALLOW TUNNEL DETECTION SYSTEM. SANDIA NATIONAL LABORATORIES.

SHEEHAN, J. R., W. E. DOLL & W. A. MANDEL. 2006A. VOID DETECTION USING SEISMIC REFRACTION TOMOGRAPHY. IN *PHILADELPHIA ANNUAL MEETING*, 526. PENNSYLVANIA.

SHEEHAN, J. R., W. E. DOLL & W. A. MANDELL (2006B) AN EVALUATION OF METHODS AND AVAIABLE SOFTWARE FOR SEISMIC REFRACTION TOMOGRAPHY ANALYSIS. *ENVIROMENTAL AND ENGINEERING GEOPHYSICS,* 10, 21-34.

SHERIFF, R. E. & L. P. GELDART. 1985. EXPLORATION SEISMOLOGY I: HISTORY THEORY AND DATA ACQUISTION. CAMBRODGE UNIV. PRESS.

SILVESTER, P. P. & R. L. FERRARI. 1990. *FINITE ELEMENTS FOR ELECTRICAL ENGINEERS (2ND. ED.).* CAMBRIDGE UNIVERSITY PRESS.

SOGADE, J., Y. VICHABIAN, A. VANDIVER, P. M. REPPERT, D. COLES & F. D. MORGAN (2004) ELECTROMAGNETIC CAVE-TO-SURFACE MAPPING SYSTEM. *IEEE TRANSACTIONS ON GEOSCIENCE AND REMOTE SENSING,* 42, 754-763.

SONG, J. L. & U. TEN BRINK. 2004. RAYGUI 2.0 - A GRAPHICAL USER INTERFACE FOR INTERACTIVE FORWARD AND INVERSION RAY-TRACING. IN *U.S. GEOLOGICAL SURVEY OPEN-FILE REPORT*.

TELFORD, W. M., L. P. GELDART & R. E. SHERIFF. 1990. *APPLIED GEOPHYSICS SECOND EDITION*.

VAN SCHOOR, M. (2002) DETECTION OF SINKHOLES USING 2D ELECTRICAL RESISTIVITY IMAGING. *JOURNAL OF APPLIED GEOPHYSICS,* 50, 393-399.

VESECKY, I. F., W. A. NIERENBERG & A. M. DESPAIN. 1980. TUNNEL DETECTION. SRI INTERNATIONAL.

VIDALE, J. (1988) FINITE-DIFFERENCE CALCULATION OF TRAVEL-TIMES. *BULLETIN OF THE SEISMOLOGICAL SOCIETY OF AMERICA,* 78, 2062-2076.

VIRIEUX, J. (1986) P-SV-WAVE PROPAGATION IN HETEROGENEOUS MEDIA - VELOCITY-STRESS FINITE-DIFFERENCE METHOD. *GEOPHYSICS,* 51, 889-901.

WIDESS, M. B. (1973) HOW THIN IS A THIN BED. *GEOPHYSICS,* 38, 1176-1180.

WILLIAMSON, P. R. (1991) A GUIDE TO THE LIMITS OF RESOLUTION IMPOSED BY SCATTERING IN RAY TOMOGRAPHY. *GEOPHYSICS,* 56, 202-207.

XIA, J. H., R. D. MILLER & C. B. PARK (1999) ESTIMATION OF NEAR-SURFACE SHEAR-WAVE VELOCITY BY INVERSION OF RAYLEIGH WAVES. *GEOPHYSICS,* 64, 691-700.

XIA, J. H., J. E. NYQUIST, Y. X. XU, M. J. S. ROTH & R. D. MILLER (2007) FEASIBILITY OF DETECTING NEAR-SURFACE FEATURE WITH RAYLEIGH-WAVE DIFFRACTION. *JOURNAL OF APPLIED GEOPHYSICS,* 62, 244-253.

XU, C. Q. & S. D. BUTT (2006) EVALUATION OF MASW TECHNIQUES TO IMAGE STEEPLY DIPPING CAVITIES IN LATERALLY INHOMOGENEOUS TERRAIN. *JOURNAL OF APPLIED GEOPHYSICS,* 59, 106-116.

YANCEY, D. J., M. G. IRNHOF, J. E. FEDDOCK & T. GRESHAM (2007) ANALYSIS AND APPLICATION OF COAL-SEAM SEISMIC WAVES FOR DETECTING ABANDONED MINES. *GEOPHYSICS,* 72, M7-M15.

YILMAZ, O. 2001. SEISMIC DATA ANALYSIS: PROCESSING, INVERSION, AND INTERPRETATION OF SEISMIC DATA (INVESTIGATIONS IN GEOPHYSICS, NO 10). SOCIETY OF EXPLORATION GEOPHYSICISTS.

ZHANG, S. X., L. S. CHAN & J. H. XIA (2004) THE SELECTION OF FIELD ACQUISITION PARAMETERS FOR DISPERSION IMAGES FROM MULTICHANNEL SURFACE WAVE DATA. *PURE AND APPLIED GEOPHYSICS,* 161, 185-201.

ZHOU, W., B. F. BECK & J. B. STEPHENSON (2000) RELIABILITY OF DIPOLE-DIPOLE ELECTRICAL RESISTIVITY TOMOGRAPHY FOR DEFINING DEPTH TO BEDROCK IN COVERED KARST TERRANES. *ENVIRONMENTAL GEOLOGY,* 39, 760-766.

APPENDIX A
DESCRIPTION OF TUNNEL SITES

In this appendix the details of each tunnel site are presented, this includes photographs of the tunnels site. The information presented is the field notes and description at each tunnel site location. The information about the target areas and motivation can be seen in Chapter 2. This appendix will be split into two parts; the first is the Oxford, MS the second is Douglas, AZ.

OXFORD, MS

The Oxford, MS test site is an old rail track that was constructed 150-160 years ago, the site has since then had its track removed and now is used as a walk path. The site is located 1 mile from the major highway and runs perpendicular from the highway so the only major sources of noise are pedestrians walking and, in the dam site, some possible 60Hz interference. The railway has multiple culverts that are used to keep from water building up along the embankment, the culverts were constructed in multiple phases since the construction of the railway. It is not known when these different tunnels/culverts were constructed but some are believed to be much older than others. These culverts, which act as surrogate tunnels for this study, providing a variety of sizes, shapes, and depths. The material above the walkway changes from site to site, but all have crushed gravel as the surface. The surveys were collected from February 5-20 , 2009 and the coordinates can be seen in Table A-1.

In general we approached each site with the same idea to try and find the subsurface culvert. First we estimated the depth of the tunnel then laid the spread length to at least 5 times the depth of the tunnel. The longer the spread the higher the depth penetration for refraction tomography, but at the cost of lost lateral resolution. Once this determined, we centered the seismic section along the surface of the old railway. We also have a 1.5 m lateral offset perpendicular from the receiver array for shot points in order to avoid damaging the geophone receivers by

driving over them with the truck that carried the weight drop. In contrast, The hammer seismic surveys did not need to be offset.

Table A-1 lists the different sites.

Tunnel:	**Tunnel Material:**	**Date Survey Performed**	**Latitude (N)**	**Longitude (W)**
Tunnel 1	Sandstone Block	February 5, 2009	34°20'11.04" N	89°33'34.14" W
Tunnel 2	Metal Pipe	February 6, 2009	34°20'42.06" N	89°32'58.80" W
Dam	Earthen Dam	February 7, 2009	34°21'5.45"N	89°33'21.96" W
Tunnel 3	Small Metal Pipe	February 13, 2009	34°20'45.54" N	89°32'56.52" W
Tunnel 4	Small Sandstone Pipe	February 13, 2009	34°19'47.52" N	89°33'58.32" W
Tunnel 5	Concrete Pipe	February 16, 2009	34°20'3.00"N	89°33'48.12" W
Tunnel 6	Concrete Blocks	February 16, 2009	34°19'30.54" N	89°34'12.48" W
Tunnel 7	Concrete pipe	February 18, 2009	34°20'18.96" N	89°33'19.68" W
Tunnel 8	Concrete Blocks	February 19, 2009	34°19'29.19" N	89°34'14.64" W

Table A-1 This is the coordinates and location of each tunnel site in Oxford, Ms

TUNNEL 1

This was the first tunnel site that had data collected on it. The site had both electrical and seismic methods gathered on it and the most types of surveys were used for this site. The site took 2 days to acquire all the data due to issues with the equipment but the data set that is used for tomography only took approximately 4 hours to gather.

The seismic survey was 120 m long with the 40 Hz geophones every 1m. To gather this data set we use a shot spacing of 1 m, starting 0.5 m from the edge of the spread with a 1m shot spacing through the line. The data was sampled at 0.125 ms and was measured for 0.5 s. The source used for this survey was an accelerated weight drop that was 1.5 m laterally offset from the geophone array. At least 3 shots were taken at each shot point for stacking purposes but the data was acquired pre-stack and stacked later in house for amplitude studies. In addition to the seismic profile along the surface of the railway, a second line of 24 3-componet geophones were laid inside the tunnel. This was a test to see the results but due to the tough ground the amplitudes of this data was poor. The data energy in field showed there was a difference in seismic energy transfer from the beginning to the other end of the spread. The seismic signal was drastically getting attenuated on the south end of the spread.

Along with the seismic surveys there was also 2 electrical surveys collected at this site using a ERT Scintrex box. The data set up includes 50 electrodes collected to a smart cable with 2 m electrode spacing. The total length of the spread was 100 m centered over the spread, the survey was set up first and was running first then the seismic survey was set up and ran. There was a dipole-dipole array that was calculated and a Wenner array. The Dipole-Dipole array was cut short due to light and power issues.

The tunnel itself can be seen in the pictures below but it consisted of blocks of stone that were fitted together and plastered into place. This tunnel was quite large being about a 1 m high and about 0.75 m wide; the tunnel was big enough to

crawl through conformably. The base of the tunnel was made of sandstone blocks fitted together, this can be seen in figures A-1 and A-2.

PICTURES

Figure A-1 This is the a picture of inside f tunnel 1. On the ground is a measuring tape used to put the 3-C geophones inside the tunnel during acquisition

Figure A-2 Picture of the south side of the tunnel entrance. Te yellow box is the geode and orange reel is the trigger line for the accelerated weight drop

TUNNEL 2

NOTES

This was the second survey collected in Oxford MS. This is a 1 m diameter corrugated metal pipe that is approximately 6m deep. The looks of this tunnel was that this was inserted after that of the railway and was used to limit wash out of the walk path. This site had both electrical and seismic surveys on it but not to the extent of tunnel 1. The site had steep slopes and had a bit rougher gravel. This survey was carried out on a Friday afternoon and had a large amount of pedestrian traffic, the survey was stopped when people were walking by but some random noise was seen. The ground here was also exposed to the sunlight and was drier than other surveys.

The seismic survey was 120 m long with 40 Hz geophone spacing of 1 m. To gather this data set we use a shot spacing of 1 m, starting 0.5 m from the edge of the spread with a 1 m shot spacing through the line. The source used for this survey was an accelerated weight drop that was 1.5 m laterally offset from the geophone array. Each shot location had at least 3 shots done for stacking purposes but the data was acquired pre-stack and stacked in house for amplitude studies. The acquisition was sampled at 0.125ms and was measured for 0.5 s.

An electrical survey was done on this site with a dipole-dipole array. The first survey that was performed had a 2 m electrode spacing with 50 electrodes having 100 m spread. The tunnel was centered on the center of the spread and was activated during the construction of the survey. During one of the QC checks during the survey a loop error was encountered and caused the survey to stop. Skipping the data made the survey continue until that electrode was found again and an open error was encountered. This was repeated until another electrode stopped working and thus caused a large amount of data not to be collected. The reason for this was a faulty smart cable and was not used for any other surveys. On Sunday February 8, 2009 the survey was performed using a 4m electrode spacing and a 100 m electrode spread. The data was collected but a lot less due to only having 25 electrodes.

PICTURES

Figure A-3 This is the south entrance of the tunnel

Figure A- this is the north hand entrance

DAM

NOTES

The dam site is technically not a dam but that is how we informally referred to it, technically this was an earthen embankment that contained some of the runoff from the power plant. The surrogate dam/tunnel is a metal pipe that is used in times of high water level, when we performed this survey there was some water that was coming out the other side in small quantities. This site is technically not part of the railway track and is in a similar region away from the highway and only source of noise is the high voltage power lines. The tunnel is approximately 5m deep and the tunnel is only about 0.5m in diameter. Compared to the other surveys the surface was a reddish clay material that was still quite moist. The seismic source had good contact but there were numerous equipment failures. There were both seismic and electrical studies performed at this site.

The seismic survey was 42 m long with 40 Hz geophone spacing of 0.6 m. To gather this data set we use a shot spacing of 0.6 m, starting 0.6m from the edge of the spread with a 0.6 m shot spacing through the line. The source used for this survey was an accelerated weight drop that was 1.5m laterally offset from the geophone array. At each shot location had at least 3 shots for stacking purposes but the data was acquired pre-stack and stacked in house for amplitude studies. The acquisition was sampled at 0.125 ms and was measured for 0.5 s. The seismic data was collected with a large number of bad geophones. At the start of the survey there were 3 bad channels and at the end there were over 10. The last line of geophones had identified loose wiring in the electrode takeout cables and was not used for the remainder of the surveys.

There were 3 dipole-dipole surveys performed over this tunnel site the reason for this is that since the last electrode takeout was removed to try and increase the data sampling we just changed the electrode spacing and kept the middle electrode the same. This was done during seismic acquisition, the ground was quite wet and the electrodes had solid contact with the ground. The surveys

consisted of a 25 m long 1m electrode spacing spread, a 50 m long 2 m electrode spacing, and a 100 m long 4m electrode spacing spread survey.

PICTURES

Figure A-5 The tunnel entrance form the on the north side of the tunnel

Figure A-6 the tunnel on the south side with the towards the drainage zone.

TUNNEL 3

NOTES

This was the 4th survey or known as tunnel 3 since the dam site was not included as part of the DHS contract. This tunnel site was a small metal pipe survey that was just off from tunnel 2. This surrogate tunnel is approximately 0.4 m in diameter and is partially filled on the south hand side of the tunnel site. This tunnel site is expected to have a kink in it since the anticipated location it should come out of is different. There were both seismic and electrical surveys done at this site. The approximate tunnel depth is around 4-6m.

The seismic survey was 45 m long with 40 Hz geophone spacing of 1 m. To gather this data set we use a shot spacing of 0.6 m, starting 0.6 m from the edge of the spread with a 0.6 m shot spacing through the line. The source used for this survey was an accelerated weight drop 1.5 m laterally offset from the geophone array. Again, at least 3 shots were done for stacking purposes at each shotpoint but the data was acquired pre-stack and stacked in house for amplitude studies. The acquisition was sampled at 0.0625 ms and was measured for 0.5 s. Unlike other surveys the actual location of the tunnel is not well known so the spread is centered on the approximate location of the tunnel.

The electrical survey carried out here had a 2m electrode spacing dipole-dipole spread, the survey was performed over the same region as the seismic profile. The estimated tunnel that is seen in the seismic survey sees the tunnel anomaly 10 m offset from this center of spread location. The resistivity section does not detect due to not getting deep enough to detect it.

PICTURES

Figure A-7 this is the south side of tunnel 3, the small metal pipe is barley visible

Figure A-8 This is the north side of the tunnel, the location was different then expected and thus we expect a kink in the result.

TUNNEL 4

NOTES

This was the 5th survey or known as tunnel 4. This tunnel site was a made up of small concrete blocks. This surrogate tunnel is approximately 0.5 m high and 0.75 m wide. There was both seismic and electrical techniques surveys. The approximate tunnel depth is around 6m. Both seismic and electrical methods should perpendicularly transect the tunnel trace at the surface. The surface was made up of crushed gravel and was quite dry.

The seismic survey was 72 m long with 40 Hz geophone spacing of 1 m. To gather this data set we use a shot spacing of 1 m, starting 0.5 m from the edge of the spread with a 1m shot spacing through the line. The source used for this survey was an accelerated weight drop that was 1.5 m laterally offset from the geophone array. Each shot location at least 3 shots were done for stacking purposes but the data was acquired pre-stack and stacked in house for amplitude studies. The acquisition was sampled at 0.125 ms and was measured for 0.5 s. There were 3 shots at each shotpoint location and vertically stacked during processing.

The electrical survey had a 2 m electrode spacing dipole-dipole, the survey was performed over the same region as the seismic. The dipole-dipole array has a 50 m electrode spread but had an issue with electrode contact. The electrodes that were placed were easily planted and did not achieve a solid contact with the earth even when put 8” into the ground.

PICTURES

Figure A-9 This is the south side entrance into tunnel 4, this tunnel si created of concrete blocks and is approximately 0.5m.x0.75m.

Figure A-10 This is the north side entrance into tunnel 4, this tunnel is created of concrete blocks and is approximately 0.5m.x0.75m.

TUNNEL 5

NOTES

This was the second smallest tunnel that was attempted to be gathered, for this survey hammer seismic was done due to only using a 28.8 m spread. There was both seismic and electrical surveys acquired, the reason for this tunnel was because it was partially filled and quite shallow. The ground was a harder pack and both the geophones and the electrodes could get good contact. The hammer seismic is shot directly between the receivers, there is no perpendicular offset from the array since the striking plate could fit between the geophones..

The seismic survey was 28.8 m long with 40 Hz geophone spacing of 0.6 m. To gather this data set we use a shot spacing of 0.6 m, starting 0.6 m from the edge of the spread with a 0.6 m shot spacing through the line. The source used for this survey was a sledge hammer that had no lateral offset from the geophone array. Each shot location at least 3 shots were done for stacking purposes but the data was acquired pre-stack and stacked in house for amplitude studies. The acquisition was sampled at 0.0625 ms and was measured for 0.5 s.

The electrical surveys had a 25 m dipole-dipole array done with 1m electrode spacing; the survey was set up before the seismic and ran while the seismic survey was running. The electrodes had solid contact and the ground was fairly compact and not loose gravel.

PICTURES

Figure A-11 this is the surface layout of tunnel 5, on the left is the ERT survey, the right is the seismic

Figure A-12, this is the north side of the tunnel 5, the culvert is partially filled

Figure A-13, this is the south side of tunnel 5. The tunnel is partially filled.

TUNNEL 6

NOTES

This was the 7th survey or known as tunnel 6. This tunnel is very similar to tunnel 4 and the acquisition was the same. The tunnel itself is slightly deeper than tunnel 4. This tunnel site was a made up of small concrete blocks. This surrogate tunnel is approximately 0.5 m high and 0.75 m wide. There were both seismic and electrical surveys done at this site. The approximate tunnel depth is around 6.5 m. Both seismic and electrical methods should transect the tunnel on the surface perpendicular. The surface was made up of crushed gravel and was quite dry. The slopes on either side of the railway were steep with evidence of erosion. Parts of the slope had a backfill of gravel on the south side of this tunnel because of this.

The seismic survey was 72 m long with 40 Hz geophone spacing of 1 m. To gather this data set we use a shot spacing of 1m, starting 0.5 m from the edge of the spread with a 1m shot spacing through the line. The source used for this survey was an accelerated weight drop that was 1.5 m laterally offset from the geophone array. Each shot location at least 3 shots were done for stacking purposes but the data was acquired pre-stack and stacked in house for amplitude studies. The acquisition was sampled at 0.125 ms and was measured for 0.5 s. There were 3 shots at each shotpoint location and vertically stacked during processing.

The electrical survey here had a 2 m electrode spacing dipole-dipole spread done, the survey was performed over the same region as the seismic. The dipole-dipole array has a 50 m electrode spread but had an issue with electrode contact. The electrodes that were placed were easily planted and did not get solid contact even when put 10 cm into the ground.

PICTURES

Figure A-14 The south side of tunnel 6, the tunnel was completely covered , but is not filled

Figure A-15 The north side of tunnel 6, we cannot see if this part of the tunnel is filled or not.

TUNNEL 7

NOTES

Only a seismic survey was performed at this survey due to time constraints, and because the ERT system was still running at tunnel 6 when this tunnel was being performed. The survey was the shallowest tunnel and is estimated at only 1.5 m deep. The survey was 42 m long, the tunnel is partially filled with water, The ground was quite hard and good contact was achieved between with the geophones and the ground

The seismic survey was 28.8 m long with 40 Hz geophone spacing of m. To gather this data set we use a shot spacing of 0.6 m, starting 0.6 m from the edge of the spread with a 0.6m shot spacing through the line. The source used for this survey was a sledge hammer that had no laterally offset from the geophone array. Each shot location at least 3 shots were done for stacking purposes but the data was acquired pre-stack and stacked in house for amplitude studies. The acquisition was sampled at 0.0625 ms and was measured for 0.5 s.

PICTURES

Figure A-16 This is the surface layout of Tunnel 7, the geophones are on the side of the path.

Figure A-17 This is the north side of the tunnel, it is partially filled

Figure A-18 This is the south side of the tunnel, there is a mixture of water, leaves and tree branches in the tunnel.

TUNNEL 8

NOTES

This was the last survey that was surveyed in Oxford, MS. The tunnel is also the second deepest at around 8 m deep. The tunnel has quite steep and both a Wenner and a dipole-dipole survey were done. This was one of the few days where wind noise was an issue and can be seen in the seismic data. The seismic data also had a string of low frequency phones at the end to see the difference between them. The tunnel itself is around 0.75 m wide and 0.75 m high, the construction is similar to Tunnel 6 and Tunnel 4 with sandstone blocks and mortar as its casing. The tunnel itself was empty and had very little debris in it

The seismic survey was 120 m long with 40 Hz geophone at spacing of 1m. In addition, the last 24 m had 10 Hz geophone attached. To gather this data set we use a shot spacing of 1 m, starting 0.5 m from the edge of the spread with a 1m shot spacing through the line. There were a large number of bad shots due to wind noise. The source used for this survey was an accelerated weight drop that was 1.5 m laterally offset from the geophone array. Due to the wind energy, the elastic band that was attached was tightened for more power. Each shot location at least 3 shots done for stacking purposes but the data was acquired pre-stack and stacked in house for amplitude studies. The acquisition was sampled at 0.125 ms and was measured for 0.5 s

Along with the seismic surveys there were also 2 electrical surveys collected at this site using an ERT Scintrex box. The data set up includes 25 electrodes collected to a smart cable with 2m electrode spacing. The total length of the spread was 50 m centered over the spread, the survey was set up first and was running first then the seismic survey was set up and ran. There was a dipole-dipole and Wenner array that were calculated.

PICTURES

Figure A-19: This is the surface layout for tunnel 8. The right has the geophones attached, the blue geophones are the 10Hz geophones, and the 10Hz geophones are red. The left hand side of the surface has the ERT survey

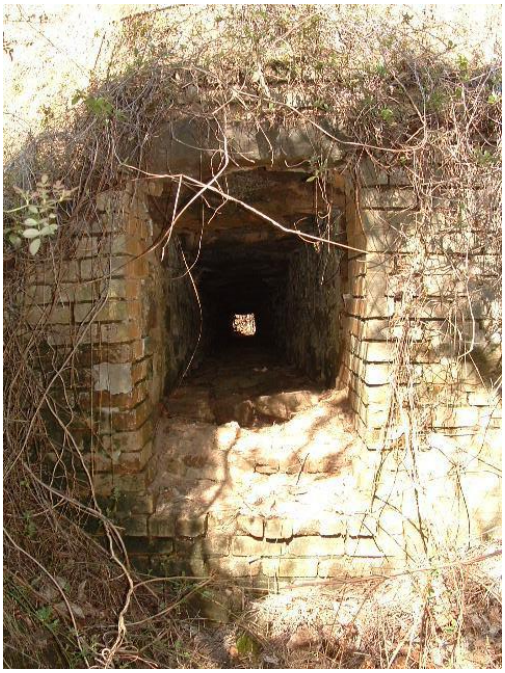

Figure A-20 The south hand side of the railway survey site for tunnel 8

DOUGLAS, AZ

The Douglas, AZ test site is a discovered clandestine tunnel that had both weapons and cocaine transferred through it. The tunnel was found in 1990 and is to date still one of the more sophisticated tunnels ever created on the US Mexico border. The tunnel was built by Corona-Verbera who was the architect for the "El Chappo" Guzman Drug Trafficking Organization. He was incarcerated for 25 years. The tunnel shaft was approximately 8 m deep on the Mexico side and had the use of an elevator like pulley system to lower the contraband into the tunnel, the tunnel had tracks for a cart in the tunnel along with a air-conditioning and electricity for lighting. The tunnel emerged in warehouse on the US side, and there is also an underground storage area for the contraband before being brought to the surface. The tunnel is also concrete lined with a water pump and drains for when the tunnel is filled full of water.

The Douglas, AZ test site is controlled by the US customs and border patrol (CBP) and while we were there we had a representative with us and also a member of the US department of homeland security (DHS). To get permission for these tests both permission from DHS and CBP was required along with The University of Mississippi.

When we arrived at the test site there were only 2 possible areas for the seismic survey to be performed. There was a zone of gravel and sand beside the road by the warehouse, and then there was ditch beside the road and was approximately 3 m below the roadside. This had loose sands and was under construction with concrete being laid some distance away. There was also an area right beside the border fence but do to safety concerns and amount of noise directly beside the fence was not done. Looking at the figures below we can see the field conditions of each seismic site.

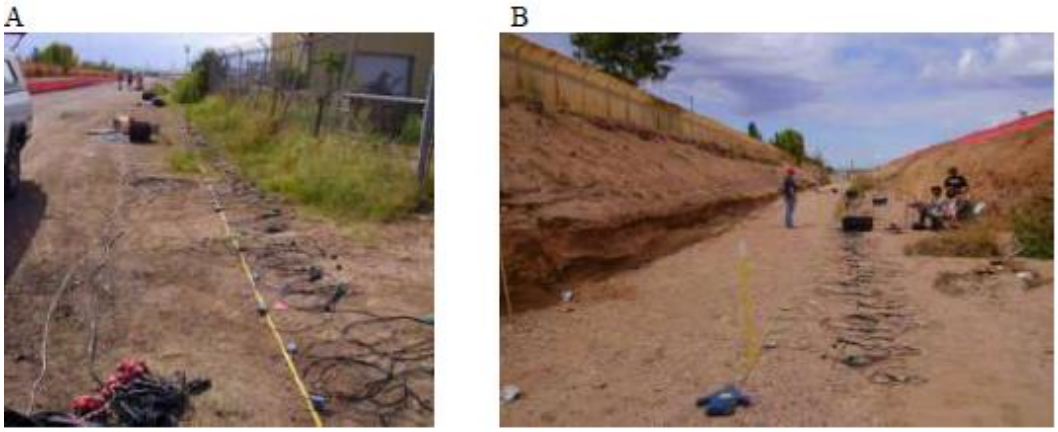

Figure A-21 Left: this is the layout for the roadside data in Douglas, AZ. This survey uses low frequency geophone. The tunnel is approximately in the middle of the warehouse running to the right. Right: This is the ditch data, the seismic was done directly in the middle and to the left hand side by the overhang the electrical survey was done. The border fence can be seen on the above the ditch on the left.

ROADSIDE

There were 4 main surveys that were acquired on the roadside data a 3-C geophone, the large hammer, small hammer and the borehole surveys. Each method was described below.

3-C survey: This was the first survey performed; it uses 24 channel 3-C geophones attached to one geode with 6 separate lines. This survey is performed by shooting 1 spread length of geophones on either side of the individual spread to increase the fold of the files. There are 6 lines, shots in-between each geophone with geophone spacing of 1 m. The shot spacing for these surveys is 1m; the small hammer was used and is hit vertical into a metal plate. The geophone spacing is 1m and goes for 60m.

Seismic 16Hz large hammer: This survey was done on Sept 2, 2009 and is the first major survey used. There were 6 separate geodes used where the first geode has the borehole component attached. On the survey file we have the first channel 1-24 as the borehole and then 25-144 as the 120 channels of the vertical component geophones. A long offset shot was taken at -30m from spread length west of the line. This was across the road and used for the borehole data exclusively. Shot spacing is

1m and is taken inline between the geophones. The total spread length for this line is 59.5 m where the tunnel is situated 18m from the west start of the line. The spread length starts from the east where 0m is the start of the line.

Seismic 16Hz small hammer: This survey was carried out just for amplitude information on the geophones which were otherwise clipped due too much energy in the close range. This data was not used for seismic refraction or reflection profiles and was gathered for amplitude studies. The shots are taken in-between the line and follow the same format as the large hammer survey.

Borehole: The data collected here is the first 1-24 channels of the large hammer survey. Channels 5-8 are the only ones active and all the rest are turned off. Channel 5 is the vertical component of the downhole tool, channel 6 is the H1 component, channel 7 is the H2 component, and channel 8 is the hydrophone. The borehole is 10.5m from the start of the line and

There were also 2 electrical surveys performed at this test site, a Wenner array and a dipole-dipole array. There was a metal fence beside the tunnel site did and also there were quite a bit of road traffic while the survey was running. The resistivity survey had a 1m electrode spacing with a 50 m electrode spread. The 50 electrodes that were used worked good until the dipole-dipole survey. Similar to the Oxford, MS data set there became a bad takeout and some of the data was lost. Since there was also another road immediately to the west of the test site we could not center the tunnel in the spread.

Ditch Data

The ditch data compromised of a dug out ditch that was fortuitously under construction at the time of the surveys. The ditch would not be covered with concrete. This area had a loose sand base and was fairly flat the electrical data that was collected was over the overhang since it was moister there and the electrodes had better contact. The seismic data was collected in the middle of the ditch and was in loose sands. The ditch had a large amount of metal debris around on the surface such as rebar, barbed wire, and other garbage. Looking at the side of the ditch we could see that there was a loosely consolidated surface by the roadside and the

material got more and more competent with depth. The ditch data was under this competent layer. There were two surveys performed for this site

There were two survey performed right after another. The first used low frequency geophones, the second used higher frequency geophones which better reduce ground roll and other surface related noise, but limit the data. The goal was to compare if the frequency change in the geophones would change the result drastically. Refraction profiles were done on both to compare the difference. The second survey was identical except there was 40 Hz geophones instead of the first one which had 14 Hz geophones.. The seismic data had a 48m spread length with a geophone spacing of 0.5m, the data was recorded for 0.5 s at a 0.0625 ms sample rate. The source spacing was 0.5 m and where the data started off by 0.25 m from the end of the spread.

The electrical data that collected was a dipole-dipole array using 1m electrode spacing with 50 electrodes. The electrodes were planted along the edge of the ditch in the shade and had water poured over them for good contact. The loose sands were causing poor contact. The

PEOPLE INVOLVED

I would like to thank the people involved for the Douglas, AZ data set for all there hard work and dedication. The people that worked on the site are

Craig Hickey	NCPA
Grey Riddle	University of Alberta
Douglas Schmitt	University of Alberta
J.D. Heffington	NCPA
Gordon Brasnett	University of Alberta
Steve Taylor	University of Alberta
Cory Schmitt	Doug Schmitt son
Lesley Blancas	DHS S&T
James Wray	CBP
Robert Shiner	CBP

PICTURES

There are no pictures of the actual tunnel. Since it is concealed and no confined space training was taken.